Astrocyte Lipid Homeostasis is Regulated by Glutamate

by

Luis Fernando Rubio Atonal

A thesis submitted in partial fulfillment of the requirements for the degree of

Master of Science

Department of Physiology
University of Alberta

Abstract

Astrocytes can store excess fatty acids in lipid droplets to avoid lipotoxicity. Fatty acids can be released from lipid droplets and catabolized to generate energy in the mitochondria. We previously found reduced astrocytic lipid droplets and increased transport of fatty acids into the mitochondria in response to glutamate, the major excitatory neurotransmitter in the brain. Whether glutamate affects fatty acid catabolism and how glutamate regulates lipid droplet homeostasis in astrocytes is unknown. Here, we show that astrocytes use glutamate directly as fuel for increased oxidative phosphorylation while decreasing their use of glycolysis for ATP production. Importantly, glutamate had no effect on fatty acid catabolism in mitochondria. Instead, increased fatty acid transport is likely used for mitochondrial maintenance as we found decreased reactive oxygen species with a concomitant increase in mitochondrial mass upon glutamate treatment. Consistent with healthier mitochondria, we observed that glutamate increased AMPK phosphorylation and supressed the induction of autophagy, which probably reduces the lipid flux into lipid droplets. Altogether, this study reveals how exogenous application of glutamate, a major excitatory neurotransmitter in the brain, regulates fatty acid homeostasis in astrocytes.

Preface

This thesis is an original work by Luis Fernando Rubio Atonal. The research project, of which this thesis is a part, received research ethics approval from the University of Alberta Animal Care and Use Committee (Inter- and intracellular trafficking of lipids in the brain, No. AUP00003358, January 26, 2020) and the Canadian Council of Animal Care (CCAC).

Chapter 3 of these thesis is being prepared for submission for publication as “Astrocytic lipid homeostasis is regulated by glutamate”; Luis F. Rubio-Atonal, Julie Jacquemyn, Jinlan Chang & Maria S. Ioannou (in preparation). Technical support was provided by Dr. Julie Jacquemyn (lipidomics), Dr. Jinlan Chang (western blotting) and Mike Wong from the Advanced Cell Exploration Core (ACE) (Seahorse) at the University of Alberta. Lipid extraction and lipidomics LC/MS workflow were performed by Dr. Jun Han and his team from The Metabolomics Innovation Centre (TMIC) at its Victoria (BC, Canada) facility. Dr. Maria Ioannou performed the mitochondrial lipid trafficking assay, corresponding to Figure 17, panels C and D. I performed the data collection and analysis from all the experiments except for those stated previously. Concept formation was done together with my supervisor, Dr. Maria Ioannou.

Acknowledgments

I would like to acknowledge Dr. Maria Ioannou for her guidance and supervision during this research project.

I would also like to acknowledge Dr. Thomas Simmen and Dr. Gregory Funk for being part of my supervisory committee and for their helpful insights and ideas during our supervisory meetings.

I am also thankful to my mentors Dr. Marisol Orozco and Dr. Benjamin Lindsey as well as my therapist Cristina Figueroa Quirino for their many hours of support and advice.

I would also like to thank all the student members of the Ioannou lab, both past and present: Julie Jacquemyn, Nathanael Lee, Wendy Cai, Kennedy Chik, Ju-Young Bae, Isha Ralhan and Ian Gatera. I got to learn a lot from you, and I appreciate all the lessons I learnt with everyone.

Dearest to my heart, my family, and my chosen family: my mom, my brother, my dad, and my partner. Without my family's unwavering support and specially, my partner's support and ability to hold down our fort while I embarked on this academic journey.

Finally, a special mention for the institutions that funded the research and awards that allowed me to perform this work: the Faculty of Medicine and Dentistry, the Women and Children's Health Research Institute, the Canadian Institutes of Health Research and the Natural Sciences and Engineering Research Council of Canada.

Table of Contents

List of Figures

List of Tables

Chapter 1: Introduction

Neurons and astrocytes

The brain is composed of multiple cell types including neurons, astrocytes, oligodendrocytes, and microglia. For this research, we will focus on astrocytes and how they respond to neuronal activity. Neurons are the functional unit of the brain, as they specialize in receiving, transmitting, and processing the information that the body receives from internal and external stimuli. Astrocytes on the other hand, coordinate a myriad of functions that support neurons: regulate water and ion transport, maintenance of the blood-brain barrier, transport of nutrients and signals that arrive from the blood, modulation of synapses through their lifecycle, as well as providing metabolic support to neurons.

All this activity in the brain requires energy in the form of adenosine triphosphate (ATP), a molecule that stores energy. The brain requires a constant supply of fuel in the form of macromolecules to sustain ATP synthesis, as the brain consumes more than 10% of the total energy produced by the body in a resting state (*1*). Most the energy in the brain comes from glucose, as low levels of glucose in the blood quickly lead to fainting. If glucose levels are not restored to normality within a few seconds, permanent damage is caused. To avoid this, the supply of fuels to the brain to produce energy must be tightly regulated. Astrocytes are uniquely positioned to contribute to the brain energy supply, as they are located in between neurons and the vasculature. Astrocytes play a crucial role in providing neurons with metabolic support. To accomplish this, astrocytes sense neuronal signals and respond to them accordingly. This implies that there is constant communication between neurons and astrocytes.

Neuron-astrocyte communication

Neuron-astrocyte communication is important for the everyday functioning of the brain. Neurons communicate with each other via synaptic neurotransmission. In synaptic transmission, neurotransmitters are released from one neuron (presynaptic neuron) and travel through the extracellular space of the synaptic cleft until they reach another neuron

(postsynaptic neuron). Neurotransmitters then bind to their corresponding receptors on the postsynaptic neuron. Receptors for neurotransmitters are proteins that respond to one or more molecules in the extracellular space. There are two types of receptors: a) Ionotropic receptors, where the receptor is an ion channel that respond directly to the neurotransmitter by passing current in the form of ions, or b) Metabotropic receptors, which produce a second messenger that signals intracellularly to induce its effect. In addition to receptors, transporters import neurotransmitters into cells and consequently clear them from the extracellular space. But where do astrocytes fit in this neuron-to-neuron synaptic neurotransmission?

The synapse is not just a neuron-to-neuron communication spot. Astrocytic processes envelop synapses, which allows them to detect neurotransmitters through their own receptors. The astrocyte capacity to detect neuronal signals is relevant for astrocytic function because it grants them the capacity to coordinate a response to support (*2*–*5*) or modulate neuronal network activity (*6*, *7*). But how do astrocytes coordinate with neurons to support their activity? The glutamatergic synapse is a great example of neuron-astrocyte communication.

Glutamatergic synapse as a hub for neuron-astrocyte communication

Glutamate is a major excitatory neurotransmitter in the brain (*3*), as around 40% of neurons in the brain are glutamatergic and around 80-90% of neurons express glutamate receptors (*8*). Moreover, astrocytes express both types of glutamate receptors: ionotropic and metabotropic glutamate receptors. On the ionotropic side, astrocytes express NMDA and AMPA/Kainate receptors (*9*, *10*); while on the metabotropic side, astrocytes express glutamate metabotropic receptors mGluR5 and mGluR2/3 (*9*, *10*). The function of ionotropic receptors in astrocytes, particularly the NMDA receptor, is still a matter of debate (*11*–*13*) while the astrocyte metabotropic receptor function is better understood and established (*10*).

In a glutamatergic synapse, glutamate is released via exocytosis from the presynaptic neuron, diffuses quickly through the synaptic cleft, and reaches the postsynaptic neuron to exert its excitatory effects. However, if glutamate accumulates in the synaptic cleft

without being removed, it induces neuronal excitotoxicity and death (*14–18*). Astrocytes take up glutamate via excitatory amino acid transporters 1 and 2 (EAAT1 and EAAT2) and convert it into glutamine in the cytosol via glutamine synthetase (GS) (*19*, *20*). This reduces the risk of neuronal excitotoxicity. Newly recycled glutamine can be secreted via SNAT3/5 to the extracellular space to then be picked up by neuronal SNAT1/2 (*21*, *22*). Neurons convert glutamine back to glutamate via the glutaminase enzyme, and then load the recycled glutamate into synaptic vesicles for reuse (*22*, *23*). This cycle is described in Figure 1. The glutamate/glutamine cycle illustrates how astrocyte glutamate-glutamine metabolism is linked to sustaining neuronal activity and function.

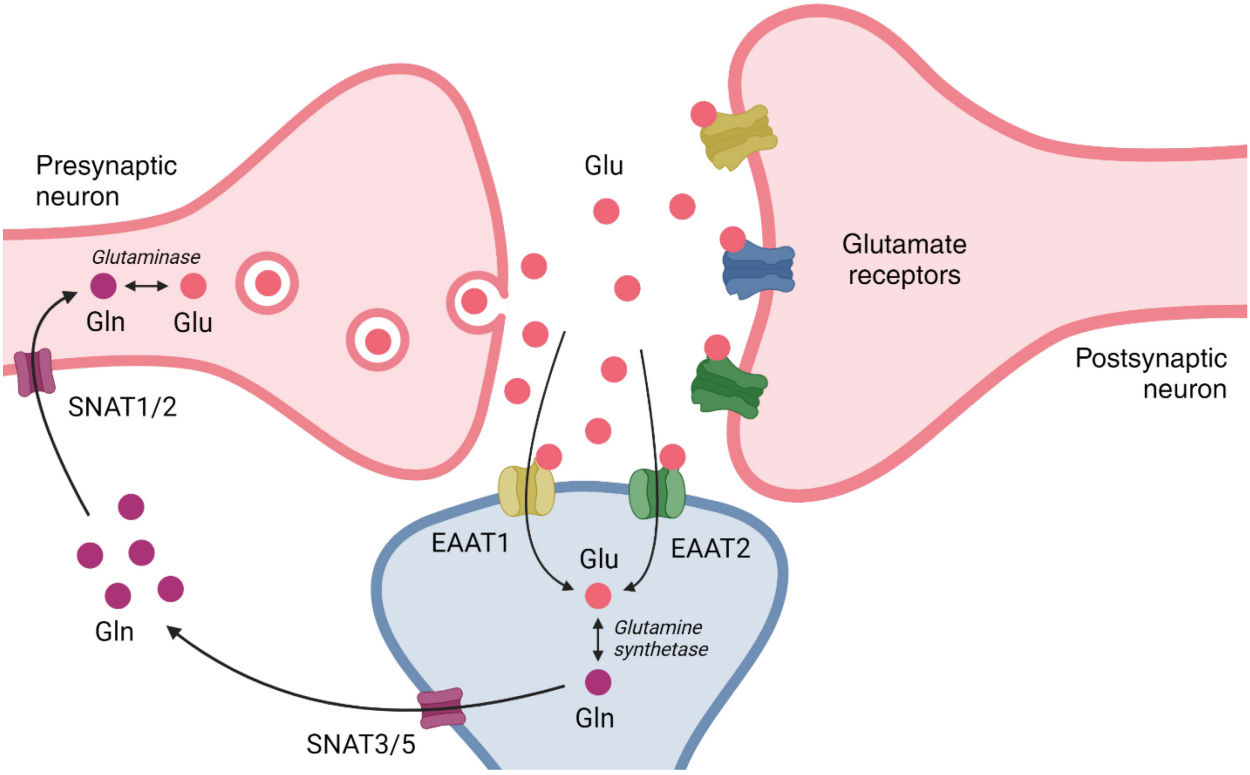

Figure 1. The glutamate/glutamine cycle.

Schematic representation of the glutamate/glutamine cycle. In the glutamatergic synapse, the presynaptic neuron releases glutamate that acts on the postsynaptic neuron glutamatergic receptors. Excess glutamate is removed by astrocytic EAAT1/EAAT2. In the astrocyte, glutamate is converted back to glutamine and then released into the extracellular space by astrocytic glutamine transporters SNAT3/SNAT5. Glutamine is then taken up by neurons via glutamine transporters SNAT1/SNAT2 and converted into glutamate via glutaminase to be recycled and loaded back into synaptic vesicles. Gln, glutamine; Glu, glutamate; EAAT1/1, excitatory amino acid transporter 1/2; SNAT1-3/5,

sodium-coupled neutral amino acid transporter 1-3/5. Figure created with BioRender.com.

Neuron-astrocyte metabolic coupling

Neurotransmission activity in the brain accounts for up to 70% of the entire brain energy expenditure according to multiple simulations (*24–26*). Most of this energy expenditure relies on glucose metabolism (*4*, *27*, *28*), as low levels of glucose in the blood can significantly alter brain function and the severity of this effect is inversely correlated with glucose levels (*29*, *30*). But where is this glucose coming from? Glucose is delivered to the brain through the vasculature. Unlike other organs in the body which associate directly with the vascular system, the brain is separated from the systemic circulation by the blood brain barrier (*31*, *32*). The blood brain barrier is a selectively permeable barrier that surrounds the brain vasculature (*31*, *33*).

In the blood brain barrier, the main glucose transporter is glucose transporter 1 (GLUT1, Slc2a1) (*34*, *35*), as it is abundantly expressed in endothelial cells and astrocytes (*35*). Other glucose transporters like sodium-dependent glucose transporter (SGLT1) are also found in the blood brain barrier (*2*, *34*, *36*). When neuronal activity is sustained, glucose is quickly transported from the blood into the brain through endothelial cells mainly via GLUT1 (*36*, *37*). Glucose is then taken up via glucose transporters by neurons (GLUT3, GLUT4) and astrocytes (GLUT1) and then metabolized (*30*, *38*, *39*).

Neurons and astrocytes can catabolize glucose via glycolysis (*30*). In neurons, the resulting pyruvate from glycolysis can be further catabolized in the mitochondria to produce more ATP (*40*). However, in astrocytes, pyruvate is converted into lactate and release it into the extracellular space where it is taken up by neurons (*40*). Once in the neuron, lactate is converted back into pyruvate and used it for ATP production (*41*, *42*). This process is known as the astrocyte-neuron lactate (ANLS) shuttle (Figure 2) and allows astrocytes to support neuronal activity (*42–45*) by providing lactate as a substrate that is used for energy production in the mitochondria.

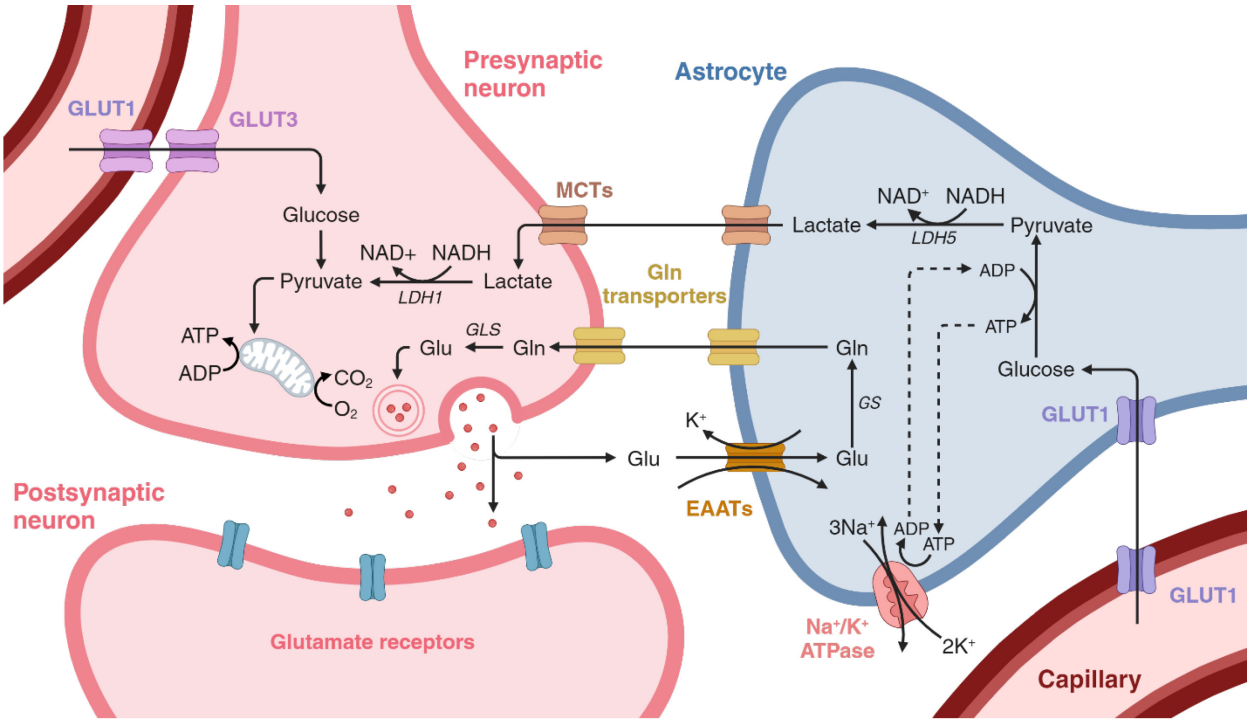

Figure 2. Astrocyte-Neuron Lactate Shuttle.

Neuronal activity induces glutamate transport into astrocytes, a significant energetic cost for astrocytes. To ensure affront these energetic costs, astrocytes upregulate glucose uptake and glycolysis. Glycolysis-derived pyruvate in astrocytes is preferentially converted into lactate. Lactate will then be secreted by astrocytes through monocarboxylate transporters (MCTs) into the extracellular space and taken up by neurons which can the use it for ATP synthesis. GLUT1/3, glucose transporter 1/3; NAD, oxidized nicotinamide adenine dinucleotide; NADH, reduced nicotinamide adenine dinucleotide; MCTs, monocarboxylate transporters; EAATs, excitatory amino acid transporters; Na^+/K^+ ATPase, sodium-potassium adenosine triphosphatase or sodium/potassium pump; LDH1/5, lactate dehydrogenase 1/5; GLS, glutaminase; Gln, glutamine; Glu, glutamate; ADP, adenosine monophosphate; ATP, adenosine triphosphate. Figure created with BioRender.com.

Additionally, neuronal activity is tightly coupled to local blood flow. Astrocytes are located in between neurons and the vasculature and respond to neuronal activity by releasing signals that regulate blood flow (*2*). These signals result in vasodilation in regions with heightened neuronal activity (*46–48*), and vasoconstriction in areas with sufficient substrate supply and/or decreased neuronal activity (*48*, *49*). This enhances oxygen and

glucose delivery to areas with high neuronal activity to meet the energetic demands (*2*, *48*).

This close intertwining of neuronal activity with astrocyte metabolism is known as neurovascular coupling. Recently, neuron-astrocyte metabolic coupling was shown to involve lipid metabolism (*50*). However, the regulation and physiological role of lipid metabolism in astrocytes is not completely understood.

Lipids

Lipids are a diverse group of organic compounds. Unlike other macromolecules that are defined by the existence of a specific functional group, lipids are identified by their solubility. If a macromolecule is more soluble in organic solvents than water, they are considered as lipids. Broadly, lipids can be split into two groups: fatty acids and sterols. Fatty acids comprise a chain composed of a backbone of carbon atoms that are surrounded by hydrogen and a terminal carboxyl group (-COOH), while sterols contain four fused carbon skeleton rings. Our research will focus on fatty acids.

Fatty acids are classified according to their chain length: short-chain fatty acids (SCFA) are composed of two to five carbon chains (C:2-C:5), medium-chain fatty acids (MCFA) contain six to twelve carbons (C:6-C:12), long-chain fatty acids (LCFA) harbor thirteen to twenty carbons (C:13-C:20) and very-long-chain fatty acids (VLCFA) possess more that twenty one carbons (≥C:21). Fatty acid chain length is relevant as it impacts fatty acid structure, function, and metabolism (*51*). But how do fatty acids get into the cell? Fatty acids can be either imported into the cell or be newly synthesized.

Fatty acid import and synthesis

Import of fatty acids into the cell is mediated by a) diffusion of fatty acids across the membrane, or b) fatty acid transport proteins. Diffusion implies the rapid movement of mostly SCFA across the cell membrane through a flip-flop mechanism (*52*, *53*). This rapid movement across the cell membrane is performed without the need of specialized proteins nor the use of energy (*54*). The use of fatty acid transport proteins implies the transport of specific fatty acids through these proteins that are expressed in the cell membrane. So far, 3 protein families have been identified in this process: fatty acid

transport proteins (FATP), fatty acid translocase (FAT), and fatty acid binding proteins (FABP). Fatty acid transport proteins facilitate the transport of LCFA into the cell and present 6 isoforms (FATP-1-6) of which FATP-1 and FATP-4 are mostly expressed in the brain (*54*–*56*). Fatty acid translocase, also known as CD36, presents affinity for LCFA although the exact transport mechanism remains to be identified (*54*, *57*). Fatty acid binding proteins are subdivided according to their cellular distribution, where we can find plasma membrane associated and cytoplasmic FABPs. Membrane associated FABPs not only bind LCFA but can also transport other lipid species like monoacylglycerol and cholesterol. Cytosolic FABP have high affinity for LCFA but can also bind to other lipid and non-lipid ligands (*58*). FABP6, FABP3, FABP5 and FABP7 have been identified in the nervous system (*59*), of which FABP5 and FABP7 have been identified in glial and neuronal cells (*60*, *61*).

In addition to the import mechanisms, fatty acids in the brain can be synthesized *de novo* by astrocytes in a process known as lipogenesis. *De novo* synthesis of fatty acids occurs in the cytosol and cytosolic acetyl-CoA serves as the main carbon building block. Cytosolic acetyl-CoA is also converted into malonyl-CoA by acetyl-CoA carboxylase 1 (ACC1). This reaction requires ATP and CO_2. Both acetyl-CoA and malonyl-CoA are necessary substrates for fatty acid synthesis. Fatty acid synthesis occurs in the cytosolic multicomplex enzyme known as fatty acid synthase (FAS) (*62*). FAS contains all the domains that are essential to synthesize fatty acids: a “mobile arm” known as the acyl-carrier binding protein (ACP) (*63*), malonyl/acetyl transferase (MAT), β-ketoacyl synthase (KS), β-ketoacyl reductase (KR), dehydratase (DH), enoyl reductase (ER), and thioesterase (TE) (*64*); and as fatty acid synthesis progresses, ACP will carry the growing fatty acid around all the complexes until synthesis is completed.

Fatty acid synthesis begins by the transfer of the acetyl group (2 carbons) from acetyl-CoA into ACP forming acetyl-ACP and the transfer of the malonyl group (3 carbons) from malonyl-CoA into a different ACP forming malonyl-ACP. This occurs in the MAT domain. This is followed by the action of the KS domain that decarboxylates malonyl-ACP (now only 2 carbons) and transfers the acetyl-group from acetyl-ACP, forming acetoacetyl-ACP (4 carbons). Acetoacetyl-ACP is then reduced by the KR domain to form β-

hydroxybutyryl-ACP which is then dehydrated by the DH domain resulting in α,β-trans-butenoyl-ACP. α,β-trans-butenoyl-ACP is then further reduced by the ER domain forming butyryl-ACP. Butyryl-ACP can then be elongated by repeating the previously described process by the addition of more malonyl groups. This forms a cycle in which each repetition will add 2 more carbons into the fatty acid until the desired length is achieved (usually 16 carbon palmitate). This triggers the end of the cycle, in which the TE domain hydrolyzes the thioester bond that links palmitate to ACP, resulting in the release of the fatty acids.

Free fatty acids are then transferred into other organelles to perform their function. Intracellular trafficking of fatty acids is dependent on their chain length. SCFA and MCFA usually diffuse through membranes (*65*–*70*) while LCFA and VLCFA need to be transported into organelles using transporters like FATP and FABP, or through organelle contact sites by the action of lipid transfer proteins (*71*–*75*).

Fatty acids cannot be directly metabolized, instead, they must be activated. This activation is done by converting free fatty acids into their equivalent acyl-CoA. This is achieved by the acylation of the free fatty acid via acyl-CoA synthetases (ACS). Like many enzymes in lipid metabolism pathways, they only activate fatty acids with a certain chain length and ACS is no exception. ACS is a family of enzymes that is split in four branches, each of which activates a different set of fatty acids based on their chain lengths: 1) short-chain acyl-CoA synthetases (ACSS), 2) medium-chain acyl-CoA synthetases (ACSM), 3) long-chain acyl-CoA synthetases (ACSL) and 4) very long-chain acyl-CoA synthetases (ACSVL) (*76*, *77*). Activation of fatty acids also result in the trapping of fatty acids inside the cell or organelle of interest (*76*, *78*).

Lipid droplets

Astrocytes uptake and synthesize lipids. When excess amount of these lipids are accumulated they are stored in organelles known as lipid droplets (LD) (*79*). Lipid droplets consist of a phospholipid monolayer enclosing a “core” filled by neutral lipids, most commonly triacylglycerols (TAG) and sterol esters (SE) (*74*, *79*–*81*) (Figure 3). While the

main components of the lipid droplets are TAGs and sterol esters, it has been proposed that other lipids as well as hydrophobic molecules might be in LDs as well (*82*).

Lipid droplets have multiple functions, among them, they provide fatty acids to fuel energy production during periods of nutrient deprivation or during high metabolic demand (*74*, *75*, *79*) They also protect cells against lipotoxicity caused by excess of free fatty acids (*74*, *75*, *79*, *83*). Although LD regulation has been explored in multiple tissues and organs like the liver or adipose tissue, the pathways regulating LDs in astrocytes have not been fully elucidated.

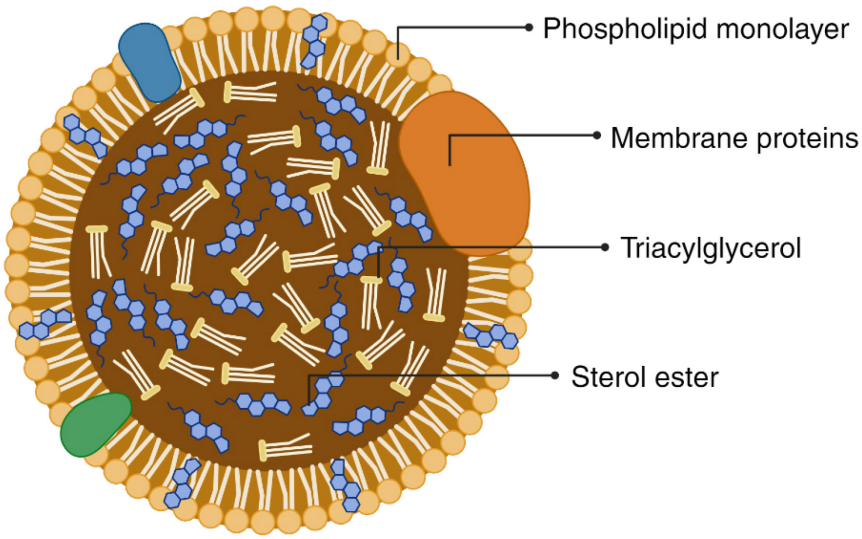

Figure 3. Lipid droplet structure.

Schematic that describes the structure of lipid droplet: a phospholipid monolayer that surrounds a core of triglycerides and sterol esters. Figure created with BioRender.com.

Triacylglycerol synthesis and lipid droplet formation

Lipid droplets form in the endoplasmic reticulum (ER) membrane, near areas with high TAG synthesis (*74*, *75*, *79*).

TAGs are synthesized from the esterification of glycerol with fatty acids and it occurs on the ER membrane (Figure 4). This begins by the formation of monoacylglycerol (MAG) by glycerol-3-phosphate acyltransferase (GPAT), which joins glycerol-3-phosphate with

a fatty acid (*74*, *75*, *81*). MAGs are then transformed into phosphatidic acid (PA) by acyl glycerophosphate acyltransferase (AGPAT), which needs a MAG and an acyl-CoA (*74*, *75*, *81*). PA is rapidly converted into diacylglycerol (DAG) by phosphatidic acid phosphatase (PAP) (*74*, *75*, *81*). Finally, TAG synthesis occurs by conversion of diacylglycerol via two possible pathways: diacylglycerol acyltransferase enzymes 1 and 2 (DGAT1, DGAT2) (*84*) or by DGAT1/2-independent enzyme synthesizing storage lipids (DIESL) (*85*).

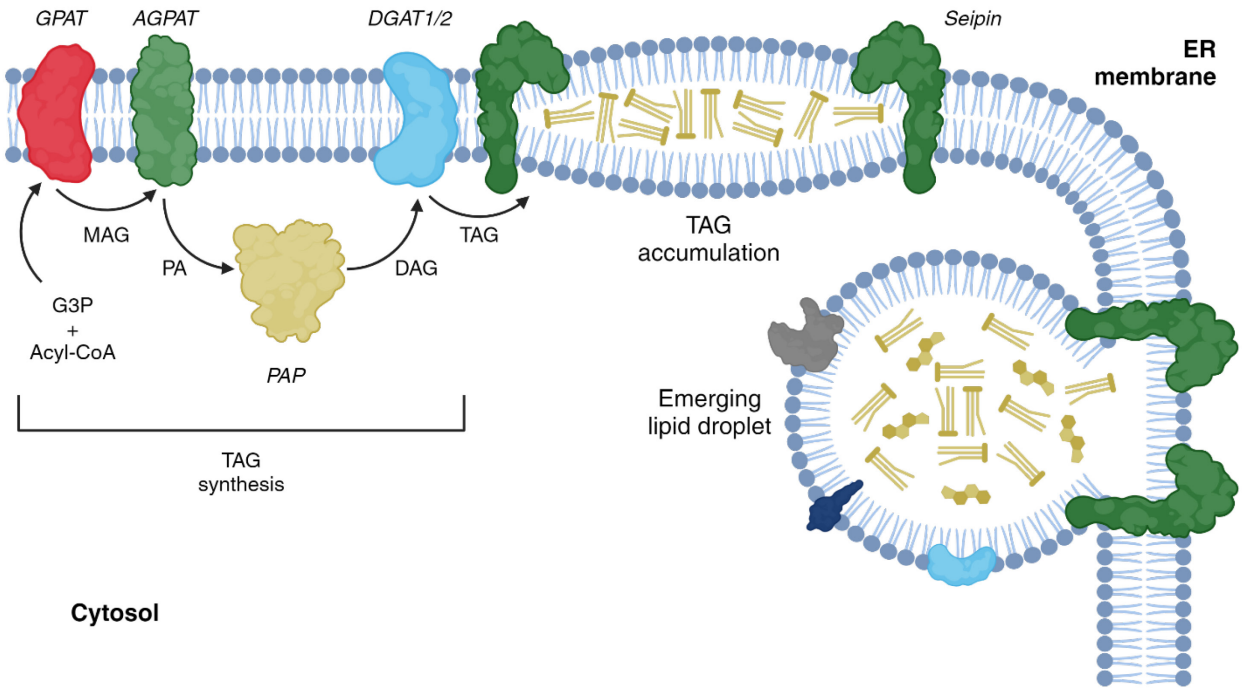

Figure 4. Triacylglycerol synthesis and lipid droplet biogenesis.

Triglyceride synthesis and lipid droplet biogenesis. TAG synthesis occurs by the sequential esterification of glycerol-3-phosphate with three free fatty acid via acyl transferases. Lipid droplet biogenesis commences with the accumulation of TAGs in between the phospholipid bilayer of the ER until the formation of a lipid lens. Through undetermined pathways, proteins that aid in lipid droplet biogenesis are recruited to the TAG accumulation site to further support this growth. G3P, glycerol-3-phosphate; GPAT, glycerol-3-phosphate acyltransferase; MAG, monoacylglycerol; AGPAT, acyl glycerophosphate acyltransferase; PA, phosphatidic acid; PAP, phosphatidic acid phosphatase; DAG, diacylglycerol; DGAT1/2, diacylglycerol acyltransferase enzyme 1/2. Figure created with BioRender.com.

Although produced physiologically, sterol ester production can increase if there is an excess of sterols (*86*). Sterol esters are made by acyl-CoA cholesterol acyltransferases 1 and 2 (ACAT1, ACAT2) (*74*, *81*) or via lecithin-cholesterol acyltransferase (LCAT) (*86*). ACATs synthesize sterol esters by esterifying cholesterols with an acyl-CoA (*81*, *86*). On the other hand, LCAT synthesizes sterol esters by esterifying cholesterol with a fatty acid removed from a cell membrane phospholipid known as phosphatidylcholine (*86*).

Lipid droplet biogenesis begins when TAGs accumulate on the ER membrane. After a concentration threshold, they will separate from the rest of the membrane lipids and form a lipid lens in between the membrane phospholipid leaflets (*74*, *75*, *87*). Lipid droplet biogenesis proteins, such as seipin (*88–90*) and fat storage-inducing transmembrane (FIT) proteins (*81*) are then recruited to the growing lens while TAGs and sterol esters continue to accumulate at the site of the nascent lipid droplet (*75*). This continues until the lipid droplet begins to bud off by changes in the asymmetry of the membrane lipid composition, among other mechanisms that remain to be identified (*74*, *75*). Proteins that are targeted to the lipid droplets are inserted through multiple mechanisms: lateral diffusion along the membrane continuity between the ER and the lipid droplet, insertion through separate membrane bridges that form at specialized ER exit sites or post-translational insertion of cytosolic proteins that contain amphipathic helix domains (*74*, *75*, *81*, *82*, *88*, *91*). Lipid droplets can then either remain bound to the ER or completely bud off.

Lipid droplet degradation

To release free fatty acids, TAGs in the lipid droplets must be converted back into free fatty acids. Lipid droplet breakdown occurs via two processes, neutral lipolysis or lipophagy.

In neutral lipolysis, cytosolic lipases recruited to the lipid droplet surface convert triacylglycerols back into fatty acid directly on the lipid droplet surface. The canonical pathway identified begins with adipose triglyceride lipase (ATGL), which catabolizes triglycerides into diacylglycerols (*92*). Then, other lipases like hormone-sensitive lipase (HSL) and monoacylglycerol lipase (MAGL) metabolize diacylglycerols and

monoacylglycerols respectively into free fatty acids. Recently, non-canonical lipases like DDHD2 have shown to possess triacylglycerol hydrolase activity in the brain (*93*, *94*).

Access of cytosolic lipases to the lipid droplets is regulated by perilipins (*95*–*97*). Perilipins are a family of proteins (PLIN1-5) that are strongly associated with lipid droplets. PLIN2 has been identified in most cell types including astrocytes (*98*). Phosphorylation of PLINs is key to achieve the regulation of lipid metabolism. Phosphorylation of PLIN1and PLIN 5 allow the recruitment of lipases and enhancement of lipase activity (*95*, *97*, *99*), while phosphorylation of PLIN2 by AMPK allows its removal from the lipid droplet surface to facilitate access to lipases (*100*).

Alternatively, lipid droplets can be catabolized by lipophagy (*101*), a process where the cell encapsulates parts of or entire lipid droplets in an autophagosomal membrane which fuses with lysosomes (*101*). In the lysosome, TAG degradation is performed by lysosomal acid lipase (LAL) (*92*, *102*), which also degrades diacylglycerols, monoacylglycerols and sterol esters (*92*, *103*).

Our laboratory discovered a reduction in the number of astrocytic lipid droplets in response to glutamate and that the lipophagic pathway was not involved (*50*). Whether astrocytic lipases on the surface of lipid droplets are activated in response to glutamate has not been investigated. We also found that glutamate increased fatty acid trafficked into the mitochondria (*50*). However, the role of lipid trafficking into the mitochondria during glutamate stimulation is not completely understood.

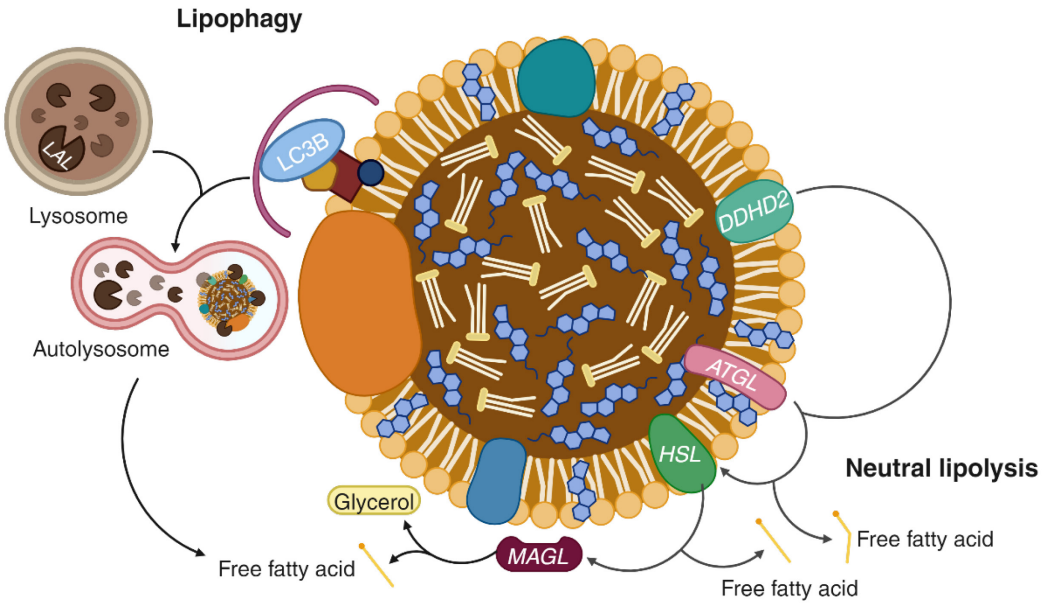

Figure 5. Lipid droplet catabolism.

Lipid droplets are catabolized through lipophagy or neutral lipolysis. Lipophagy uses the autophagic machinery and will engulf parts of or the complete lipid droplet in an autophagic vesicle that will fuse with lysosomes, resulting in the triacylglycerol degradation by action of lysosomal acid lipase and release of free fatty acids. Neutral lipolysis breaks down triacylglycerides by sequentially removing one free acid. LAL, lysosomal acid lipase; LC3B, microtubule-associated proteins 1A/1B light chain 3B; DDHD2, DDHD-domain-containing 2 protein; ATGL, adipose triglyceride lipase; HSL, hormone sensitive-lipase; MAGL, monoacylglycerol lipase. Figure created with BioRender.com.

Astrocyte metabolism and mitochondrial bioenergetics

Mitochondria play an integral role in energy production and are a key hub in signalling pathways that regulate a wide variety of cellular functions like cell death, stress response, metabolic switching, among others (*104*, *105*). Mitochondria synthesize ATP by degrading acetyl-CoA and α-ketoglutarate, products of the degradation of macromolecules such as carbohydrates, lipids, and proteins (Figure 6). This degradation of acetyl-CoA (and α-ketoglutarate) is known as the tricarboxylic acid (TCA) cycle. Degradation of these molecules produces energy that is conserved in the form of electrons transferred to electron carriers like nicotinamide adenine dinucleotide (NAD)

and flavin adenine dinucleotide (FAD). These carriers will eventually cede their electrons to a chain of enzymes that use the transfer of those electrons to produce a proton gradient that will provide the energy necessary to drive ATP synthesis.

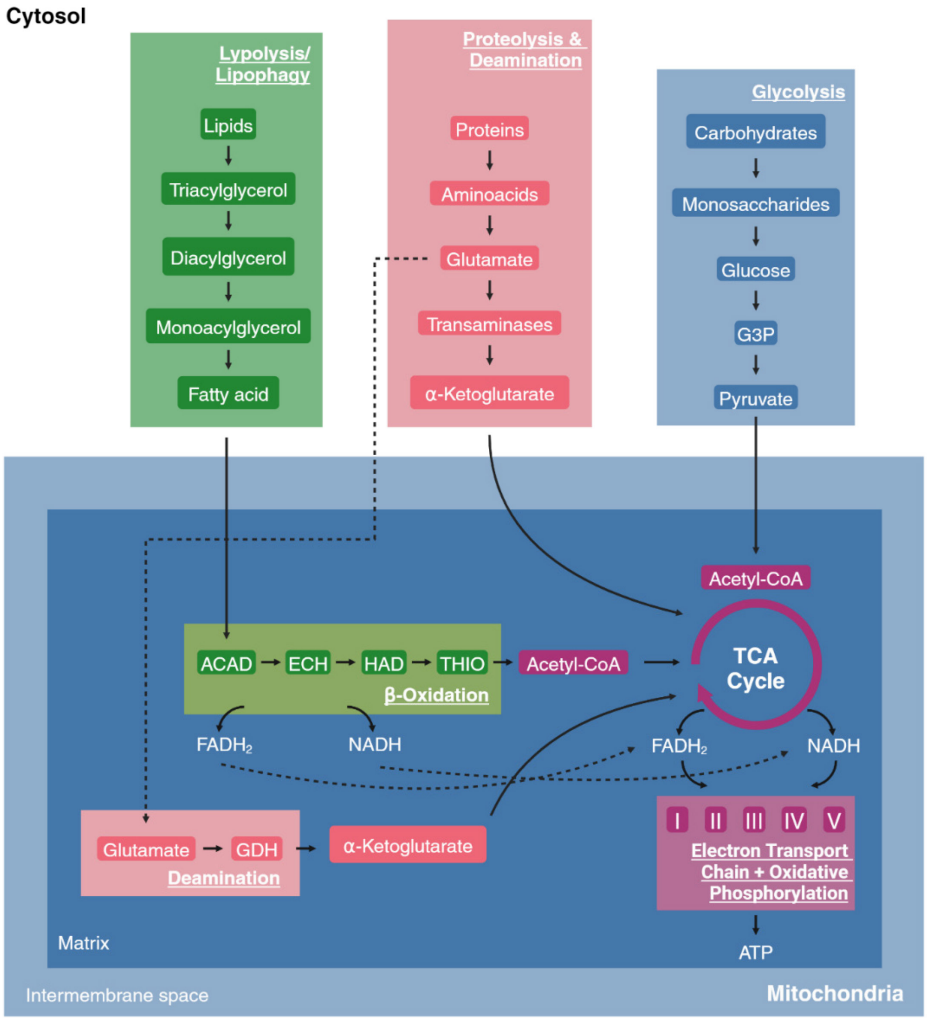

Figure 6. Overview of astrocyte bioenergetic pathways leading to ATP synthesis.

Catabolism of multiple macromolecules result in the formation of metabolic intermediates acetyl-CoA or α-ketoglutarate that enter the tricarboxylic acid cycle. This cycle produces electron carriers whose electrons will be used by the electron transport chain to produce a proton gradient that is necessary for ATP synthesis in a step known as oxidative phosphorylation. G3P, Glucose-3-phosphate; ACAD, acyl-CoA dehydrogenases; ECH, enoyl-CoA hydratases; HAD, 3-hydroxyacyl-CoA dehydrogenase; THIO, thiolases; GDH, glutamate dehydrogenase; I-V, electron transport chain complexes 1-5; NADH, reduced nicotinamide adenine dinucleotide; $FADH_2$, reduced flavin adenine dinucleotide. Figure created with BioRender.com.

Glucose metabolism

Traditionally, astrocytes are considered a glycolytic cell type. As previously mentioned, astrocytes import glucose via glucose transporters (GLUT), mainly through GLUT1. Once imported, glucose is phosphorylated by hexokinase, converting it glucose-6-phosphate (G6P) (*106*) which can enter the glycolysis or the pentose-phosphate pathway (*107*, *108*).

In glycolysis (Figure 7), the first step is the conversion of G6P into fructose-6-phosphate (F6P) via phosphohexose isomerase (*106*, *109*). This step is followed by F6P being phosphorylated by phosphofructokinase to generate fructose 1,6-bisphosphate (F1,6-bisP) (*106*, *109*). In a third step, the enzyme aldolase cleaves F1,6-bisP to produce glyceraldehyde 3-phosphate (Gly3-P) and dihydroxyacetone phosphate (DHAP) (*106*, *109*). Gly3-P is converted to 1,3-bisphosphoglycerate (1,3-bisPG) via glyceraldehyde 3-phosphate dehydrogenase (*106*, *109*). This conversion generates nicotinamide adenine dinucleotide (NAD), a coenzyme that acts electron carrier (*107*, *109*). When the oxidized NAD gains an electron, it becomes NADH, and this electron will be important for a later step in the production of ATP (*107*, *108*).

Next, 1,3-bisPG is dephosphorylated by phosphoglycerate kinase into 3-phosphoglycerate (3-PG) (*106*, *109*). This conversion yields ATP. 3-PG is further dephosphorylated to form 2-phosphogylcerate (2-PG) by phosphoglycerate mutase (*106*, *109*). 2-PG is immediately dehydrated by enolase into phosphoenolpyruvate (PEP) (*106*, *109*). Finally, PEP is phosphorylated by pyruvate kinase into pyruvate (*106*, *107*, *109*). This conversion also yields ATP (*106*, *109*).

Pyruvate can then follow one of the following routes: a) it can enter the mitochondria via pyruvate carriers to be converted into acetyl CoA by pyruvate dehydrogenase (*107*–*109*) and participate in the tricarboxylic acid cycle (TCA cycle) or, 2) be converted into lactate via lactate dehydrogenase (LDH) (*42*, *110*). If pyruvate is directed into the mitochondria for further processing and higher ATP yield, this process is known as aerobic glycolysis; instead, if pyruvate is directed towards lactate formation, this process is then known as anaerobic glycolysis.

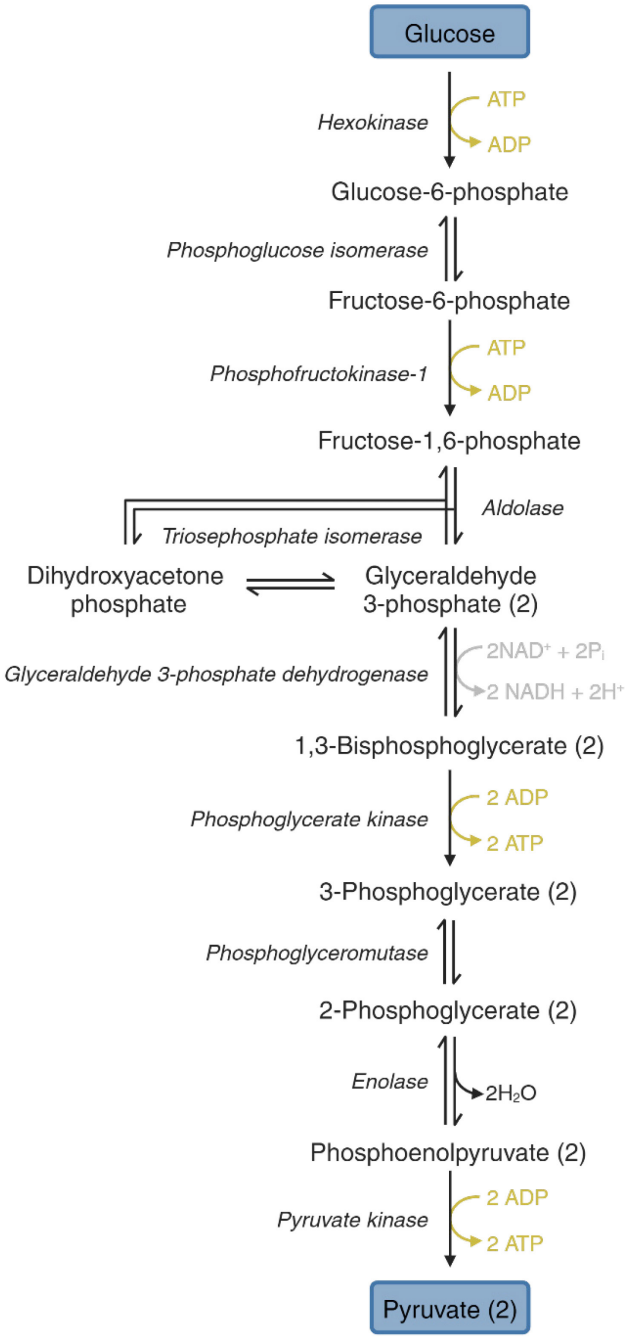

Figure 7. The glycolysis pathway.

Glucose, in a series of enzymatic reactions, is catabolized into two molecules of pyruvate. This pathway yields 2 net ATP molecules as well as electron carrier NADH. ATP, adenosine triphosphate; ADP, adenosine diphosphate; NAD, nicotinamide adenine dinucleotide; NADH, reduced nicotinamide adenine dinucleotide; FAD, flavin adenine dinucleotide; $FADH_2$, reduced flavin adenine dinucleotide. Figure created with BioRender.com.

The astrocyte-neuron lactate shuttle hypothesis (Figure 2) proposes that, in response to neuronal activity, astrocytes favor anaerobic glycolysis, where they convert pyruvate into lactate via LDH5 (*4*, *42*). Lactate is then released to the extracellular media by astrocyte specific monocarboxylate transporters 1 and 4 (MCT1, MCT4) and taken up by surrounding neurons via MCT2 (*37*, *42*, *111*). In neurons, LDH1 is the main LDH isoform, and, in opposition to astrocytic LDH5, LDH1 converts lactate back into pyruvate (*42*, *112*). Neurons then use this lactate-derived pyruvate to fuel oxidative metabolism during activity (*41*, *113*). However, this hypothesis is currently under debate, as recent research has shown that lactate formation in astrocytes can also be derived from pyruvate that comes from glutamate metabolism and not glycolysis (*114–116*). Others have also shown that neurons seem to prefer glucose over lactate for energy (*117–120*).

Astrocytes also utilize the pentose-phosphate pathway (*121*), assisting in neutralizing reactive oxygen species and in nucleotide synthesis. This pathway is split in two phases: an oxidative and a nonoxidative phase (Figure 8). In the oxidative phase, G6P is oxidized via glucose 6-phosphate dehydrogenase (G6-PDH) into 6-phosphoglucono-δ-lactone and NADPH is formed (*107–109*). This NADPH is key to reducing glutathione (GSH) from oxidized glutathione (GSSG) via glutathione reductase. This is crucial for astrocytes, as they release GSH as well as glutathione precursors cysteinyl-glycine and γ-glutamyl-cysteine, which are taken up by neurons and used to neutralize reactive oxygen species (*122–125*). 6-phosphoglucono-δ-lactone is hydrolysed by lactonase to produce 6-phosphogluconate. In turn, 6-phosphogluconate is converted into ribulose 5-phosphate (R5P) via 6-phosphogluconate dehydrogenase (*107–109*). This reaction produces one more NADPH as well as CO_2. R5P then enters the nonoxidative phase of the pathway. Here, R5P is isomerized either into ribose-5-phosphate which is then used for nucleotide biosynthesis or into xylulose 5-phosphate (X5P) (*107–109*). X5P can then be converted into glyceraldehyde-3-phosphate and fructose-6-phosphate (F6P), with the latter being able to isomerize back to G6P (*107–109*). Both metabolites can then be fueled back into the glycolysis pathway.

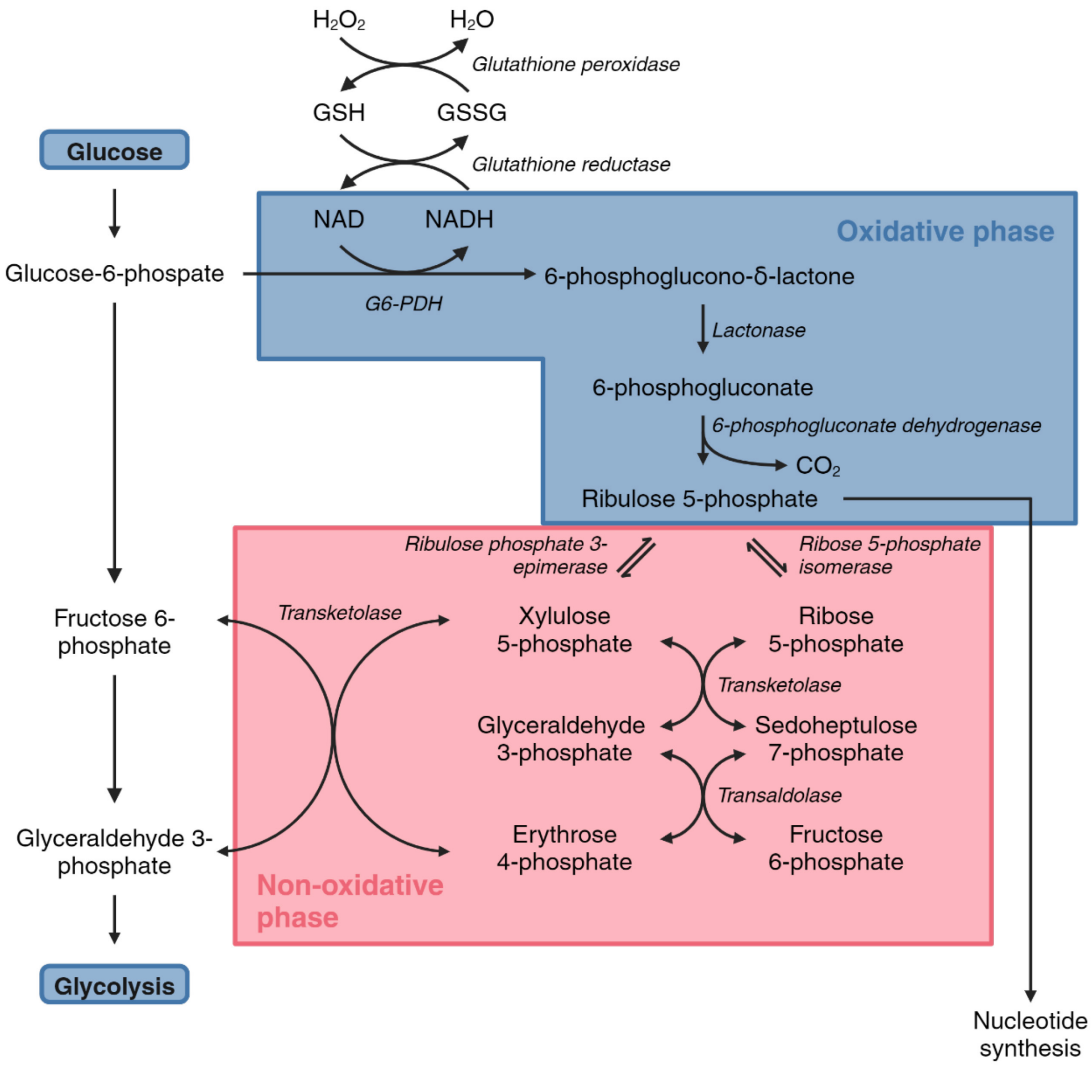

Figure 8. The pentose-phosphate pathway and its two phases: oxidative and non-oxidative phase.

The pentose-phosphate pathway role is to regenerate NADH that is then used to aid in the neutralization of damaging reactive oxygen species as well as producing ribulose-5-phosphate which can be directed towards producing nucleotides needed for DNA replication and transcription. This pathway is intertwined with glycolytic activity, as it diverts glucose-6-phosphate, an immediate metabolite of glycolysis. If no nucleotide synthesis is needed, ribulose-5-phospohate undergoes the non-oxidative phase and is reintegrated into glycolysis. GSH, glutathione; GSSG, oxidized glutathione; NAD, nicotinamide adenine dinucleotide; NADH, reduced nicotinamide adenine dinucleotide; G6-PDH, glucose 6-phosphate dehydrogenase. *Figure created with BioRender.com.*

When excess glucose is available, astrocytes store it as glycogen (*126*). Glycogen is made from many glucose molecules joined together to form a branched structure through a process called glycogenesis. In this process, G6P is converted into glucose-1-phosphate (G1P) by phosphoglucomutase (*107–109*). Then, G1P is converted into uridine diphosphate glucose (UDP-glucose) by the action of the enzyme UDP-glucose pyro phosphorylase (*107–109*). This process is initiated by glycogenin, an enzyme needed to create the initial short glycogen chains (*107*). Once glycogen chains are established, they are lengthened by the addition of UDP-glucose by glycogen synthase and branched by glycogen branching enzyme (*109*).

In periods of high neuronal activity, astrocytes quickly break down glycogen back into G6P in a process known as glycogenolysis (*127*, *128*). In this process, phosphorylase cleaves the terminal glucose in a glycogen branch, releasing G1P, which is then converted into G6P that enters glycolytic pathway. Astrocytic glycogen reserves are mainly located in processes with high synaptic density (*126–129*).

Mitochondrial metabolism: tricarboxylic acid cycle, electron transport chain and oxidative phosphorylation

In astrocytes, glucose metabolism is a major source of energy for astrocyte in periods of high neuronal activity (*40*, *44*, *45*, *130*). However, there is accumulating evidence showing that astrocytes use mitochondrial metabolism for ATP production (*116*, *131*, *132*). Alteration of mitochondrial metabolism in astrocytes can induce alterations in brain function resembling Alzheimer's disease, such as memory impairment, changes in synaptic activity and astrocyte reactivity (*133*). This shows the importance of astrocyte mitochondrial metabolism.

To synthesize ATP in the mitochondria, acetyl-CoA and α-ketoglutarate, products of the degradation of macromolecules like glucose, glutamate, or fatty acids, must go trough further degradation in the TCA cycle (Figure 9). In this cycle, the breakdown of these products results in the transfer of the energy released by their degradation to electron carriers NAD and FAD (*134*). These electron carriers release electrons that are transported through the electron transport chain (ETC) in the inner mitochondrial

membrane (*134*). As the electrons go through the complexes of the ETC, they provide the energy necessary to generate a mitochondrial membrane potential that is then used to drive ATP synthesis (*134*). This process requires the presence of oxygen, hence the name oxidative phosphorylation (OXPHOS). Recent research shows that astrocytes degrade all the main groups of macromolecules and fuel the resulting acetyl-CoA and α-ketoglutarate into the TCA cycle (*135*–*138*). Thus, in the next sections, we will look at how each degradation product will be metabolized in the mitochondria.

Pyruvate from glycolysis is actively transported into the mitochondrial matrix via the mitochondrial pyruvate carrier 1 (MPC1) (*139*). Once in the matrix, pyruvate is converted into acetyl-CoA by pyruvate dehydrogenase (PDH) (*109*, *134*, *140*). This step generates NADH as well as CO_2. Acetyl-CoA is then combined with oxaloacetate (OAA) to generate citrate by citrate synthase, followed by the isomerization of citrate into isocitrate via the aconitase enzyme (*109*, *134*, *140*). The cycle continues by converting the isocitrate into α-ketoglutarate (α-KG) by isocitrate dehydrogenase, yielding NADH and CO_2 (*109*). Next, α-ketoglutarate dehydrogenase transforms α-KG into succinyl-CoA, also yielding CO_2 and NADH (*109*). Later, succinyl-CoA is converted into succinate by action of succinyl-CoA synthase, generating guanosine triphosphate (GTP) (*109*, *134*). Succinate is then oxidized by succinate dehydrogenase (SDH) into fumarate, yielding $FADH_2$ (*109*, *134*, *140*). Importantly, succinate dehydrogenase also forms part of the ETC (*140*). Immediately, fumarate gets converted into malate via fumarase, followed by the conversion of malate into OAA via malate dehydrogenase (MDH) (*109*, *134*). The cycle continues with the entry of new acetyl-CoA repeat the TCA cycle.

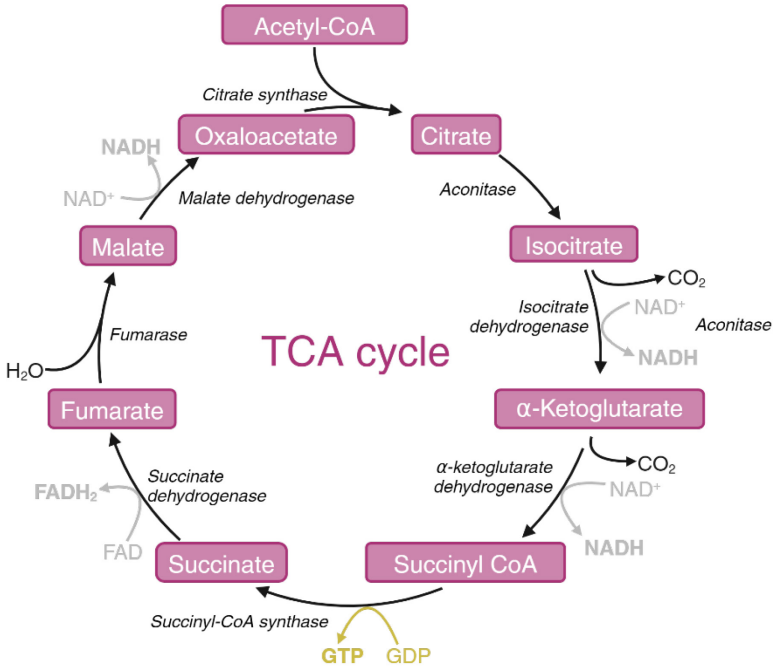

Figure 9. The tricarboxylic acid cycle.

Depiction of the TCA cycle. Acetyl-CoA or α-ketoglutarate enter (α-ketoglutarate entry not shown) this cycle and are degraded, loosing carbons along the way, and generating electron carriers NADH and $FADH_2$ that are necessary for ATP synthesis. NAD, nicotinamide adenine dinucleotide; NADH, reduced nicotinamide adenine dinucleotide; GDP, guanosine diphosphate; GTP, guanosine triphosphate; FAD, flavin adenine dinucleotide; $FADH_2$, reduced flavin adenine dinucleotide. Figure created with BioRender.com.

From a perspective of energy production, the TCA cycle generates electrons that are transferred to electron carriers NAD and FAD, becoming NADH and $FADH_2$ respectively (*141*, *142*). The ETC is a set of redox reactions that involve the oxidation of NADH and $FADH_2$ and the transport of those electrons through enzyme complexes (Figure 10) (*141*). These complexes use the energy provided by the electron transport to then transport protons across the inner mitochondrial membrane and into the intermembrane space to generate an electrochemical gradient which provides the energy necessary to synthesize ATP (*141*, *142*).

The ETC consists of 5 complexes linked to each other by the electron carriers ubiquinone (Q) and cytochrome C (*109*, *143*). There are two paths for electron transport in the ETC: Complex I/III/IV, with NADH being the electron donor (*141*), and complex II/III/IV (*144*), with $FADH_2$ instead being the electron donor.

In complex I, also known as NADH-ubiquinone oxidoreductase, NADH transfers electrons to ubiquinone via a flavin mononucleotide (FMN) (*107*, *109*, *142*). FMN receives a pair of electrons from NADH to form $FMNH_2$ (*142*, *145*). The electrons are then passed into an iron/sulphur cluster and then onto ubiquinone (Q), which is reduced to ubiquinol (QH_2) (*142*, *146*). This transfer of electrons powers the relocation of 4 protons through complex I from the mitochondrial matrix to the intermembrane space (*142*). On the other hand, $FADH_2$ transfers its electrons to Complex II (*109*, *140*, *147*). Complex II is also known as SDH, which is part of the Krebs cycle. $FADH_2$ donates its electrons to another iron/sulphur cluster (just as in complex I) (*142*, *145*) which then transfer these two electrons to Q, reducing it to QH_2. Unlike complex I, complex II does not pump protons (*142*, *147*).

QH_2 then travels across the inner mitochondrial membrane where it reaches complex III, also known as coenzyme Q-cytochrome c reductase (*142*, *144*, *146*). Here, QH_2 is oxidized into ubisemiquinone (QH^-), and transfers an electron to another iron/sulphur cluster while releasing two protons into the intermembrane space (*142*, *144*, *146*). The iron/sulphur cluster then transfers this electron into cytochrome C_1, while the other electron is used to regenerate QH^- to Q (*142*). Accompanying these events, the iron/sulphur cluster transfers one electron onto cytochrome C_1, which then transfers it to cytochrome C (*142*, *145*, *146*).

Cytochrome C then transports electrons into complex IV, also known as cytochrome c oxidase (*142*, *148*). In complex IV, cytochrome C transfers electrons to the terminal electron acceptor O_2 which is reduced to water, resulting in a net total of two protons pumped by complex IV (*142*, *145*, *148*, *149*).

The protons pumped by complex I, III and IV generate an electrochemical gradient (*142*, *145*, *148*). This occurs as protons accumulate in the intermembrane space making this side of inner mitochondrial membrane positively charged relative to the side facing the

matrix (*109*, *142*). This electrochemical gradient is used by complex V to synthesize ATP. Complex V, also known as F_1F_0 ATP synthase, is responsible for the synthesis of ATP and consists of two domains: F_1 and F_0 (*145*, *146*, *148*, *149*). To synthesize ATP, protons pass through the F0 domain from the intermembrane space towards the matrix. This transfers the energy stored in the electrochemical gradient to the F1 domain. This energy is then used to phosphorylate ADP into ATP.

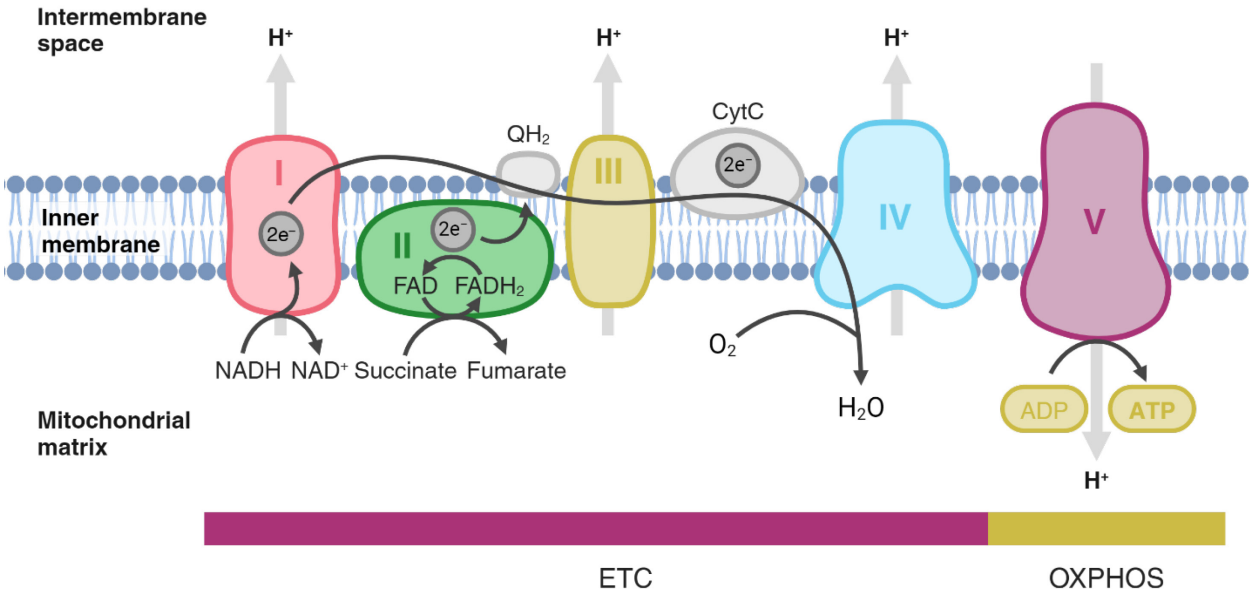

Figure 10. The electron transport chain and oxidative phosphorylation.

The ETC uses the flow of electrons provided by electron carriers NADH and $FADH_2$ to generate an electrochemical proton gradient. The proton gradient is created by the transport of protons from the mitochondrial matrix to the intermembrane space by the activity of mitochondrial complexes I, III and IV. This flow of protons towards the mitochondrial matrix induced by the formation of the gradient is then used by complex V to synthesize ATP. NAD, nicotinamide adenine dinucleotide; NADH, reduced nicotinamide adenine dinucleotide; FAD, flavin adenine dinucleotide; $FADH_2$, reduced flavin adenine dinucleotide; QH_2, ubiquinol; CytC, cytochrome C; *ATP, adenosine triphosphate; ADP, adenosine diphosphate; ETC, electron transport chain; OXPHOS, oxidative phosphorylation. Figure created with BioRender.com.*

One of the consequences of electron transport during the ETC is the generation of reactive oxygen species (ROS) which are generated when electrons leak from the ETC (*142*, *145*, *150*). This causes the reduction of oxygen into superoxide (O_2^-). O_2^- is

chemically unstable, and can cause direct damage to proteins, lipids, and DNA. The ETC has seven main sites where electrons can escape and generate ROS (*142*, *145*).

ROS can function as secondary messengers that regulate multiple cellular pathways (*140*). For example, in normal physiology, ROS has been shown to modulate the instability and failure of the mitochondrial network in cardiac cells (*151*). Physiological ROS target peroxiredoxin proteins, which then oxidize of a further set of effector proteins like Tpx1 (*152*). These effector proteins change their function and induce the expression of transcription factors like Pap1 (*152*–*154*). ROS have also been shown to be key in the induction of gene transcription in hypoxia (*105*). In the case of astrocytes, mitochondrial ROS are critical in the modulation of astrocyte glucose metabolism and coordinating antioxidant defense for neurons, as recent research showed that, at physiological level, astrocytic mitochondrial ROS supress the pentose phosphate pathway and attenuates release of extracellular ROS release (*121*). Moreover, decreased mitochondrial ROS in astrocytes lead to neuronal degeneration and alterations in cognition (*121*).

Conversely, excess ROS results in oxidative stress which can similarly lead to neurodegeneration (*155*, *156*). Therefore, ROS homeostasis needs to be tightly regulated (*142*, *157*) and as such, cells possess antioxidant systems such as superoxide dismutase, glutathione and the thioredoxin/peroxiredoxin systems, among others (*155*).

Amino acid metabolism

Amino acid degradation products can also participate in the TCA cycle for ATP synthesis. After transporting glutamate into the astrocyte via EAAT1 and EAAT2, glutamate can follow two pathways (Figure 11): a) conversion of glutamate to glutamine by glutamine synthetase (GS) and eventual glutamine release, or b) converted to α-KG and take part in the TCA cycle (*116*, *158*, *159*).

The first pathway is straightforward, as GS converts glutamate to glutamine in the cytosol (*20*, *160*). This reaction needs ATP and NH_4^+. As described in previous sections, glutamine is then exported to neurons. In the second pathway, glutamate is transported into the mitochondria via glutamate carrier 1 (GC1) or by the glutamate/aspartate exchanger (Aralar) (*161*–*163*). Once in the mitochondria, multiple enzymes can convert

glutamate into α-KG. Glutamate can be converted into α-KG via glutamate dehydrogenase or mitochondrial aminotransferases (*19*, *158*, *159*, *164*). Branched-chain aminotransferase (BCAT), aspartate aminotransferase (AAT) or alanine aminotransferase (ALT) are the enzymes that have been identified to perform this conversion (*159*, *165*), although AAT is the enzyme that contributes the most in this conversion (*166*).

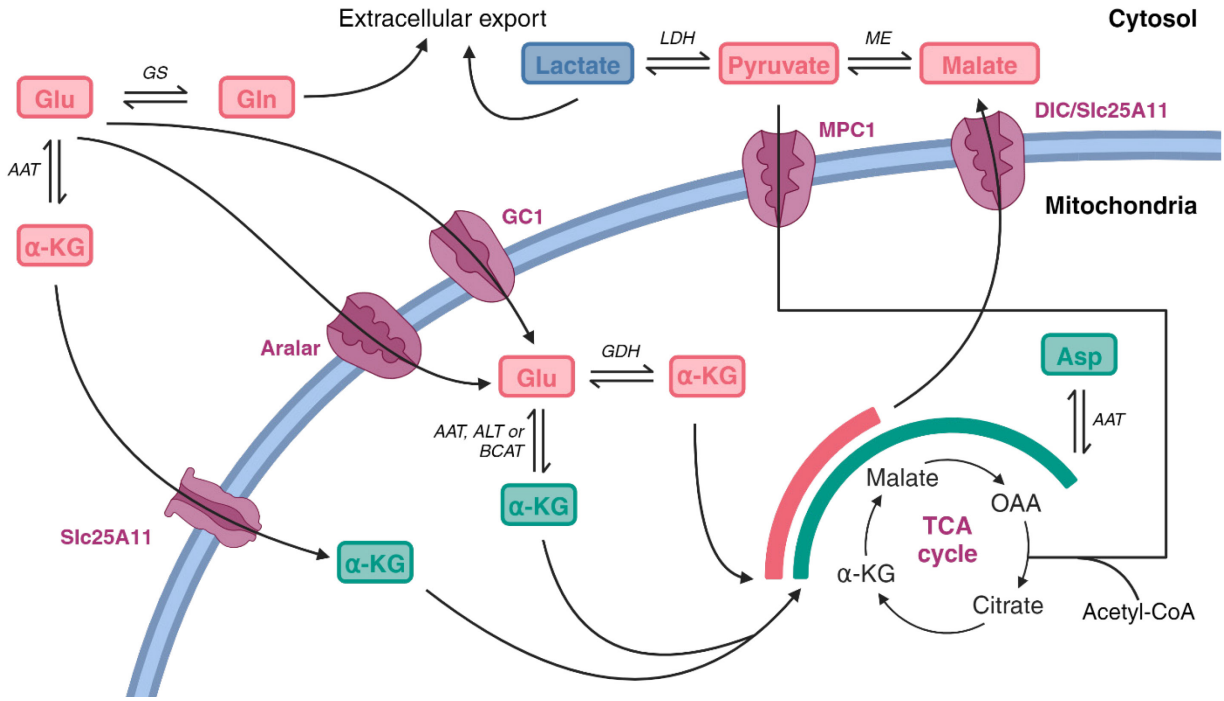

Figure 11. Glutamate metabolism in astrocytes.

Glutamate in astrocytes can follow multiple metabolic pathways: conversion into glutamine by GS or conversion of glutamate into α-KG to participate TCA cycle. Glutamate processing by aminotransferases results in α-KG leaving as OAA. Processing by GDH on the other hand, results in α-KG leaving as malate. Malate is then converted into pyruvate by malic enzyme and the can either be exported or re-enter the TCA for further oxidation. Glu, glutamate; Gln, glutamine; α-KG, α-ketoglutarate; GC1, glutamate carrier 1; Aralar, glutamate/aspartate exchanger; Slc25A11, solute carrier family 25 member 11 protein or mitochondrial 2-oxoglutarate/malate carrier protein; DIC, mitochondrial dicarboxylate carrier; MPC1, mitochondrial pyruvate carrier 1; GS, glutamine synthetase; AAT, aspartate aminotransferase; ALT, alanine aminotransferase; BCAT, branched-chain aminotransferase; GDH, glutamate dehydrogenase; ME, malic enzyme; LDH, lactate dehydrogenase; Asp, aspartate. Figure created with BioRender.com.

Once converted, α-KG enters the TCA cycle. Alternatively, glutamate can also be converted into α-KG in the cytosol by cytosolic AAT and be transported into the mitochondria by the solute carrier family 25 member 11 protein (Slc25A11, also known as the mitochondrial 2-oxoglutarate/malate carrier protein) (*163*).

α-KG derived from aminotransferases leaves the TCA cycle as OAA (Figure 11, teal α-KG box). OAA is then used again by AAT but for production of aspartate instead, which is then used for other metabolic processes (*19*, *167*). Yet, glutamate derived from GDH (Figure 11, pink α-KG box) leaves the TCA cycle as malate (*168*–*170*). Malate will then be metabolized by the malic enzyme (ME), forming pyruvate (*167*, *168*). Pyruvate can either be exported as lactate or re-enter the TCA, undergoing further oxidation (*167*, *168*).

In this point its important to reiterate that although most consider astrocytes a glycolytic cell type, research in glutamate metabolism, and more recently in lipid metabolism, show that astrocytes metabolize other fuels for energy production (*135*, *137*).

Lipid metabolism

Astrocytes can also catabolize lipids for ATP synthesis. Astrocytes can transport fatty acids into the mitochondria (*50*), and this transport is dependent on the chain length of the fatty acids. SCFA and some MCFA can freely diffuse into the mitochondria (*65*–*70*). Once inside the mitochondria, they are trapped via acylation by ACSS/ACSM (*76*). However, LCFA need to be transported into the mitochondria. This transport is mediated by carnitine-palmitoyl transferase 1 (CPT-1), which preferentially transports fatty acids from C:6 and up to C:18 (*77*, *171*–*173*). CPT-1 acts by converting long-chain acyl-CoA to a long-chain acylcarnitine and transport it across the outer mitochondrial membrane (*174*, *175*). Once in the intermembrane space, acylcarnitines are transported across the inner mitochondrial membrane via carnitine/acylcarnitine translocase (CACT) (*176*). Once in the matrix, the long-chain acyl-CoA is then converted back into a long-chain acyl-CoA by carnitine-palmitoyl transferase 2 (CPT-2) (*174*).

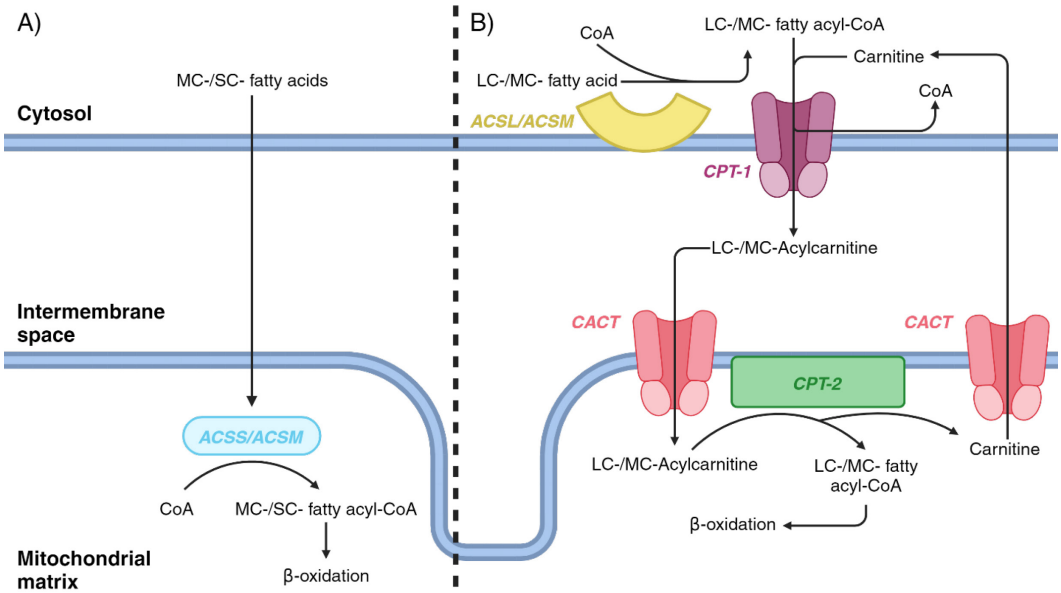

Figure 12. Transport of fatty acids into the mitochondria.

A) *SCFA and some MCFA diffuse freely across the mitochondrial membranes and are only retained in the organelle through the activation of the fatty acid by its corresponding ACS.* ***B)*** *LCFA are transported into the mitochondria in a carnitine-dependent manner and by using CPT-1, a LCFA transporter. CoA, Coenzyme A; CPT-1/2, carnitine-palmitoyl transferase 1/2; CACT, carnitine/acylcarnitine translocase; ACSS, short-chain acyl-CoA synthetases; ACSM, medium-chain acyl-CoA synthetases. Figure created with BioRender.com.*

Fatty acid acyl chains are broken down in a process known as β-oxidation (Figure 13). β-oxidation is a cycle that involves a set of chain length-specific enzymes that shorten fatty acids by removing two carbons from the hydrocarbon chain per cycle to generate acetyl-CoA, which goes into the TCA cycle (*175*, *177*). β-oxidation also generates $FADH_2$ that is used in the ETC for ATP synthesis (*178–180*).

β-oxidation occurs both in the mitochondria and in the peroxisome, another cellular organelle (*181–183*). However, they differ in the type of fatty acids they process. SCFA, MCFA, and LCFA are processed in the mitochondria while VLCFA, and branched-chain fatty acids undergo β-oxidation in the peroxisomes (*174*, *181–185*). We will focus on mitochondrial β-oxidation, which occurs in the mitochondrial matrix.

β-oxidation consists of four steps: oxidation, hydration, a second oxidation and thiolysis (*67*, *175*, *180*). In the first step, the fatty acyl-CoA is dehydrogenated by an acyl-CoA dehydrogenase producing a trans-2-Enoyl-CoA (*107*, *109*, *177–179*). This step also generates $FADH_2$, used in the ETC. In a second step, an enoyl-CoA hydratase hydrates the trans-2-enoyl-CoA and produces a (S)-3-hydroxyacyl-CoA (*107*, *109*, *177*, *180*). Third, the (S)-3-hydroxyacyl-CoA is transformed into a 3-ketoacyl-CoA by a (S)-3-hydroxyacyl-CoA dehydrogenase (*107*, *109*, *180*). This step also generates NADH used in the ETC. In the fourth and last step, 3-ketoacyl-CoA thiolase cleaves 3-ketoacyl-CoA into a shortened fatty acyl-CoA and an acetyl-CoA (*107*, *109*, *180*). The acetyl-CoA then enters the TCA cycle while the shortened fatty acyl-CoA is ready to undergo another cycle of β-oxidation (*107*, *109*, *180*).

As mentioned before, enzymes responsible for fatty acid catabolism are highly selective for chain length. For example, for acyl-CoA dehydrogenases there is a very-long-chain acyl-CoA dehydrogenase (VLCAD), a long-chain acyl-CoA dehydrogenase (LCAD), a medium-chain acyl-CoA dehydrogenase (MCAD) and a short-chain acyl-CoA dehydrogenase (SCAD) (*175*, *177*). The same principle applies to enoyl-CoA hydratases, where we can find long-chain enoyl-CoA hydratase (LCEH) and crotonase (short-chain enoyl-CoA hydratase, SCEH) (*175*, *177*); (S)-3-hydroxyacyl-CoA dehydrogenases where we find a long-chain (S)-3-hydroxyacyl-CoA dehydrogenase (LCHAD), a medium-chain (S)-3-hydroxyacyl-CoA (MCHAD), and a short-chain acyl-CoA dehydrogenase (SCHAD) (*175*, *177*); and finally, the 3-ketoacyl-CoA thiolases where we find a long-chain 3-ketoacyl-CoA thiolase (LCKAT) and a medium-chain 3-ketoacyl-CoA thiolase (MCKAT) (*175*, *177*).

In the mitochondria, these enzymes have different localization. LCEH, LCHAD, and LKAT form a complex known as the mitochondrial trifunctional protein (MTP) while VLCAD exists on its own (*178*, *179*). They are both bound to the matrix-facing side of the inner mitochondrial membrane. On the other hand, MCAD, SCAD, crotonase, SCHAD and MCKAT are in the lumen of the mitochondrial matrix (*178*, *179*).

Using the example of β-oxidation of a long-chain fatty acid, the process would be as follows: initial rounds of β-oxidation (depending on the chain length), the long-chain fatty

acid will be processed by membrane-bound VLCAD and/or MTP. Once enough carbons have been removed to be considered a medium-chain fatty acid, β-oxidation will proceed in the mitochondrial matrix first through MCAD, crotonase, MCHAD, and MCKAT. Once its a short-chain fatty acid, β-oxidation will be performed by SCAD, crotonase, SCHAD and MCKAT.

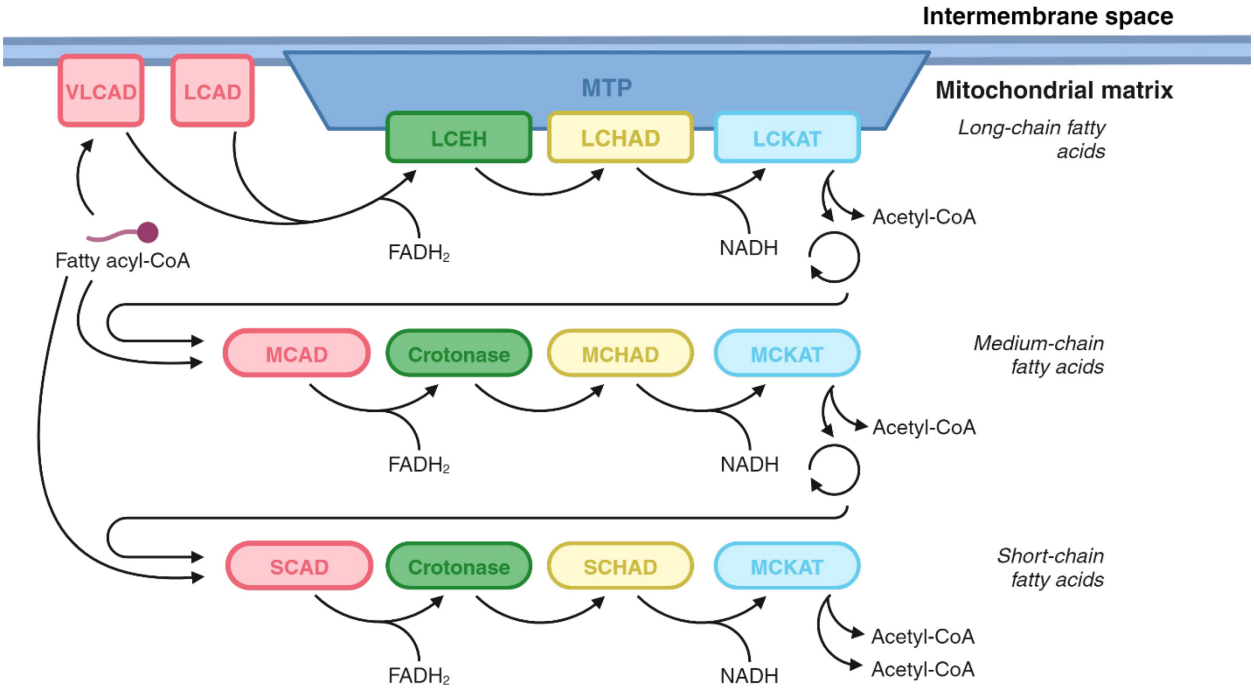

Figure 13. Mitochondrial β-oxidation of fatty acids.

B-oxidation occurs in the mitochondrial matrix. Each round of beta oxidation results in one acetyl-CoA, one FADH2, and one NADH. The acetyl-CoA can then enter the TCA cycle while NADH and FADH donate their electrons to the ETC to allow OXPHOS. VLCAD, very-long-chain acyl-CoA dehydrogenase; LCAD, long-chain acyl-CoA dehydrogenase; long-chain enoyl-CoA hydratase; LCHAD, long-chain (S)-3-hydroxyacyl-CoA dehydrogenase; LCKAT, long-chain 3-ketoacyl-CoA thiolase; MCAD, medium-chain acyl-CoA dehydrogenase; MCHAD, medium-chain (S)-3-hydroxyacyl-CoA; MCKAT, medium-chain 3-ketoacyl-CoA thiolase; SCAD, short-chain acyl-CoA dehydrogenase; SCHAD, short-chain acyl-CoA dehydrogenase; $FADH_2$, reduced flavin adenine dinucleotide; NADH, reduced nicotinamide adenine dinucleotide. Figure created with BioRender.com.

All the information previously presented only apply if the fatty acids are saturated fatty acids; that is, lacking double bonds between carbons in the acyl chain. β-oxidation of

mono and polyunsaturated fatty acids, those with double bonds, require a set of auxiliary enzymes: 2,4-dienoyl-CoA reductase (DECR), the Δ3,5-Δ2,4-dienoyl-CoA isomerase, and the Δ3, Δ2-enoyl-CoA isomerase (ECI) (*107*, *175*). For brevity, we will not review the modified β-oxidation of these fatty acids. But we will mention that this set of auxiliary enzymes reduce and isomerize mono and polyunsaturated fatty acids in their double bonds to the trans-configuration, which grants the re-entrance of the now trans-2-enoyl-CoA into the β-oxidation cycle (*107*, *175*).

Astrocyte lipid metabolism is relevant for regulation of glucose metabolism (*121*), ROS production and signalling (*121*), induction of astrocyte reactivity (*186*), generation of neurotoxic lipid species (*187–189*) and production of hydroxybutyrate, a metabolite that also supports neuronal activity (*190*). However, much remains unknown regarding the role and regulation of mitochondrial fatty acid metabolism in astrocytes.

Regulation of astrocyte bioenergetics and mitochondrial metabolism

AMP-activated protein kinase (AMPK) is an enzyme that is considered the master regulator of the cellular energy metabolism and homeostasis. Its phosphorylation leads to the up regulation or down regulation of multiple metabolic pathways (Figure 14) that dramatically affect cellular metabolism (*191–193*).

Moreover, AMPK phosphorylation acts as a switch in the activity of metabolic pathways and depends on cellular energy requirements. For example, when nutrients are abundant, AMPK is dephosphorylated, inducing an upregulation of anabolic pathways that increase ATP consumption but leads to the synthesis of multiple relevant macromolecules necessary for cell function (*192–195*). On the other hand, when nutrient availability is scarce, AMPK is phosphorylated, resulting in upregulation of catabolic pathways that will sustain ATP production (*192–195*).

AMPK is a heterotrimeric complex consisting in three subunits: 1) catalytic α-subunit, 2) a regulatory β-subunits and, 3) a regulatory γ-subunit (*194*, *195*). α- and β-subunits posses two isoforms, while the γ-subunit has three (*194*). This suggests that AMPK can potentially have twelve different conformations(*194*, *195*). However, whether these

different conformations result in differential localization, specificity and effects is a matter of debate.

AMPK α-subunit is responsible for its kinase activity and contains the Thr172 phosphorylation site required for this kinase activity (*194*). Adenosine monophosphate (AMP) or adenosine diphosphate (ADP) are important allosteric modulators of AMPK kinase activity, as they bind to the γ-subunit, while ATP on the hand acts as a competitive inhibitor (*194*). AMPK's ability to bind ATP, ADP and AMP allows it can sense the energetic state of the cell (*193*). AMPK not only responds to the energetic state of the cell, but is also modulated by other processes like overnutrition, obesity, inflammation, exercise, ageing, caloric restriction, circadian rhythms, and calcium cell signalling (*195*).

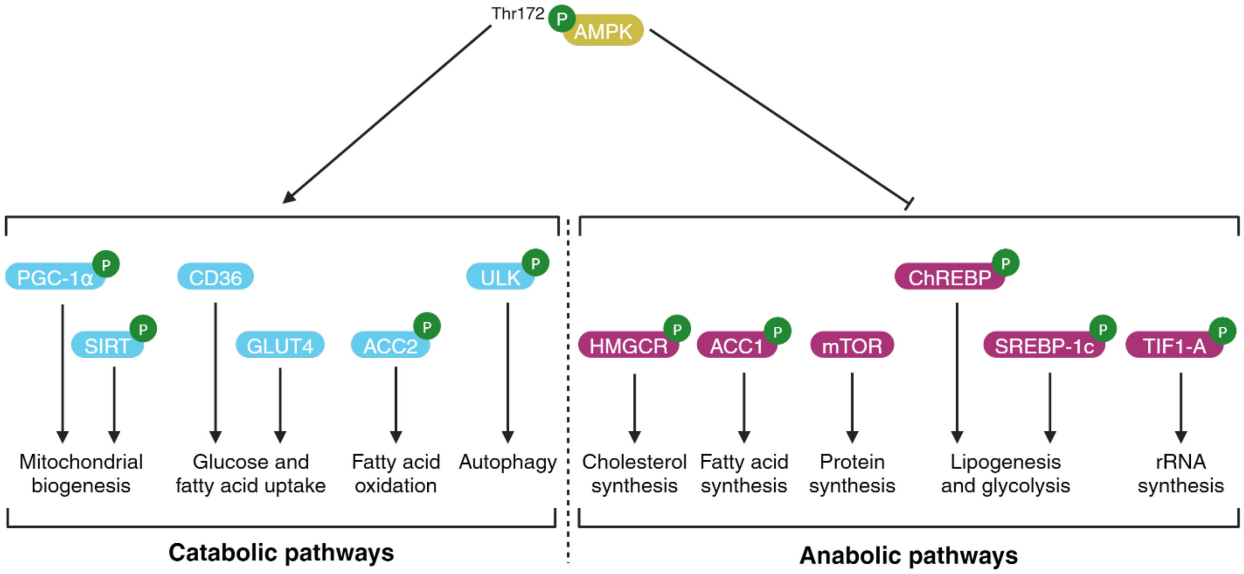

Figure 14. AMPK acts as a master regulator of cell metabolism.

Phosphorylation of AMPK α-subunit at Thr172 is required for its kinase activity. Although AMPK is able to regulate multiple metabolic pathways, its action can be differentiated in two main effects: AMPK phosphorylation upregulates catabolic pathways while inhibiting anabolic pathways to sustain ATP synthesis. PGC1α, peroxisome proliferator-activated receptor-gamma coactivator 1-alpha; SIRT, sirtuins; CD36, fatty acid translocase; GLUT4, glucose transporter 4; ACC2, acetyl-CoA carboxylase 2; ULK, Unc-51-like kinase 1; HMGCR, 3-hydroxy-3-methyl-glutaryl-coenzyme A reductase or HMG-CoA reductase; ACC1, acetyl-CoA carboxylase 2; mTOR, mammalian target of rapamycin; ChREBP, carbohydrate-responsive element-binding protein; SREBP-1c, sterol regulatory element-binding protein 1; TIF1-A, transcriptional intermediary factor 1α. Figure created with BioRender.com.

AMPK's effect on metabolism can be broadly categorized in two main effects: the downregulation of anabolic pathways and the upregulation of catabolic pathways. AMPK downregulates anabolic pathways by inhibiting glycogen storage by glycogen synthase, inhibiting ribosomal biogenesis by acting on Transcription Intermediary Factor 1-Alpha, as well as inhibiting fatty acid and sterol synthesis affecting sterol regulatory element-binding protein 1 (SREBP1), carbohydrate-responsive element-binding protein (ChREBP), HMG-CoA reductase (HMGCR) and ACC1 (*191*, *192*, *195*). AMPK can upregulate catabolic pathways such as β-oxidation by promoting transport of fatty acids into the mitochondria via ACC2, increasing lipolysis by targeting ATGL, inducing mitochondrial biogenesis through PGC1α, and increasing glucose uptake and glycolysis by affecting GLUT1, GLUT4, or PFKFB3 (*191*, *192*, *195–197*). As we can see from these examples, AMPK activity regulates numerous pathways involved in glucose metabolism, lipid metabolism and protein synthesis (*191–195*). AMPK has also been shown to affect autophagy, mitochondrial homeostasis, DNA damage, DNA repair and lysosomal homeostasis (*192*, *194*, *195*).

Focusing on lipid metabolism, AMPK phosphorylation targets downstream acetyl-CoA-carboxylase 1 and 2 (ACC1, ACC2) (*191*, *195*). ACC catalyzes the conversion of acetyl-CoA into malonyl-CoA. Malonyl-CoA from ACC2 inhibits carnitine palmitoyl transferase 1 (CPT-1), the main transporter of LCFA into the mitochondria for β-oxidation (*191*, *198*). Phosphorylation of ACC2 by AMPK blocks ACC2 activity (Figure 15), resulting in decreased malonyl-CoA and thereby increasing fatty acid transport into the mitochondria (*198*, *199*). On the other hand, ACC1 acts as the rate-limiting step in the synthesis of fatty acids, since phosphorylation of ACC1 by AMPK stops ACC1 from providing the malonyl-CoA necessary for de novo fatty acid synthesis (*198*, *199*).

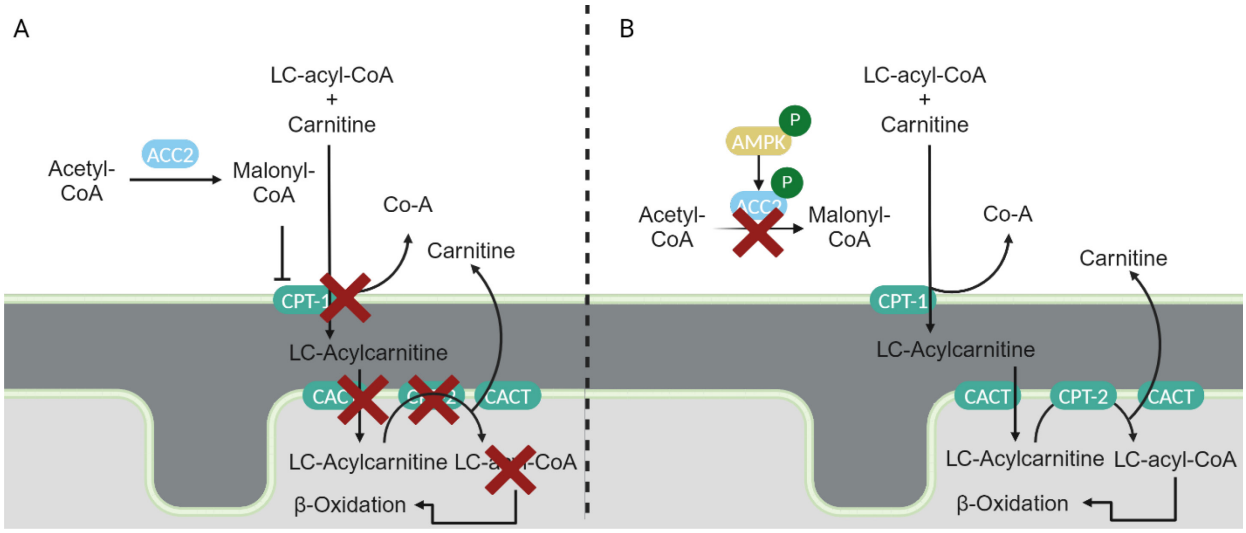

Figure 15. Regulation of the transport of LCFA into the mitochondria by AMPK.

A) *Malonyl-CoA from ACC2 inhibits CPT-1, main transporter of LCFA into the mitochondria.* ***B)*** *AMPK phosphorylation results in phosphorylation of ACC2, which inactivates it reducing malonyl-CoA production and allowing the transport of LCFA into the mitochondria by CPT-1. ACC2, acetyl-CoA carboxylase 2; Co-A, coenzyme A; CPT-1/2, carnitine-palmitoyl transferase 1/2; CACT, carnitine/acylcarnitine translocase. Figure created with BioRender.com.*

Links between astrocytic lipid metabolism and neuronal activity

While it is well-established that neuronal activity induces significant changes in astrocyte gene expression, morphology and metabolism, the relationship between lipid metabolism and neuronal activity has only recently begun to be studied.

Recent studies have shown that neuronal activity regulates gene expression, morphology, and function of astrocytes (*200*, *201*). For example, Notch signalling from neurons induced upregulation of astrocytic genes involved in glucose transport, uptake, and metabolism of neurotransmitters (GABA, glutamate, biogenic amines [dopamine, norepinephrine, epinephrine, serotonin, histamine]) (*200*). The changes in gene expression were dependent on the presence of neurons (*201*) and resulted in changes in astrocyte metabolism like increased glutamate transport (*200*) as well as changes in cortical organization (*201*). Moreover, synaptic activity induced cAMP/PKA-dependent CREB activation that led to upregulation of most of the enzymes involved in the anaerobic

glucose pathway as well as increased pyruvate and lactate production (*200*). Overall, research shows that neuronal activity can alter astrocyte metabolism through multiple pathways.

Emerging evidence suggests that lipid droplets within astrocytes play a crucial physiological and protective role in the central nervous system. Disruptions in lipid metabolism, structure, and signaling within astrocytes have been associated with various neurological disorders (*98*, *202*, *203*). Altered expression of enzymes in the TCA cycle and ETC induced altered lipid metabolism, lipid accumulation and behavioral symptoms that resemble Alzheimer's disease (*133*). Inhibition of fatty acid transport into the mitochondria results in increased efficiency of the ETC due to increased formation of mitochondrial super complexes (*121*). Inhibition of mitochondrial fatty acid trafficking also causes neuronal degeneration due to increased extracellular ROS production and significant cognitive impairment (*121*).

More evidence shows that astrocytes in distress accumulate lipid droplets. Metabolic stressors like nutrient deprivation, fatty acid overload or hypoxia induced lipid droplet accumulation (*204*). Moreover, norepinephrine, a catecholamine neurotransmitter linked to anxiety, stress and hyperactivity also mimicked the effect of metabolic stressors, resulting in increased lipid droplets (*204*). Stroke also induced lipid droplet accumulation in astrocytes while induced increased neuronal activity increased transfer of lipid from neurons to astrocytes (*50*).

Taken together, multiple lines of evidence suggest that astrocyte lipid metabolism and astrocyte mitochondrial metabolism are modulated by neuronal activity. While excessive neuronal activity induces transport of lipids into astrocytes, glutamate at physiological concentrations can regulate lipid droplet numbers (*50*). How glutamatergic neuronal activity influences astrocytic lipid homeostasis has not been established.

Hypothesis and objectives

Based on the current understanding of astrocyte metabolism and our findings that glutamate altered astrocyte lipid droplet population, the overall aim of this research is to understand how glutamate regulates astrocyte lipid homeostasis. To achieve this, we set

two objectives: a) Determine the effects of glutamate on astrocyte lipid metabolism and b) Determine the effects of glutamate on astrocyte mitochondrial health.

Chapter 2: Methods

Primary astrocyte cell culture

Primary hippocampal astrocyte cultures were prepared from P2/P3 Sprague-Dawley rat pups. Tissue was dissected and then digested using Papain for 25 minutes at 37°C. Cells were then suspended in Astrocyte Based Media (ABM), a previously defined serum-free media (*205*, *206*) or traditional astrocyte growth media (MD/10% FBS media).

ABM media is conformed by 1:1 mixture of Neurobasal medium (Gibco/Life Technologies, C.N. 21103) and DMEM high glucose (Fisher Scientific, C.N. SH30022FS) in addition to a final concentration of 1x Antibiotic-Antimycotic (Fisher Scientific, C.N. 15240062), 1x Glutamax (Fisher Scientific, C.N. 35050061), 1x Sodium Pyruvate (Fisher Scientific, C.N. 11360070), 5ng/ml Heparin-binding epithelial growth factor (HBEGF), 5µg/ml of N-Acetyl-L-Cysteine (NALC) and 1x ABM Supplement. ABM supplement consists of 1:1 mixture of Neurobasal medium (Gibco/Life Technologies, C.N. 21103) and DMEM high glucose (Fisher Scientific, C.N. SH30022FS) in addition to final concentration in the media of 100µg/ml Bovine Serum Albumin (BSA) (Millipore Sigma, C.N. A2058), 100µg/ml Apo-Transferrin Human (Millipore Sigma, C.N. T1147), 16µg/ml Putrescine Dihydrochloride (Millipore Sigma, C.N. P5780), 60ng/ml Progesterone (Millipore Sigma, C.N. P8783) and 40ng/ml Sodium Selenite (Millipore Sigma, C.N. S5261).

MD/FBS media consists of Basal Medium Eagle (BME) (Fisher Scientific, C.N. 21010046) in addition of 0.45% D-Glucose (Millipore Sigma, CN. G5146), 1x Antibiotic-Antimycotic (Fisher Scientific, C.N. 15240062), 1x Glutamax (Fisher Scientific, C.N. 35050061), 1x Sodium Pyruvate (Fisher Scientific, C.N. 11360070) and 10% Fetal Bovine Serum (FBS) (Gibco, C.N. 10437028).

After counting the cells in suspension using an automated hematocytometer, cells were seeded on KOH-treated and Poly-D-Lysine-coated (PDL) (Millipore Sigma, C.N. P6407) 12mm coverslips, 25mm coverslips, 96-well Seahorse plates, 6-well plates, 60mm culture dishes or 15cm culture dishes in an experiment-dependent way. After 20 minutes, we performed a complete media change to eliminate contaminating cell types from the

cultures. After 24 hours, we performed another complete media change. Primary cultures were maintained by changing the culture media every 2 days with half media change. Cultures were treated at 4 or 6 DIV when they reached around 60%-80% confluency.

Immunofluorescence

Cells were fixed for 20 minutes with a 4% paraformaldehyde (PFA) solution (Fisher Scientific, C.N. 50980488). Cells were then blocked and permeabilized for 1 hour with a 2% BSA (Millipore Sigma, C.N. 810037) + 0.2% Triton-X 100 in 1x PBS solution. Next, we incubated the cells for 1 hour in primary antibodies, washed with 0.2% Triton-X 100 in 1X PBS Wash Buffer solution and then incubated for another hour in the secondary antibodies. Finally, we counterstained with DAPI (Abcam, C.N. ab228549) to identify cell nuclei. Coverslips were then mounted on slides using DAKO Mounting Media (Agilent Technologies Canada Inc., C.N. S302380-2).

Table 1. Antibodies used for immunofluorescence.

Antibody	Source	Dilution	Vendor	Catalogue Number
Glial Fibrillary Acidic Protein (GFAP)	Chicken polyclonal	1:1000, FBS astrocytes. 1:500, ABM astrocytes	Abcam	ab4674
Ionized Calcium Binding Adaptor Molecule 1 (Iba1)	Rabbit polyclonal	1:1000 (FBS, ABM astrocytes) 1:500 (Tissue)	Wako	019-19741
Translocase of Outer Mitochondrial Membrane 20 (ToMM-20)	Rabbit monoclonal	1:500	Abcam	ab186735
Tubulin β3 (TUBβ3)	Mouse monoclonal	1:1000	BioLegend	801202
Alexa Fluor 647 (Anti-chicken)	Goat	1:750	Thermo Fisher Scientific	A21449
Alexa Fluor 647 (Anti-rabbit)	Donkey	1:750	Thermo Fisher Scientific	A31573
Alexa Fluor 594 (Anti-mouse)	Donkey	1:1000	Thermo Fisher Scientific	A21203
Alexa Fluor 488 (Anti-rabbit)	Goat	1:500	Thermo Fisher Scientific	A11008

Western Blot

Astrocytes were lysed using a whole-cell HEPES lysis buffer containing: 20 mM HEPES pH 7.4, 100 mM NaCl, 1% Triton X-100, 5 mM EDTA (Fisher Scientific, C.N. PI78440), Protease and Phosphatase inhibitor (Fisher Scientific, C.N. PI78440). Cell lysates were analyzed by Western blotting. We used primary antibodies against the corresponding protein of interest to blot the nitrocellulose membrane and used HRP-conjugated secondary antibodies to visualize our protein bands. Chemiluminescence from HRP-conjugated antibodies was detected using a ChemiDoc Imaging System (Bio-Rad). Blot images were opened on ImageJ with the Grayscale LUT, images were then inverted, resulting in a white background with dark immunoreactive bands. Images were rotated horizontally to align the protein bands. We then quantified protein band density using densitometry analysis in the ImageJ software.

Table 2. Antibodies used for western blotting

Antibody	Source	Dilution	Vendor	Catalogue Number
AMPKα	Rabbit monoclonal [D63G4]	1:1000	Cell Signalling Technology	5832S
Phospho-AMPKα (Thr172)	Rabbit monoclonal [40H9]	1:1000	Cell Signalling Technology	2535S
ACC	Rabbit monoclonal	1:1000	Cell Signalling Technology	3676
Phospho-ACC (Ser79)	Rabbit polyclonal	1:1000	Cell Signalling Technology	3661
B-Actin	Mouse monoclonal	1:1000	Cell Signalling Technology	3700S
LC3B	Rabbit polyclonal	1:1000	Abcam	ab48394
Anti-mouse HRP		1:10000	Thermo Fisher Scientific	A16072
Anti-rabbit HRP		1:10000	Thermo Fisher Scientific	A16104

Cell culture purity determination

6DIV astrocytes grown in MD/10% FBS or ABM media were fixed for 20 minutes in a 4% paraformaldehyde (PFA) solution (Fisher Scientific, C.N. 50980488). Cells were then blocked, permeabilized and stained against astrocyte marker glial fibrillary acidic protein (GFAP), neuronal marker β3-tubulin or microglial marker ionized calcium binding adaptor Molecule 1 (Iba1). After secondary antibody incubation, we then counterstained with DAPI (Abcam, C.N. ab228549). Imaging was performed using a Leica STELLARIS 5 (Leica Microsystems, Germany), obtaining 10 single-plane images per coverslip. Cells were manually quantified using the “Multi-point” tool in ImageJ (NIH, USA) according to the expression of the cell type markers previously mentioned.

Mitochondrial lipid trafficking assay

6DIV astrocytes were incubated in 2μM BODIPY 558/568 C12 (Red-C12) (Thermo Fisher Scientific, C.N. D3835) in ABM overnight. Next morning, astrocytes were washed three times in DPBS (Fisher Scientific, C.N. SH3002803) to remove any trace of remaining Red-C12. After the wash, astrocytes were treated with or without 100μM glutamate (Cayman, C.N. 30377) in ABM media for four hours. 30 minutes before the end of the experiment, astrocytes were incubated in 500nM MitoTracker Deep Red (Thermo Fisher Scientific, C.N. M22426). After, astrocytes were washed three times in DPBS (Fisher Scientific, C.N. SH3002803) to remove any trace background Red-C12. Astrocytes were then fixed in 4% PFA and counterstained with DAPI (Abcam, C.N. ab228549).

Extracellular Flux Analyzer Seahorse XFe96 assays

Seahorse XF Real-Time ATP Rate Assay Kit

Astrocytes were grown in Xfe96/XF Pro cell culture microplates and seeded at a density of $1.1x10^5$ for 4DIV. Astrocytes were treated with or without 100μM glutamate (Cayman, C.N. 30377) and after 4 hours were submitted to an induced Seahorse XF Real-Time ATP Rate Assay Kit (Agilent, C.N. 103592-100). In this assay, cells are subjected to the sequential addition of 1.5μM Oligomycin (Complex V inhibit) followed by a mixture of 0.5μM Rotenone (Complex I inhibitor) + Antimycin A (Complex III inhibitor). Oxygen consumption rate (OCR) and extracellular acidification rate (ECAR) are measured

approximately every 3 minutes. This assay allowed for the calculation of total, mitochondrial and glycolysis derived ATP production rates.

Seahorse XF Long-Chain Fatty Acid Oxidation Stress Kit

Astrocytes were treated with or without 100μM glutamate (Cayman, C.N. 30377) and, after 4 hours, were submitted to an induced Seahorse XF Long-Chain Fatty Acid Oxidation Stress Kit (Agilent, 103672-100). This assay was performed following the manufacturer specifications for all reagents in the kit. 100μM glutamate-treated astrocytes were co-treated with or without 4μM Etomoxir, an inhibitor of carnitine palmitoyl transferase I (CPT1), the main transporter of long-chain fatty acids into the mitochondria. After etomoxir treatment, the Seahorse performed a sequential injection of 1.5μM Oligomycin (Complex V inhibitor), followed by 1μM FCCP (a mitochondrial decoupling agent) and finally, a mixture of 0.5μM Rotenone (Complex I inhibitor) with Antimycin A (Complex III inhibitor). OCR and ECAR were measured. By detecting changes in the OCR of the mitochondria in response to CPT-1 inhibitor Etomoxir in a control or glutamate treated condition, this assay allows us to determine the effects of glutamate treatment on long-chain fatty acid oxidation activity.

Seahorse XF Mito Fuel Flex Test Kit

Astrocytes were treated with or without 100μM glutamate (Cayman, C.N. 30377) for 4 hours, after which they were submitted the Seahorse XF Mito Fuel Flex Test Kit (Agilent, 103260-100). This assay takes advantage of inhibitors of the transporters of the three main metabolites needed by mitochondria to use as a source of energy to produce ATP: pyruvate, fatty acids, and glutamine/glutamate catabolism. UK5099 (2μM) inhibits the mitochondrial pyruvate carrier which transports pyruvate, the end-product of glycolysis, into mitochondria. Etomoxir (20μM), as previously mentioned, inhibits CPT1, the main transporter of long-chain fatty acids into the mitochondria. Finally, BPTES (3μM) inhibits glutamine synthetase, the enzyme responsible of converting glutamine into glutamate, which is then transported into the mitochondria for energy production. However, astrocytes can directly import glutamate from the extracellular media via EAAT1 and EAAT2 (*162*, *207*). Due to this, we modified this assay by adding 200nM TFB-TBOA (Tocris, C.N. 2532), an inhibitor of EAATs, in addition to BPTES. By sequentially inhibiting

of each of the mitochondrial fuel pathways, this kit determines the dependency, capacity, and flexibility of the cell to oxidize glucose, long-chain fatty acids and glutamate/glutamine respectively.

Lipid droplet catabolism assays

Glutamate-treated (100μM) astrocytes were cotreated with or without 200nM of excitatory amino acid transporter inhibitor (3S)-3-[[3-[[4-(Trifluoromethyl) benzoyl] amino] phenyl] methoxy]-L-aspartic acid (TFB-TBOA, Tocris, C.N. 2532) or 2μM of the non-canonical DDHD2 lipase inhibitor KLH45 (Sigma Aldrich, C.N. SML1998) for 4 hours. Astrocytes were then fixed in 4% PFA and stained with DAPI (Abcam, C.N. ab228549) and BODIPY 493/503 (Thermo Fisher Scientific, C.N. D3922) for one hour. Imaging was performed using a Zeiss LSM 900 Airyscan (Carl Zeiss, Germany) microscope, obtaining 10 Z-stack images per coverslip. Images were then submitted to a maximum projection and lipid droplets stained with BODIPY493/503 (green channel) were thresholded using the “Renyi Entropy” algorithm followed by water shedding. We then used the “Analyze particles” command and quantified the number and average size of lipid droplets.

Metabolomic profiling

Cultured primary astrocytes were treated with or without 100 μM glutamate (Cayman, C.N. 30377) for 1 hour 45 minutes. Cells were then scrapped and collected in ice-cold methanol and immediately frozen in liquid nitrogen and stored at -80° C. Using previously described methods, short, medium and long-chain fatty acids (*208*) and acylcarnitines (*209*) were extracted, concentrated, and then analyzed via LC-MS in collaboration with The Metabolomics Innovation Center (TMIC) at the University of Victoria (BC, Canada).

Analysis of mitochondrial morphology

Astrocytes were treated with or without 100μM glutamate (Cayman, C.N. 30377) for 4 hours. 30 minutes before completing the experiment, astrocytes were incubated in CellTracker Green (1:1000 dilution, Thermo Fisher Scientific, C.N. C2925). Cells were then fixed with 4% paraformaldehyde, blocked, permeabilized and later stained against ToMM20 (a mitochondrial marker) and counterstained with DAPI. Imaging was performed using a Zeiss LSM 900 Airyscan (Carl Zeiss, Germany) microscope, obtaining 10 Z-stack

images per coverslip. Using ImageJ (NIH, USA), CellTracker Green channel was submitted to thresholding at its brightest plane using the “Li” algorithm. The threshold data was then used as input for the “3D Object Counter” function. The resulting 3D image was then submitted to a maximum projection to create a ROI that allowed us to quantify mitochondria inside a particular cell. We then thresholded mitochondria on the ToMM20 channel at their brightest point using the “IsoData” algorithm. Next, using the ROI obtained from the CellTracker Green channel, we thresholded mitochondria providing the threshold provided by the IsoData algorithm for the “3D Object Counter” function. We quantified object number, average mitochondrial volume, average mitochondrial volume and cell volume.

Autophagy assay

Glutamate-treated astrocytes were co-treated with 100μM Bafilomycin A1 (BAF A1) (Millipore Sigma, C.N. C974N95), an inhibitor of autophagosome fusion with the lysosome, for 4 hours. Cells were then lysed in a whole-cell HEPES lysis buffer. Western blot was performed as described in the Western blot section. Membranes were immunoprobed with autophagosomal membrane marker LC3B and loading control β-Actin. LC3B-I and LC3B-II were distinguished by the difference in their weight. The ratio of LC3B-II/LC3B-I normalized to our loading control was calculated by densitometry as previously described in the western blot section.

ROS assay

Astrocytes were treated with 100μM glutamate (Cayman, C.N. 30377) for 4 hours. To detect ROS production, each treatment group was incubated with 2.5 mM CellROX Green (Thermo Fisher Scientific, C.N. C10444) for 30 min at 37 °C before the conclusion of the experiment. Astrocytes were then fixed in 4% PFA and counterstained with DAPI (Abcam, C.N. ab228549) for 10 minutes. Imaging was performed using a Zeiss LSM 900 Airyscan (Carl Zeiss, Germany) microscope, obtaining 10 z-stack images per coverslip. We then selected one plane where the nucleus of cells was in focus for analysis. Nuclei on the DAPI channel were thresholded using the “Otsu” algorithm. We then used this image as an ROI and quantified mean gray value and integrated density on the CellROX Green channel.

Mitochondrial dynamics assay

Astrocytes were transfected with MitoTimer (addgene, plasmid # 50547), a mitochondria-targeted doxycycline-induced fluorescent protein that shifts its fluorescence from green to red over a period of 48 hours (*210*, *211*). MitoTimer (0.5µg/µL) was transfected when cultured astrocytes reached 3 DIV by using 3.75µl of Lipofectamine 3000 (Fisher Scientific, C.N. L3000015) in ABM media. After a 4-hour incubation with the construct, astrocytes were washed three times with DPBS (Fisher Scientific, C.N. SH3002803) to remove any trace of MitoTimer DNA that was not taken up by the cells. After the washes, ABM media was resupplied. MitoTimer was then expressed in two 4-hour 2µg/ml doxycycline (Abcam, C.N. ab141091) pulses: one at 4 DIV and a second one at 6 DIV. After the first pulse, astrocytes were washed three times with DPBS to remove any trace of doxycycline to avoid constant expression of the MitoTimer construct. ABM media was resupplied after the DPBS wash. Additionally, during the second doxycycline pulse, we treated astrocytes with or without 100µM glutamate (Cayman, C.N. 30377) for four hours. Astrocytes were then fixed in 4% PFA and counterstained with DAPI (Abcam, C.N. ab228549) for 10 minutes. Imaging was performed using a Zeiss LSM 900 Airyscan (Carl Zeiss, Germany) microscope, obtaining 6-8 z-stack images per coverslip. Using ImageJ (NIH, USA), we created a maximum projection to create an ROI to only quantify mitochondria inside a cell. Then, within the obtained ROI, each channel was independently analyzed by applying the automated threshold included “3D Object Counter” function. We quantified the mean gray value of each channel.

Microscopy

Imaging was performed using the following microscopes: Leica STELLARIS 5 (Leica Microsystems, Germany) or Zeiss LSM 900 Airyscan (Carl Zeiss, Germany). For imaging experiments, we took 10 images per experiment in aleatory and non-overlapping areas of the coverslip. The only exception to this was our MitoTimer assay, in which we took between 6 to 10 pictures per experiment and actively searched for cells that expressed the MitoTimer construct. Previous to image analysis, images were subjected to background subtraction by applying a Gaussian Blur filter (10 for lipid droplets, 50 for mitochondria and cell nuclei) to duplicate images which was then subtracted to the

original image. Images taken were then analyzed using image analysis software ImageJ (NIH, USA) as described in each experiment section.

Statistical Analysis

Statistical analysis will be performed using GraphPad Prism 10 (GraphPad Software LLC). Differences between groups were determined via Student's T, one-way ANOVA, Kruskal-Wallis, or two-way ANOVA, depending on the experimental design and the characteristics of the data obtained.

Chapter 3: Results

Results

To explore the effects of glutamate on astrocyte physiology, we cultured primary rat astrocytes in a previously defined serum-free media containing heparin binding epidermal growth factor (*205*) known as ABM. These astrocytes have a more ramified morphology relative to the fibroblast-like appearance of those grown in serum (Figure 16A), and approximately 95% of cells are positive for the astrocyte marker GFAP (Figure 16B-D). Consistent with previous reports (*50*), these astrocytes respond to glutamate by reducing the number of lipid droplets (Figure 16E-F). Lipid droplet size was unaffected by glutamate treatment in both complete media and HBSS (Figure 16G-H).

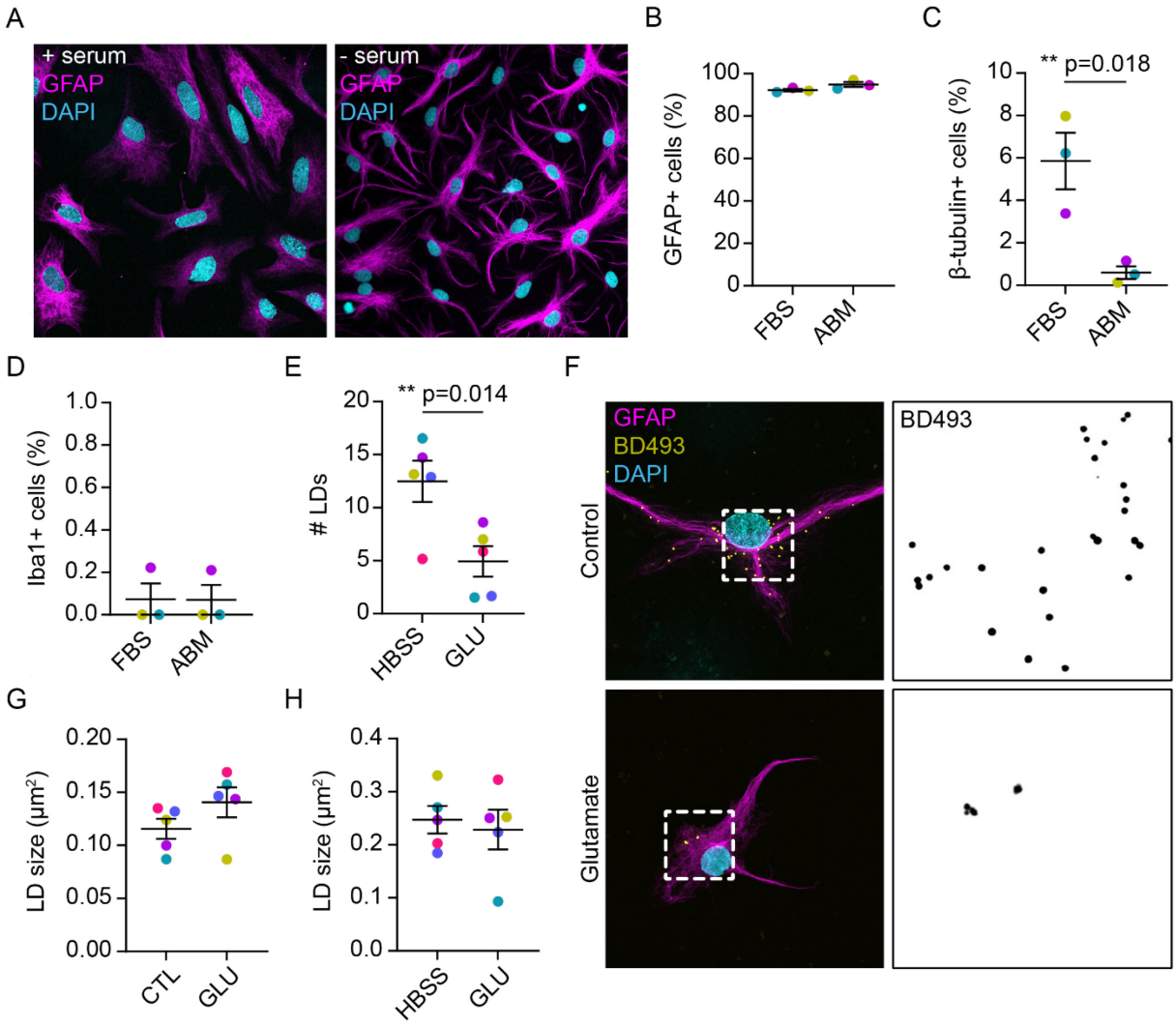

Figure 16. ABM astrocytes possess a morphology that better resembles in-vivo astrocytes and recapitulates lipid droplet degradation in response to glutamate.

A) *Super resolution images of astrocytes grown in MD/10%FBS (+ serum) or ABM (- serum) media. Astrocytes (GFAP, 647nm) are pseudo colored in magenta, nuclei in blue (DAPI, 461nm).* ***B, C, D)*** *Quantification of cell purity using our stablished culture methods. Astrocytes (GFAP) are quantified in B, neurons (β-tubulin) in C and microglia (Iba1) in D. Unpaired T-test, n=3, duplicates, mean +/- SEM.* ***E)*** *Quantification of the number of lipid droplets stained with neutral lipid dye BODIPY493/503. Unpaired T-test, n=3, duplicates, mean +/- SEM.* ***F)*** *Representative super resolution images of astrocyte lipid droplets when cells were treated with or without glutamate. Astrocytes (GFAP, 647nm) are pseudo colored in magenta, nuclei in blue (DAPI, 461nm) and lipid droplets in yellow (BODIPY 493/503, 508nm).* ***G, H)*** *Quantification of the size of lipid droplets stained with neutral lipid dye BODIPY493/503. Unpaired T-test, n=3, duplicates, mean +/- SEM.*

Glutamate decreases lipid droplet numbers and increases fatty acid trafficking to mitochondria in astrocytes

Previously, we found that glutamate promotes fatty acid trafficking from the lipid droplets to the mitochondria (*50*). To test if this also occurs in serum-free astrocytes, astrocytes in serum-free complete media were treated with glutamate. Astrocytes responded by decreasing the number of lipid droplets (Figure 17A-B). We then loaded astrocytes with the fluorescently tagged fatty acid BODIPY 558/568 C12 (Red-C12) overnight. Using microscopy, we then quantified the intensity of Red-C12 in mitochondria following glutamate treatment. Accordingly, astrocytes treated with glutamate had increased Red-C12 signal intensity in mitochondria labelled with MitoTracker Deep Red (Figure 17C-D). Collectively, this data indicates that glutamate affects lipid homeostasis in astrocytes.

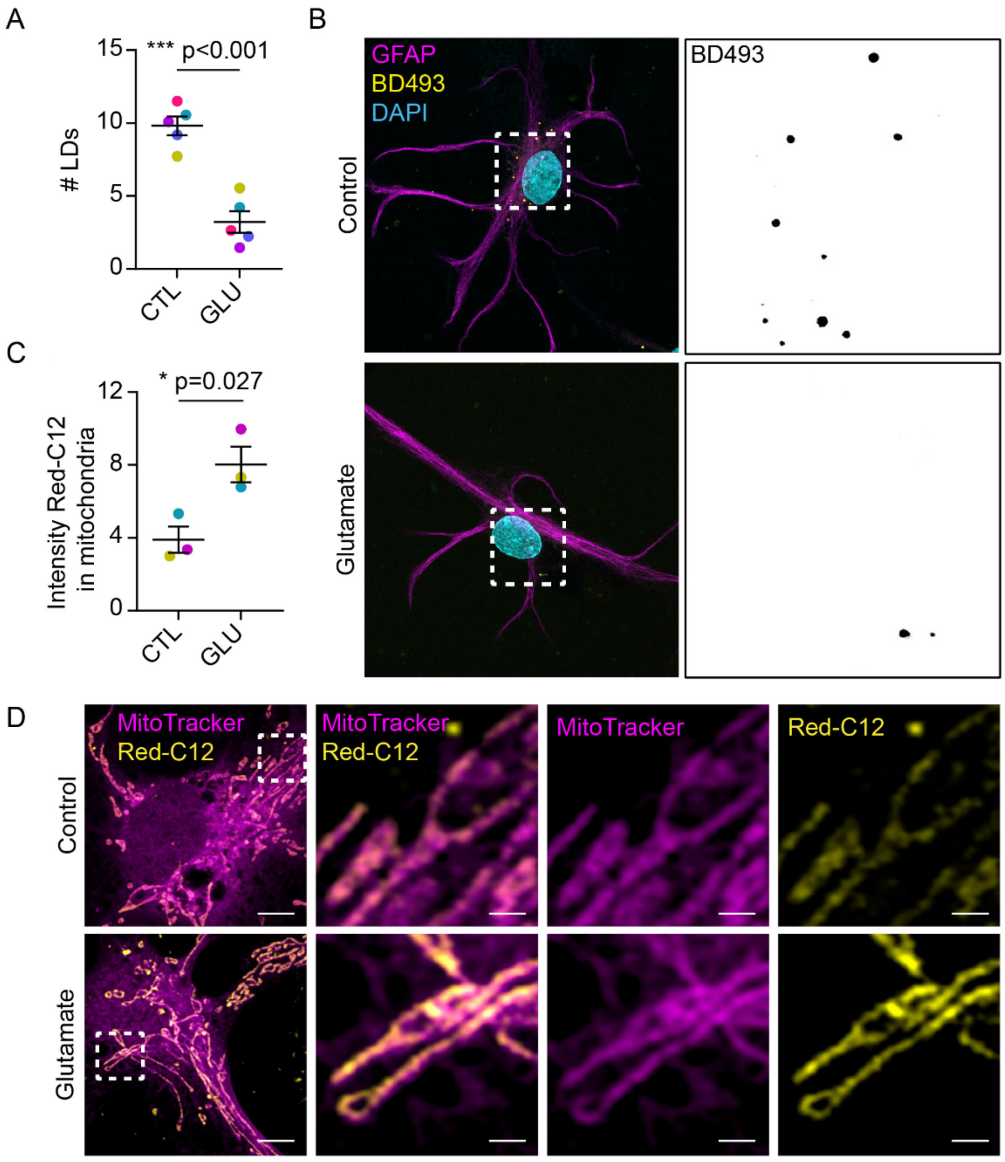

Figure 17. Glutamate decreases lipid droplets and increases fatty acid trafficking into astrocyte mitochondria.

A) *Quantification of astrocyte lipid droplet number using neutral lipid dye BODIPY493/503. Unpaired t-test, n=5, mean +/- SEM.* ***B)*** *Representative image of astrocytes treated with or without glutamate.* ***C)*** *Quantification of fluorescent intensity of lipid BODIPY 558/568 C12 (Red-C12) inside astrocyte mitochondria.* ***D)*** *Representative super resolution images of mitochondrial BODIPY 558/568 C12 intensity in glutamate-treated astrocytes. First column is an overview of the astrocytes, following columns are a zoom in of the indicated white dashed area on the first column. MitoTracker Green FM (511nm) is pseudo colored in magenta, Red-C12 in yellow (567nm). Unpaired t-test, n=3, mean +/- SEM. Scale bar, 5μM on soma view, 1 μm on zoom.*

Glutamate increases mitochondrial respiration

As lipid droplet homeostasis is dependent on cell metabolism and glutamate is an important metabolic substrate (*138*, *158*, *159*, *212*), we next explored how glutamate affects metabolism in astrocytes. As expected, astrocytes increase ATP production rate in response to glutamate (Figure 18A). This increase in ATP production rate is derived from the mitochondria, as it coincides with an increase in the oxygen consumption rate with glutamate treatment (Figure 18D) and increased ATP production rate in the mitochondria (Figure 18B). At the same time, glutamate decreased ATP production from glycolysis as indicated by the decreased extracellular acidification rate (Figure 18E) and decreased ATP production rates from glycolysis (18C). These data shows that glutamate increases mitochondrial activity and mitochondria-derived ATP production rate while inhibiting glycolytic activity.

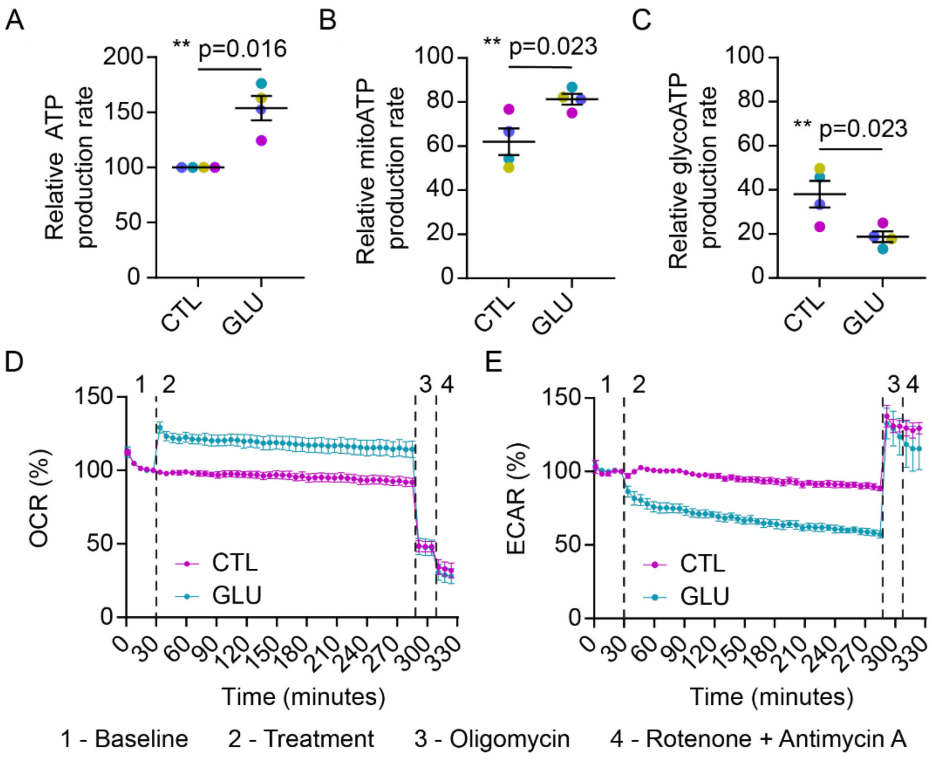

Figure 18. Glutamate enhances mitochondrial ATP production rate and oxygen consumption while decreasing glycolysis-derived ATP production rate.

A) *Total ATP production rate in control and glutamate-treated groups. Data normalized to control group. Welch's t-test, p≤ 0.05, n=4, ≈44 replicates per experiment, mean +/- SEM.* ***B)*** *Mitochondrial ATP production rate in control and glutamate-treated group. Data*

is relative to total ATP production in the corresponding group. Two-Way ANOVA, post-hoc Šídák, p≤ 0.05, n=4, ≈44 replicates per experiment, mean +/- SEM. ***C)*** *Glycolysis-derived ATP production rate in control and glutamate-treated group. Data is relative to total ATP production in the corresponding group. Two-Way ANOVA, post-hoc Šídák, p≤ 0.05, n=4, ≈44 replicates per experiment, mean +/- SEM.* ***D)*** *Astrocyte oxygen consumption rate in control and glutamate-treated group. Data normalized to the last measurement in our baseline period before treatment injection. Multiple unpaired t-tests, Šídák-Bonferroni correction, p≤ 0.05, n=4, ≈ 44 replicates per experiment, mean +/- SEM.* ***E)*** *Astrocyte extracellular acidification rate in control and glutamate treated astrocytes. Data normalized to the last measurement in our baseline period before treatment injection. Multiple unpaired t-tests, Šídák-Bonferroni correction, p≤ 0.05, n=4, ≈ 44 replicates per experiment, mean +/- SEM.*

Glutamate does not affect fatty acid oxidation

Since glutamate increases fatty acids transport into the mitochondria in addition to increased mitochondrial respiration, we hypothesized that these fatty acids are used for fatty acid oxidation. To test this, we co-treated astrocytes with glutamate and etomoxir, a carnitine palmitoyltransferase-1 inhibitor, to prevent fatty acid entry into mitochondria. We observed that glutamate treatment increased ATP-linked respiration, however, etomoxir had no effect on ATP-linked respiration (Figure 19A) or mitochondrial ATP production rate (Figure 19B-C). The dependency of astrocytes on fatty acid oxidation was low regardless of whether glutamate was present (Figure 19D) and their capacity to metabolize fatty acids remained low even when other fuel pathways were inhibited (Figure 19E). Consistently, we observed no alterations in total levels of free fatty acids (Figure 19F). Instead, astrocytes preferentially use glutamate as a fuel source for oxidative metabolism (Figure 19GH), while reducing their dependence on pyruvate (Figure 19I-J). Collectively, these data indicate that glutamate does not influence fatty acid oxidation which remains stable in astrocytes.

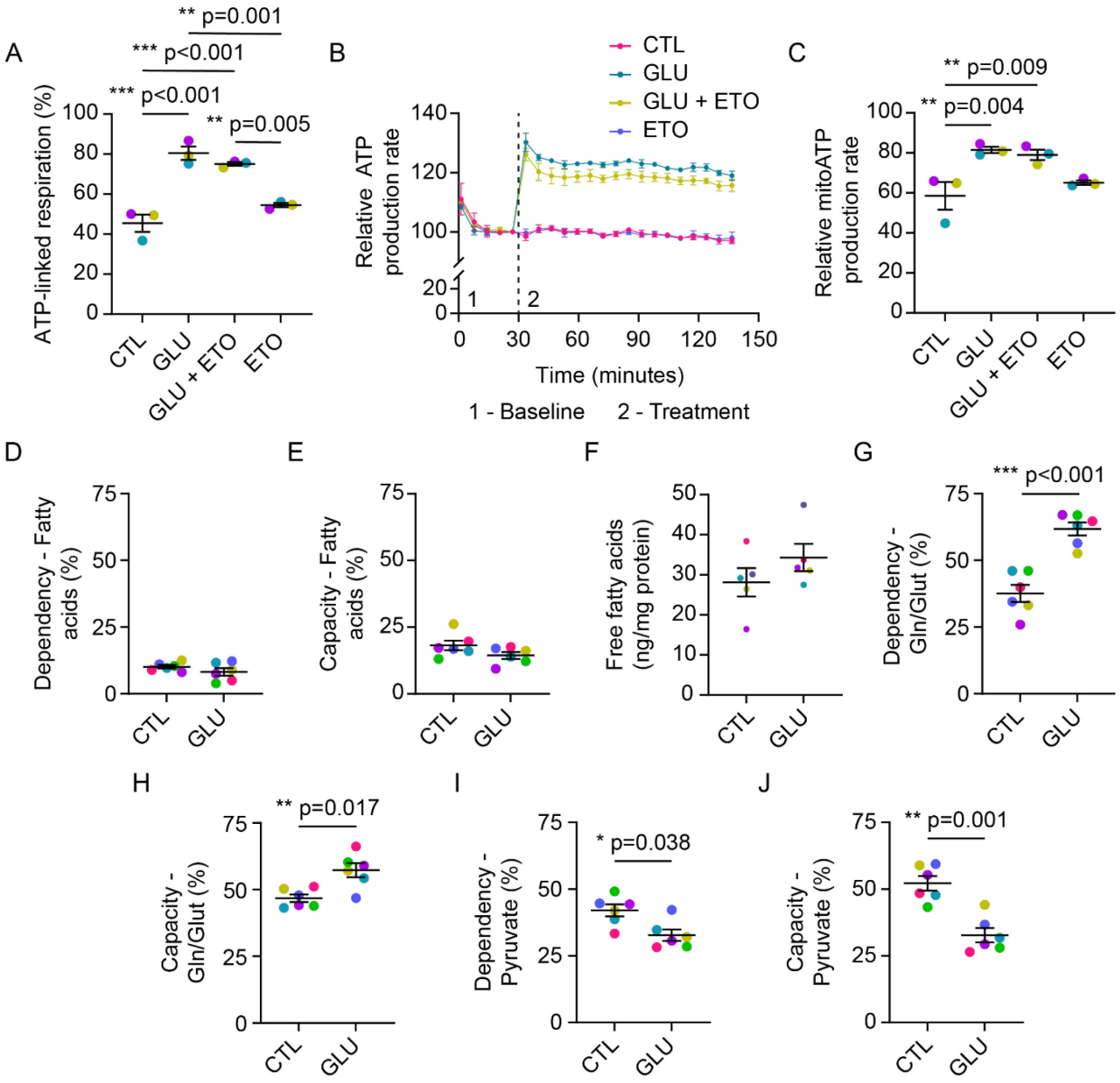

Figure 19. Glutamate treatment does not significantly affect mitochondrial fatty acid oxidation but increases glutamate oxidation while decreasing glucose oxidation

A) *ATP-linked respiration in astrocytes. Data is normalized total OCR per group. One-Way ANOVA, post-hoc Šídák's, p≤ 0.05, n=3, ≈ 20 replicates per experiment, mean +/- SEM.* ***B)*** *ATP production rate over time. Data is normalized to the last baseline measurement before treatment. Two-Way ANOVA, post-hoc Šídák, p≤ 0.05, n=3, ≈ 20 replicates per experiment, mean +/- SEM.* ***C)*** *Mitochondrial ATP production rate relative to total ATP production rate on glutamate-treated astrocytes cotreated with etomoxir. Two-Way ANOVA, post-hoc Šídák, p≤ 0.05, n=6, ≈8 replicates per experiment, mean +/- SEM.* ***D, E)*** *Dependency and capacity of fatty acid oxidation in control and glutamate treated astrocytes. Data relative to total OCR. Multiple unpaired t-tests, Šídák-Bonferroni*

correction, p≤ 0.05, n=6, ≈8 replicates per experiment, mean +/- SEM. ***F)*** *Total content of fatty acids (≥C8) present on control and glutamate treated astrocytes. Unpaired t-test, p≤ 0.05, n=5, duplicates, mean +/- SEM.* ***G, H)*** *Dependency and capacity of astrocytes to oxidize glutamate in control and glutamate-treated groups. Data relative to total OCR. Multiple unpaired t-tests, Šídák-Bonferroni correction, p≤ 0.05, n=6, ≈8 replicates per experiment, mean +/- SEM.* ***I, J)*** *Dependency and capacity of astrocytes to metabolize pyruvate in control and glutamate-treated groups. Data relative to total OCR. Multiple unpaired t-tests, Šídák-Bonferroni correction, p≤ 0.05, n=6, ≈8 replicates per experiment, mean +/- SEM.*

Glutamate lowers astrocytic acylcarnitines

As previously shown, glutamate induces fatty acid trafficking to the mitochondria, but not for ATP production. For long-chain fatty acids to enter mitochondria, they need to be converted to acylcarnitines. Faulty β-oxidation of fatty acids could explain the lack of contribution towards ATP production which would lead to a toxic accumulation of long-chain acylcarnitines (*213*, *214*). Therefore, we assessed whether astrocytes were accumulating free fatty acids as acylcarnitines. By lipidomic profiling, we discovered a reduction in total acylcarnitine levels upon glutamate treatment (Figure 20A). The most significant changes were observed in short-chain acylcarnitines, as they were mostly downregulated (including acetyl carnitine [C:2], 2-methylbutyril carnitine [C:5], Isovaleryl carnitine [C:5] and butyrobetaine) (Figure 20B). Two other acylcarnitine species (C:4, C:6) were upregulated (Figure 20B). While the effects of altered short-chain acylcarnitines remain unclear, the absence of toxic long chain acylcarnitine accumulation indicates that glutamate is not disrupting the mitochondria's ability to process incoming fatty acids.

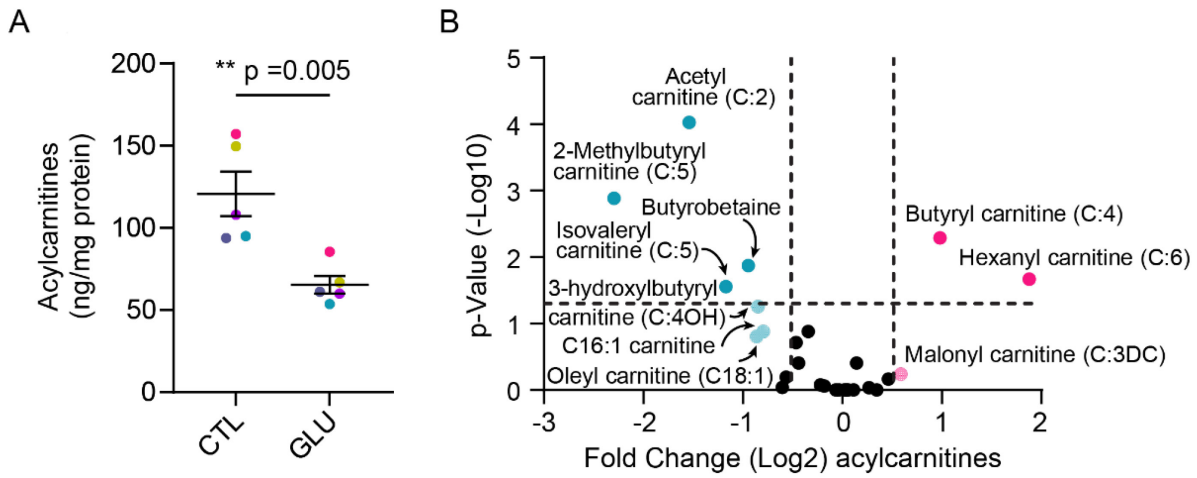

Figure 20. Analysis of changes in the profile of fatty acyl-carnitines in glutamate-treated astrocytes.

A) *Total content of acylcarnitines in control and glutamate treated astrocytes. Unpaired t-test, p≤ 0.05, n=5, duplicates, mean +/- SEM.* ***B)*** *Volcano plot depicting the changes in fatty acyl-carnitines obtained following MS data processing in control and glutamate-treated groups. Multiple unpaired t-tests, Holm-Šídák correction, p≤0.05, n=5, 3 replicates per experiment. Fold change considered significant when Log2 >0.5 or <0.5.*

Glutamate decreases lipid droplets independent of its uptake

Astrocytes play an important role in clearing extracellular glutamate by internalizing it via transporters and use this glutamate as fuel for oxidative phosphorylation in the mitochondria. Since lipid droplet formation and breakdown is highly dependent on the cell's metabolic state, we next wondered whether glutamate uptake, and subsequently its catabolism, is required for the effects seen on lipid droplets. The major glutamate transporters responsible for glutamate uptake by astrocytes are the excitatory amino acid transporters (EAAT1 and EEAT2) which can be blocked by the pan-EEAT inhibitor TFB-TBOA in cultured astrocytes (Figure 21A). Inhibiting EAAT transporters had no effect on the number or size of lipid droplets (Figure 21B-D). Therefore, the effects of glutamate on lipid droplets occur independently from its uptake and catabolism.

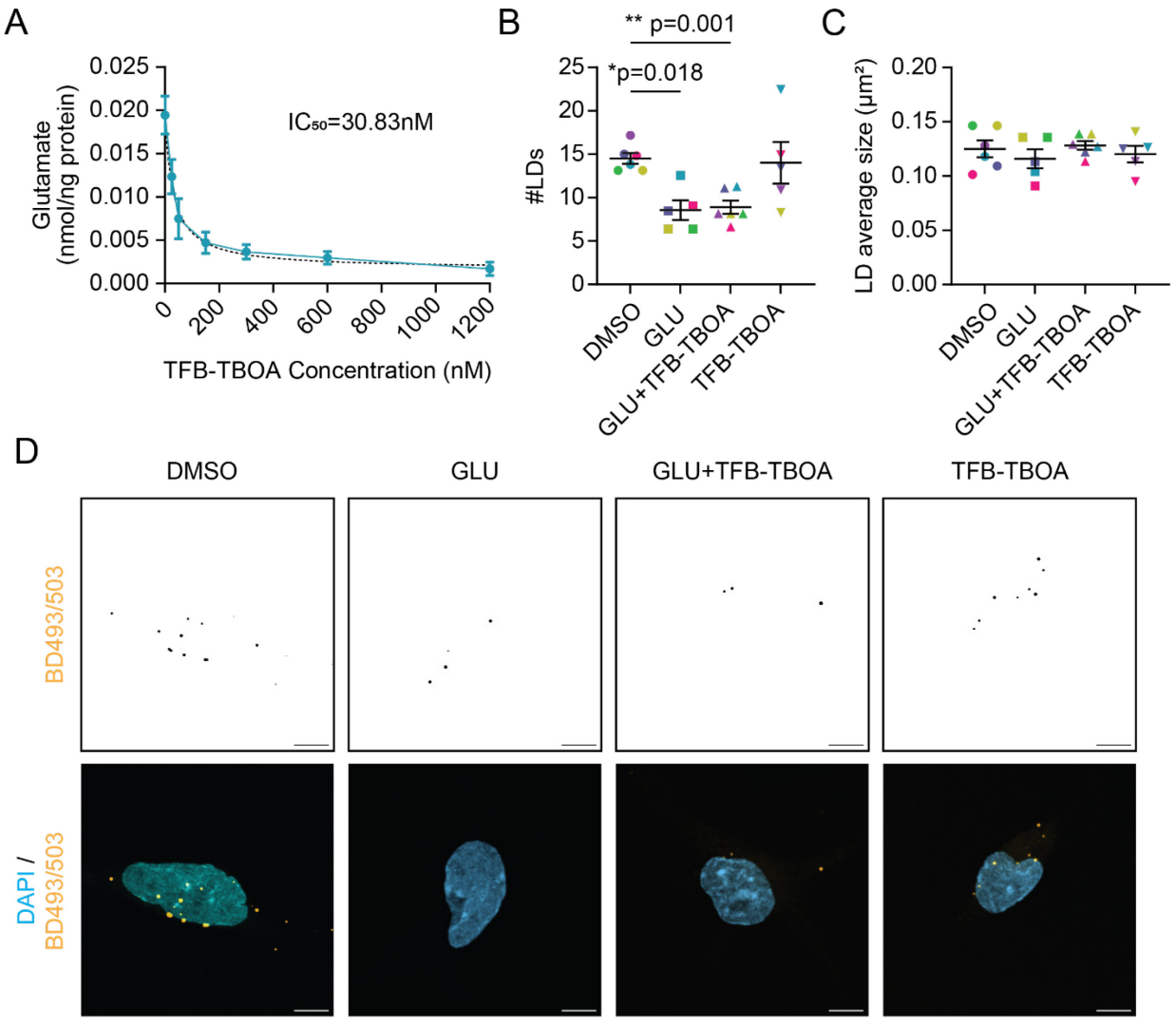

Figure 21. Glutamate receptors and not glutamate transporters are responsible for lipid droplet catabolism.

A) *Inhibition curve of EAAT-mediated glutamate transport in astrocytes treated with TFB-TBOA at multiple doses.* ***B)*** *Quantification of astrocyte lipid droplets stained by BODIPY 493/503. Welch's ANOVA, post-hoc Dunnett's T3, p≤ 0.05, n=6, duplicates, mean +/- SEM.* ***C)*** *Average size of astrocyte lipid droplets stained by BODIPY 493/503. Welch's ANOVA, post-hoc Dunnett's T3, p≤ 0.05, n=6, duplicates, mean +/- SEM.* ***D)*** *Representative super resolution images of each treatment group. Nuclei are pseudo colored in blue (DAPI, 461nm) and lipid droplets in orange (BODIPY 493/503, 508nm). Scale bar 5µm.*

Glutamate increases AMPK and ACC phosphorylation

If glutamate uptake is not required for changes in lipid metabolism, we reasoned that glutamate signalling could be involved by recruiting downstream pathways that affect lipid metabolism like AMPK and ACC. To test this, we treated astrocytes with glutamate and then analyzed the phosphorylated and total AMPK and ACC protein, as these proteins play an important role in regulating metabolism and lipid droplet physiology (*100*, *191*, *192*, *198*, *199*).

We discovered that after glutamate treatment, AMPK phosphorylation was increased at 15 minutes with no affect on total AMPK levels (Figure 22A-C). ACC, downstream target of AMPK, also showed changes after glutamate treatment. More specifically, increased phosphorylation of ACC after glutamate treatment at earlier (15 and 45 minutes) and later time points (75 and 105 minutes) (Figure 22D-F). Overall, these experiments show that glutamate increases AMPK and ACC phosphorylation which may affect downstream lipid metabolism and storage.

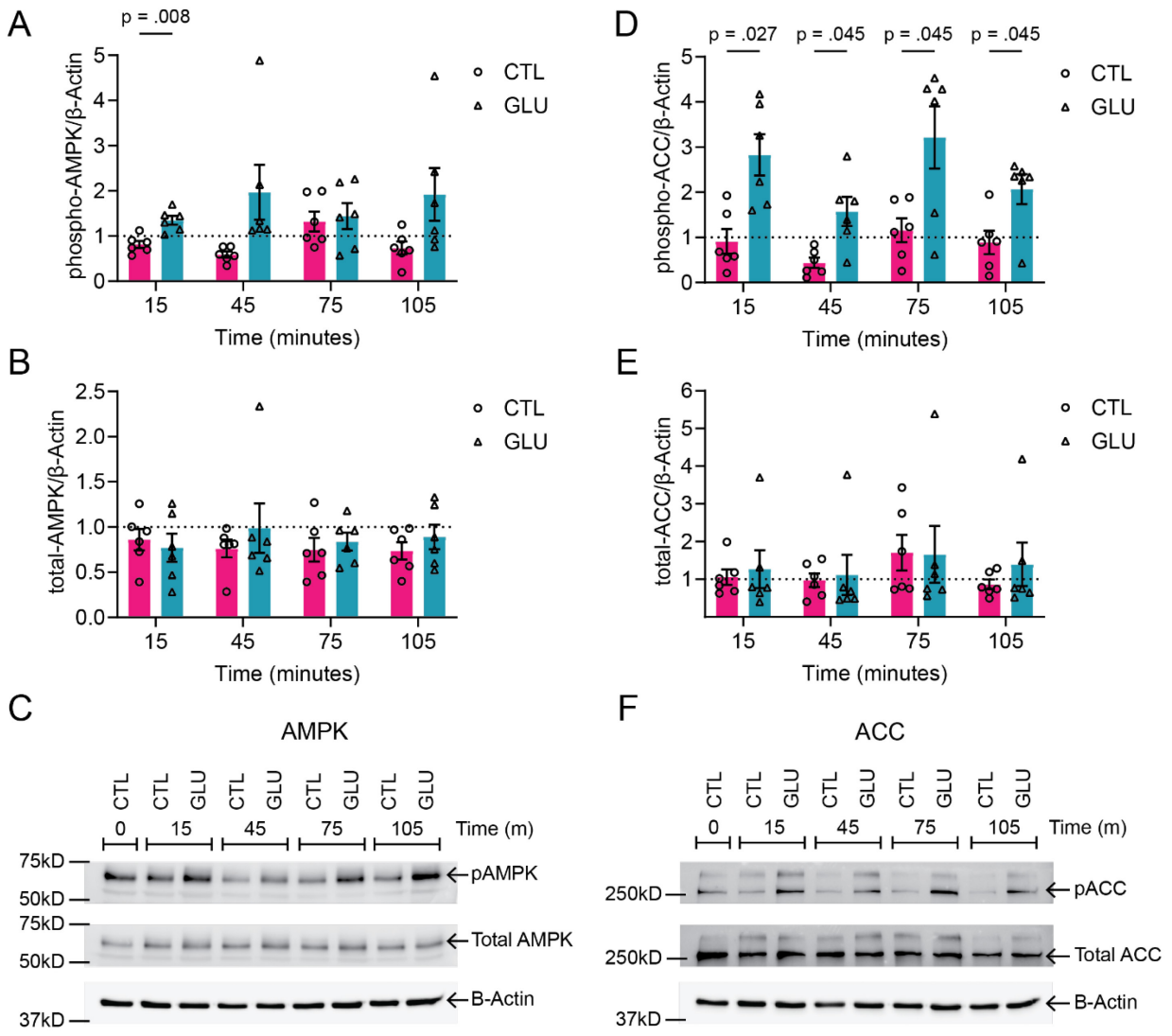

Figure 22. Glutamate induces AMPK and ACC phosphorylation.

A, B) *Quantification of phosphorylation of AMPKα and total AMPKα normalized to our loading control. Multiple unpaired Welch t-tests, Holm-Šídák correction, p≤ 0.05, n=6, duplicates, mean +/- SEM.* ***C)*** *Representative images of pAMPKα, total AMPKα and β-Actin of astrocytes treated with or without glutamate at the timepoints tested.* ***D,E)*** *Quantification of phosphorylated ACC, total ACC and loading control β-Actin. Multiple unpaired Welch t-tests, Holm-Šídák correction, p≤ 0.05, n=6, duplicates, mean +/- SEM.* ***F)*** *Representative images of pACC, total ACC and β-Actin at multiple timepoints.*

Astrocytes catabolize lipid droplets via non-canonical lipase DDHD2

Lipid droplet catabolism is performed via two pathways: neutral lipolysis and lipophagy. In lipophagy, lipid droplets (or parts of it) are engulfed by an autophagosome, which then fuse with lysosomes, in turn breaking down lipid droplets via lysosomal acid lipase. Previous research from our laboratory suggests that lipophagy is not responsible for glutamate-induced reduction in lipid droplets (*50*). Moreover, the lipase inhibitor DEUP prevented glutamate-induced reduction in lipid droplet numbers (*50*). However, whether glutamate regulates lipases on the lipid droplet surface is unclear. In canonical neutral lipolysis, adipocyte triglyceride lipase (ATGL) is responsible for initiating the breakdown of triglycerides from lipid droplets. More recent research suggests that non-canonical lipase DDHD2 acts as the main triglyceride lipase in the brain (*93*, *94*, *215*).

To test if DDHD2 is affected with glutamate treatment, astrocytes were co-treated with or without 2 μM KLH45, a specific inhibitor of DDHD2 (*93*). As previously observed, astrocytes treated with glutamate have decreased lipid droplet numbers (Figure 23A) and no changes in lipid droplet average size (Figure 23B). Co-treatment with KLH45 rescued the number of lipid droplets in glutamate treated astrocytes to control levels (Figure 23A). This confirms that DDHD2 is the main triglyceride lipase in astrocytes. KLH45 also increased lipid droplet size, whereas glutamate had no effect on lipid droplet size (Figure 23B). This suggests that glutamate acts on lipid droplets independent of DDHD2, which is constitutively active. This is also consistent with no difference in free fatty acids with glutamate treatment detected by lipidomics (Figure 19F), further supporting no change in lipolysis of triglycerides.

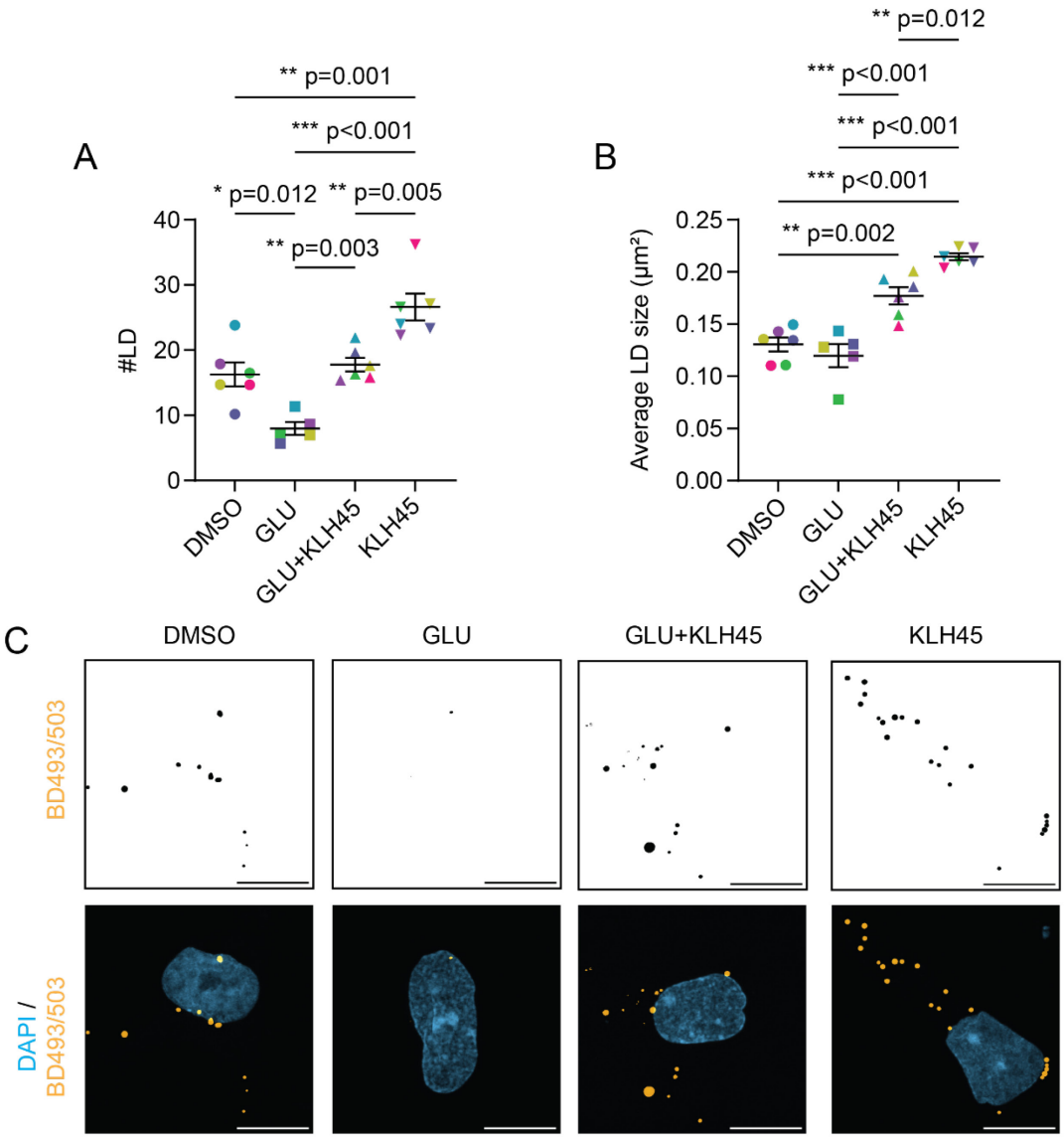

Figure 23. DDHD2 lipase is the main triglyceride lipase in astrocytes.

A) *Quantification of astrocyte lipid droplets stained with BODIPY 493/503. Welch's ANOVA, post-hoc Šídák, p≤ 0.05, n=6, duplicates, mean +/- SEM.* ***B)*** *Average size of astrocyte lipid droplets stained with BODIPY 493/503. One-Way ANOVA, post-hoc Dunnett T3, p≤ 0.05, n=6, duplicates, mean +/- SEM.* ***C)*** *Representative super resolution images of astrocyte lipid droplets. Nuclei are pseudo colored in blue (DAPI, 461nm) and lipid droplets in orange (BODIPY 493/503, 508nm). Scale bar 10µm.*

Glutamate reduced the induction of autophagy

Since glutamate reduces lipid droplet numbers independent of DDHD2 activity, we next wondered whether it instead regulates the influx of lipids into lipid droplets. Degradation of membranes by autophagy generates lipids that are then stored in lipid droplets (*92*, *102*, *216*). We therefore reasoned that glutamate may reduce lipid droplet numbers by reducing macroautophagy. To test this, we evaluated the lipidation of LC3 upon glutamate treatment. First, we measured the LC3B-II/LC3B-I ratio in the presence of Bafilomycin A1 (BAF A1) to block autophagosome-lysosome fusion. We observed decreased LC3B-II/LC3B-I ratio upon glutamate treatment, and therefore reduced induction of autophagy, (Figure 24A,C). We next compared the LC3B-II/LC3B-I ratio in the presence and absence of BAF A1. This showed no difference on the autophagic flux in the presence of glutamate (Figure 24B-C). Collectively these data reveals decreased induction of autophagy in the presence of glutamate which is consistent with a reduced need for lipid storage.

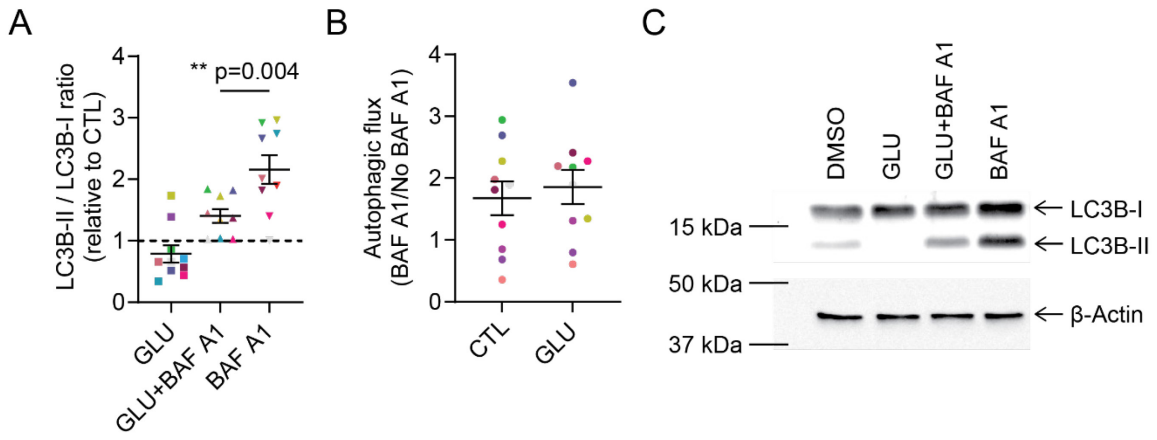

Figure 24. Glutamate decreases autophagy induction.

A) *Analysis of densitometry quantification of the ratio of autophagy marker LC3B-II/LC3B-I normalized to β-Actin. One-Way ANOVA, post-hoc Šídák, p≤ 0.05, n=10, mean +/- SEM.* ***B)*** *Densitometric analysis of the autophagic flux (LC3ii/i ratio in the presence of BAF) / (LC3ii/i ratio in absence of BAF). Student's T, p≤ 0.05, n=10, mean +/- SEM.* ***C)*** *Representative image of LC3B and housekeeping protein β-Actin blots.*

Glutamate decreases ROS

One trigger of autophagy is oxidative stress. While increased mitochondrial oxidative metabolism is a major source of ROS generation, previous work from our lab found a reduction in ROS in astrocytes treated with glutamate (*50*). We wanted to confirm whether the same was true for astrocytes grown in the absence of serum. We measured the amount of superoxide and hydroxyl radicals by staining astrocytes with CellRox Green (*217*). We found that glutamate-treated astrocytes showed decreased CellROX fluorescence (Figure 25A-B). This suggests that despite increased oxidative metabolism, glutamate compensates by engaging astrocyte antioxidant capacity. This is also consistent with decreased autophagy.

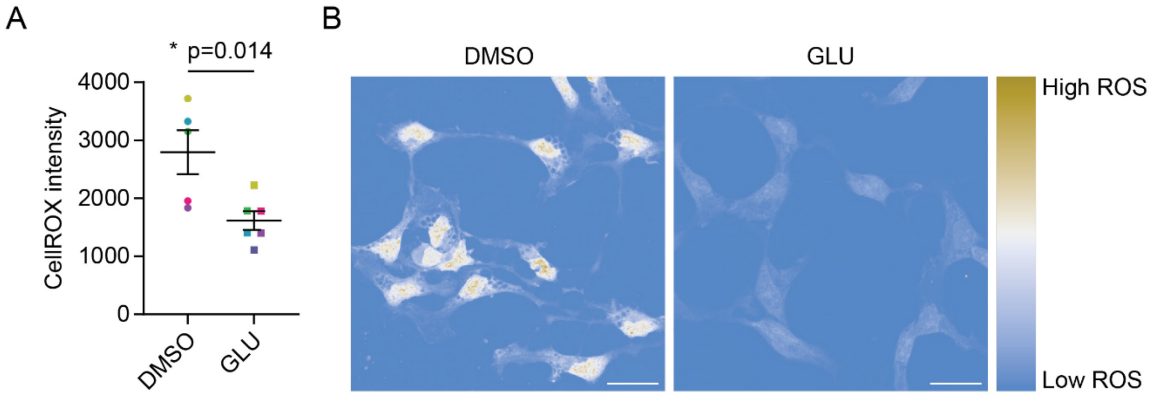

Figure 25. Glutamate decreases intracellular ROS.

A) *Fluorescence intensity of ROS-sensitive probe CellROX Green in astrocytes treated with or without glutamate. Unpaired t-test, n=6, p≤ 0.05, duplicates, mean +/- SEM.* ***B)*** *Representative picture of astrocytes treated with or without glutamate. Pseudo color gradient shows CellROX fluorescent signal as high if yellow and low if blue. Scale bar 20µm.*

Glutamate expands the mitochondrial mass of astrocytes

Considering that fatty acids are transported into the mitochondria but not catabolized, we wondered whether glutamate induced any changes in the mitochondrial network. We treated astrocytes with or without glutamate for 4 hours and then stained for translocase of the outer membrane 20 (ToMM20), a mitochondrial marker. We found that glutamate-

treated astrocytes had increased number and volume of mitochondria with no change in cell volume (Figure 26A-E). There was an overall shift in the size distribution towards larger mitochondria (Figure 26D), indicating that glutamate does not induce mitochondrial fragmentation as it does in neurons. Collectively, these data point to an enhanced mitochondrial mass in astrocytes in response to glutamate.

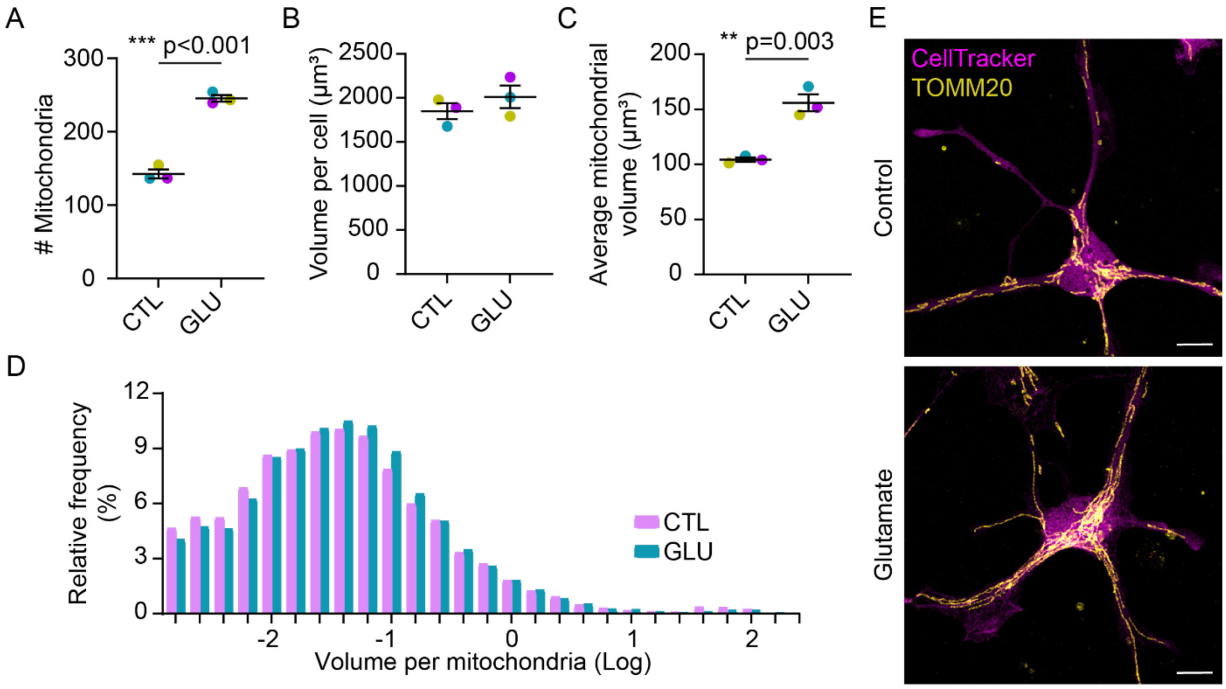

Figure 26. Glutamate treatment increased mitochondrial quantity, mass and a shift in distribution in mitochondrial size.

A) *Quantification of mitochondria stained by ToMM20 in control and glutamate-treated astrocytes. Unpaired t-test, p≤ 0.05, n=3, 2 replicates, mean +/- SEM.* ***B)*** *Cell volume quantification of control and glutamate-treated astrocytes by CellTracker Green. Unpaired t-test, p ≥ 0.05, n=3, 2 replicates, mean +/- SEM.* ***C)*** *Quantification of the average mitochondrial volume in control and glutamate treated astrocytes. Unpaired T-test, p≤ 0.05, n=3, 2 replicates per experiment, mean +/- SEM.* ***D)*** *Distribution of the relative frequency of mitochondrial volume. Kolmogorov-Smirnov test, p≤ 0.05, n=3* ***E)*** *Representative super resolution images of astrocytic mitochondria stained with mitochondrial marker ToMM20. Cytosol (CellTracker Green CMFDA, 516nm) is pseudo colored in magenta and mitochondria in yellow (ToMM20, 647nm). Scale bar 10µm.*

Glutamate does not alter mitochondrial turnover rate

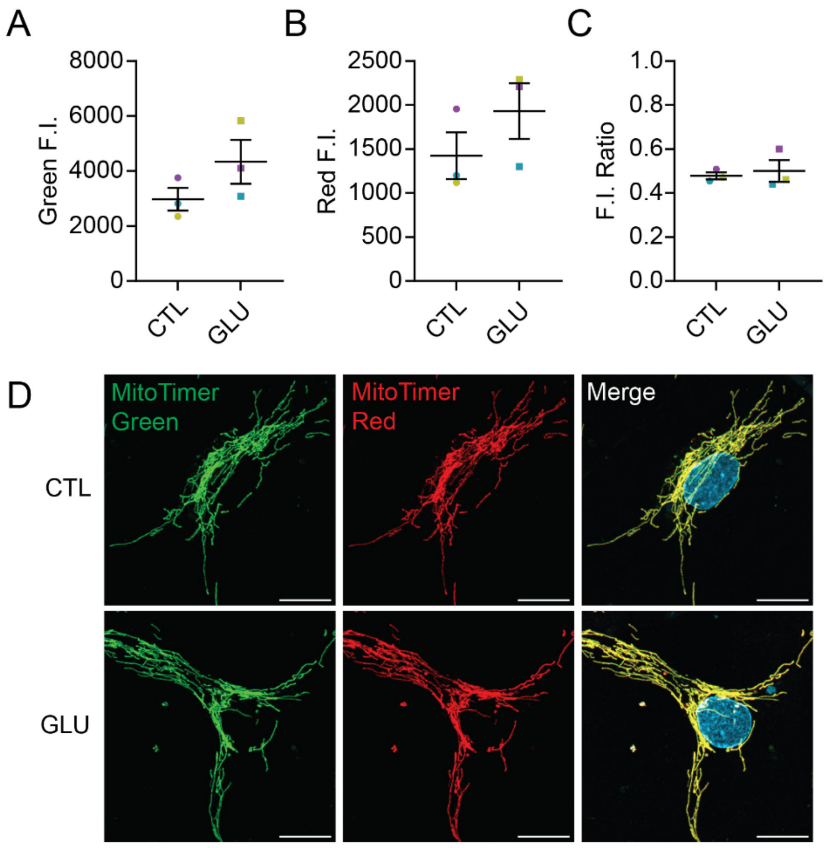

Figure 27. Glutamate does not alter mitochondrial turnover.

A) *Fluorescence intensity on the green channel of control and glutamate-treated astrocytes. Unpaired t-test, p≤ 0.05, n=3, 2 replicates, mean +/- SEM.* ***B)*** *Fluorescence intensity on the red channel of control and glutamate-treated. Unpaired t-test, p≤ 0.05, n=3, 2 replicates, mean +/- SEM.* ***C)*** *Ratio of Green/Red fluorescence intensity. Unpaired t-test, p≤ 0.05, n=3, 2 replicates, mean +/- SEM.* ***D)*** *Representative images of astrocytes transfected with MitoTimer in both control and glutamate groups. Scale bar 10μM.*

Since we observed decreased autophagy inductions and increased mitochondrial quantity, we wondered whether these changes would alter mitochondria turnover as mitochondrial biogenesis and mitophagy are key regulators of mitochondrial turnover and health. To test this, we transfected our astrocytes with doxycycline-induced MitoTimer (*210*, *211*), a mitochondrially-targeted fluorescent protein that shifts from green to red over time. By inducing two pulses, this allowed us to, in the first pulse to identify all “old” mitochondria in the red channel while our second pulse (48 hours later) was performed

to identify both the “new” mitochondria as well as the import of MitoTimer into currently functional mitochondria in the green channel. During our second pulse, we also treated astrocytes with or without glutamate, allowing us to compare whether glutamate changed the rate of degradation of “old” mitochondria. We can also determine whether glutamate altered the mitochondrial turnover by calculating the ratio of “new/functional” mitochondria over “old/non-functional”.

Glutamate treatment did not affect either the import of MitoTimer into the mitochondria (Figure 27A, D) nor mitochondrial degradation (Figure 27B, D), resulting in no significant change in the ratio of mitochondrial turnover (Figure 27C). These results suggest that glutamate treatment does not alter mitochondrial dynamics, rather, may be sustaining the balance of this dynamics in spite of significant mitochondrial activity. This is further supported by the decreased ROS and the lack of accumulation of toxic acylcarnitine species.

Chapter 4: Discussion

Summary

Astrocytes can store excess fatty acids in lipid droplets to avoid lipotoxicity. Fatty acids can be released from lipid droplets and catabolized to generate energy in the mitochondria. We previously found reduced astrocytic lipid droplets and increased transport of fatty acids into the mitochondria in response to glutamate, the major excitatory neurotransmitter in the brain. But whether glutamate affects fatty acid catabolism and how glutamate regulates lipid droplet homeostasis in astrocytes is unknown. Here, we show that astrocytes use glutamate directly as fuel for increased oxidative phosphorylation while decreasing their use of glycolysis for ATP production. Importantly, glutamate had no affect on fatty acid catabolism in mitochondria. Instead, increased fatty acid transport is likely used for mitochondria maintenance as we found decreased reactive oxygen species with a concomitant increase in mitochondrial mass upon glutamate treatment. Consistent, with healthier mitochondria, glutamate increased AMPK phosphorylation, supressed the induction of autophagy which ultimately reduced the flux of lipids into lipid droplets. Altogether, this study reveals how astrocytes regulate fatty acid homeostasis in response to glutamate.

Effects of culture media on astrocyte physiology

Previous work showing that astrocytes alter lipid homeostasis in response to glutamate were performed in serum-containing cultures. We confirmed that astrocytes grown in the absence of serum (*205*, *206*, *218*) also respond to glutamate by reducing the number of lipid droplets and increasing lipid transport into the mitochondria (*50*). This is important as most studies used cultured astrocytes grown in serum. However, transcriptomic analysis has identified astrocytes grown in serum as reactive (*219–221*) Compared to acutely isolated astrocytes, serum-gown astrocytes present significant alterations in gene expression (*205*, *222*) that indicate a reactive state that occurs during physiological stress and disease (*219*). Reactive astrocytes have different metabolism (*223–225*) and function (*188*, *189*, *226–229*) than resting state astrocytes in the brain. Multiple reactive astrocytic states exist that are dependent on the insult type and severity (*219*), which might result

in differences in their metabolic programming. The effects of glutamate on lipid metabolism in astrocytes grown with or without serum suggests that this signalling pathway may be unaffected by astrocyte activation. However, further research is needed to test this possibility directly, since lipid metabolism and mitochondria-related gene expression is altered in reactive astrocytes (*219*).

Glutamatergic receptors in fatty acid homeostasis

Defining the pathways activated by glutamate is key to understanding how it can be modulated. We showed that the effects of glutamate on lipid metabolism are independent of glutamate import through EAATs. This points to the regulation of lipid homeostasis via signaling pathways likely activated downstream of glutamatergic receptors.

Since astrocytes were treated with exogenous glutamate, we suspect that glutamatergic neuronal activity in the brain might have similar effects as we have reported in here. However, further research using astrocyte-neuron co-cultures might address this question.

An important limitation of our study is that we have yet to determine which glutamate receptor(s) are involved in regulating lipid droplets. Previous work from our lab using serum-containing astrocytes found that activation of the NMDA receptor with glutamate agonist NMDA also reduced lipid droplets (*50*). NMDA receptor subunits have been detected in astrocytes at the mRNA and protein levels by multiple studies (*230*–*232*). However, their function in astrocytes is still heavily debated (*12*, *232*–*238*). For example, one study showed that mechanically-isolated astrocytes responded to NMDA by generating inward currents that were blocked by the NMDA receptor antagonist AP5 (*238*), but another study showed that in cell cultures with advantageous conditions for NMDA activation, no currents were detected (*235*). Moreover, recent studies have identified that NMDA receptors present metabotropic-like activity (*239*), as block of ion flow of the NMDA receptor through NMDA receptor antagonists still induced NMDA-dependent shrinkage and retraction of dendritic spines (*239*). Another possibility is that different culture conditions affect the expression of NMDA receptor subunits. For example, the expression of multiple NMDA receptor subunits is affected by the presence of neurons in the culture (*200*, *231*). It is likely that the presence of serum (and likely

reactive state) and/or contaminating cell types in these cultures accounts for the differences in NMDA's affects on lipid metabolism. More work is needed to determine the role(s) of NMDA on astrocytic metabolism during different physiological states.

Another consideration is the potential role of glutamate on system xc^-. System xc^- is a Na^+-dependent cystine/glutamate antiporter that transports cystine into astrocytes and exports glutamate into the extracellular space (*240*). However, system xc^- is not sufficient to counteract the glutamate import through EAATs as we see a net influx of glutamate into astrocytes (Figure 21A). Alternatively, high concentrations of extracellular glutamate, such as those seen during excitotoxicity, can reverse the system xc^- function (*241*, *242*). However, reversal of xc^- function is associated with ferroptotic cell death (*243*), which includes increased oxidative stress, fragments and reduced mitochondrial mass (*242*, *244*, *245*). Since we use physiological concentrations of glutamate, and observe decreased oxidative stress and increased mitochondrial mass, it is unlikely that transport through system xc^- is being altered.

Finally, neurotransmitters in addition to glutamate could affect lipid metabolism. However very few studies exist on this topic. For example, lipid droplet accumulation was induced by treating astrocytes with noradrenaline, which activates adrenergic GPCR receptors α_2 and $\beta_{1\text{-}3}$ (*204*). This indicates that astrocyte lipid metabolism can respond to multiple neurotransmitters.

Glutamate treatment correlates with the activation of signaling pathways involved in astrocytic fatty acid homeostasis

We next examined the effect of glutamate on metabolic signalling in astrocytes. We found that glutamate treatment correlated with the activation of AMPK and ACC. Our results are in line with multiple studies showing that phosphorylation of AMPK induces ACC phosphorylation (*191*, *195*, *198*, *199*, *246–248*). Further experiments are needed to confirm if AMPK directly activates ACC in astrocytes, or whether additional signalling pathways are involved (*196*, *249*).

Since ACC can regulate the transport of fatty acids into the mitochondria, this might explain why we observe increase fatty acid content in mitochondria (Figure 19D-F). As

explained previously, malonyl-CoA produced by ACC2 inhibits CPT-1 (*195*), the main transporter of long-chain fatty acids into the mitochondria (*191*). ACC2 is inactivated by phosphorylation, thereby allowing CPT-1 to import fatty acids into the mitochondria (*176*, *191*). Fatty acids imported into the mitochondria can then enter the β-oxidation pathway, or alternatively can be used for the turnover of mitochondrial phospholipids such as cardiolipin (*250*, *251*). As discussed in more detail below, we believe glutamate is stimulating fatty acid import to support the latter.

One limitation in our experiment is that the antibodies used against ACC and phospho-ACC recognize both isoforms of ACC: ACC1 and ACC2. This is important because these isoforms serve different functions in regulating metabolism (*248*). Like ACC2, ACC1 also produces malonyl-CoA but uses this as a substrate for the *de novo* synthesis of long-chain fatty acids (*198*). Lack of *de novo* synthesis by phosphorylation of ACC2 could also explain the observed changes in lipid droplet numbers in response to glutamate. Although we cannot differentiate between ACC1 and ACC2 in our blots, we speculate that the effects are not likely through ACC1 as we observed no difference in free fatty acids of any chain length by lipidomics. This limitation however could be tested directly using either isoform-specific ACC antibodies or using specific inhibitors of ACC1 or ACC2 activity.

Astrocytes catabolize lipid droplets at a steady state

We also explored the mechanisms through which astrocytic lipid droplets release fatty acids. Since our previous studies showed that lipophagy was not involved in lipid droplet catabolism in response to glutamate (*50*), we tested the role of the triglyceride lipase DDHD2. We found that lipid droplets grew in both size and number with DDHD2 inhibition. This occurred in both control and glutamate treated cells. By promoting efflux of fatty acids from lipid droplets, neutral lipolysis results in smaller lipid droplets (*252*). Indeed, inhibition of DDHD2 resulted in larger lipid droplets consistent with reduced lipid efflux (*252*). We reasoned that if glutamate acted directly on lipases, that it would also influence lipid droplet size, but this was not the case. Lipid droplet size was unaffected by glutamate treatment. Therefore, we drew two conclusions from these experiments: first, that DDHD2 is the main triglyceride lipase in astrocytes as it is constitutively catabolizing triglycerides

from lipid droplets; second, that glutamate is acting on lipid droplet homeostasis independent of lipase activity.

ATGL/PNPLA2 is the main triglyceride lipase in other lipid-enriched cell types like adipocytes and hepatocytes (*79*, *95*, *253*, *254*), but recent literature points out that this is not the case in the brain (*93*, *94*). Recent evidence has also confirmed that ATGL is not the main triglyceride lipase in the brain, as treatment with ATGListatin (an inhibitor of ATGL) did not induce significant accumulation of triacylglycerols (*255*), however, ATGL was found to interact with DDHD2 and potentiate its effect in neurons (*255*). Thus, ATGL might be a modulator of DDHD2 activity in astrocytes, prompting further research to determine if this interaction is happening in astrocytes.

Effect of glutamate on ATP production

Seeing the effects of glutamate on lipid droplet homeostasis as well as the increased transport of lipids into the mitochondria, we then analyzed the effects of glutamate on astrocyte mitochondrial energy dynamics. We originally hypothesized that the increased transport of fatty acids into the mitochondria would lead to increased ATP production from mitochondrial fatty acid oxidation. However, our results showed that while glutamate increased ATP production, this was not from the oxidation of fatty acids. Rather, an analysis of mitochondrial fuel consumption showed that astrocytes use glutamate as a substrate for mitochondrial oxidation with a concurrent reduction in the use of glucose.

The increased ATP production rate in response to glutamate is consistent with previous work (*45*, *130*, *165*, *256*, *257*). Neuronal activity increases astrocyte energetic demand, as glutamate clearance by astrocytes results in increased activity of the Na^+/K^+ ATPase pump and the Na^+/Ca^+ exchanger (NCX) to maintain ion homeostasis (*43*–*45*, *258*). Since the activity of the Na^+/K^+ ATPase pump is ATP-dependent, astrocytes must increase ATP production to sustain the pump's activity (*43*–*45*, *258*). Interestingly, ATP can also be incorporated into vesicles and released into the extracellular space where is acts as a neuromodulator (*259*–*265*). Several groups have described the ability of glutamate to trigger ATP released from astrocytes (*260*, *261*, *263*, *266*–*270*).

One limitation regarding extracellular flux analysis is that it does not directly measure the transport and utilization of glucose. Instead, the oxygen consumption rate (OCR) and the acidification of the media (ECAR), are used to estimate metabolic activity (*271*, *272*). In the case of ECAR, it can represent both mitochondrial (through the release of CO_2 and formation of H^+ and HCO_3) and glycolytic activity (through lactate production which releases H^+ to the extracellular media) (*271–273*). Although the mitochondrial contribution to media acidification is factored in using a CO_2 Contribution Factor (*273*), the contribution of CO_2 from other non-glycolytic pathways cannot be completely discarded (*271*, *272*).

To address these limitations of the extracellular flux analysis, further experiments could be used to confirm the effects on ATP. To measure increase in ATP levels, we could use commercially available kits to detect the ATP/ADP ratio in control versus glutamate-treated astrocytes + inhibitors of each pathway to assess changes in this ratio. Another option could be transfecting astrocytes with an ATP biosensor based on fluorescence intensity known as iATPSnFR (*274*).

Effects of glutamate on glucose utilization

Our finding that glutamate reduced both aerobic and anaerobic glycolysis was unexpected as several early papers describe astrocytes as a constitutively glycolytic cell type (*4*, *5*, *45*, *130*, *257*, *275*) and inhibition of the electron transport chain in astrocytes did not affect survival in comparison to neurons (*275*). There is considerable evidence that glutamate upregulates glucose transport, glycolytic activity and even inhibits OXPHOS in astrocytes (*38*, *39*, *44*, *45*, *118*, *130*, *257*, *276*). This results in diverting pyruvate away from the mitochondria and instead towards the production and release of lactate (*42*, *45*) to support neuronal activity. However, these findings can be challenged, as there is evidence for non-existent or even decreased glucose utilization and increased glutamate utilization in astrocytes (*116*, *256*, *277*). Other studies have also shown that glutamate effectively competes with glucose as a substrate for OXPHOS (*116*, *278*, *279*). To further confirm the decrease in glycolytic activity, we could directly measure a) extracellular glucose concentrations before and after glutamate treatment, b) lactate concentrations before and after glutamate treatment, c) activity of glycolytic enzymes like

hexokinase, phosphofructokinase or pyruvate kinase, or d) use ^{13}C-labeled glucose and quantify ^{13}C in glycolytic metabolites by mass spectrometry.

To our knowledge, this is the first report of the effect of glutamate in serum free media, where astrocytes more closely resemble astrocytes at steady state. It is possible that these metabolic changes reflect differences in the way physiological and reactive astrocytes respond to the stimulus (*223*–*225*). Further studies of astrocyte metabolism are needed to better understand the effect of glutamate on astrocyte metabolism.

Effects of glutamate on fatty acid utilization

Inhibiting of the transport of medium and long chain fatty acids into the mitochondria did not affect glutamate-induced mitochondrial ATP or fatty acid oxidation. This was confirmed by our targeted lipidomics, were we observed no changes in medium and long chain free fatty acids. This was unexpected given the increased transport of fatty acids into the mitochondria in response to glutamate. We confirmed that astrocytes metabolize fatty acids in a basal state which is consistent with reports that astrocytes possess all the machinery needed to perform fatty acid oxidation (*280*–*282*) and that astrocytes functionally metabolize fatty acids (*186*, *190*, *281*, *283*–*285*), more specifically, of medium- and long-chain fatty acids (*138*, *281*, *284*, *285*). However, their dependency and capacity to oxidize fatty acids remains lower than other energy substrates regardless of glutamate treatment.

One limitation of these experiments is the use of etomoxir to inhibit CPT-1, the main transporter of fatty acids into the mitochondria. CPT-1 preferentially transports acyl chains from C:6 to C:18 (*77*, *171*–*173*), while fatty acids with shorter chains freely diffuse into the mitochondria (*65*, *66*, *68*–*70*) where they eventually get trapped via acylation (*77*). Our lipidomic experiments have a similar limitation in that we were unable to measure short-chain fatty (<C:8). This may be due to evaporation of SCFA as volatile compounds during the process of lipid extraction and concentration (*286*). Since we were unable to assess the impact of glutamate on SCFA, we cannot draw conclusions on the contribution of its oxidation. To address this limitation, we could inhibit β-oxidation directly by treating astrocytes with 4-bromocromotic acid (*287*, *288*) or ranolazine (*289*–*291*), compounds that inhibit the 3-Ketoacyl CoA thiolases. Regardless of whether there are affects on the

oxidation of SCFA, glutamate still increased the import of RedC12, a C:12 medium chain fatty acid.

The role for fatty acid import into astrocytic mitochondrial in the absence of oxidation remains relatively unexplored. Blocking fatty acid entry into the mitochondria via etomoxir in addition to lipid overload induces astrocyte reactivity and cognitive impairment (*133*) Another report using CPT1A knockout animals had increased formation of mitochondrial super complexes (*292*). Increased mitochondrial supercomplexes decrease ROS production, increase basal respiration, and increase mitochondrial oxygen consumption (*150*, *292*). They propose that fatty acid oxidation, through a yet unidentified mechanism, maintains the astrocytic ETC in an inefficient conformation that favours ROS production (*150*, *292*). This finding might explain the inflexibility of fatty acid oxidation, as mitochondria may maintain a minimum amount of ROS production necessary for ROS signalling to occur.

Glutamate as a direct energy substrate

Rather than fatty acid oxidation, we found that glutamate was used as the fuel for increased ATP production. This occurs at the expense of glucose metabolism. After being transported into astrocytes, glutamate can follow two main metabolic pathways: a) conversion into glutamine and released, b) converted to α-ketoglutarate by glutamate dehydrogenase or via transamination enzymes for partial or complete oxidation (*158*, *159*). Previous work shows that as glutamate concentration increases, it is consumed by mitochondrial oxidation until saturation of the transamination enzymes (*19*, *159*, *168*, *293*). If the exposure to glutamate remains elevated or is repetitive, its usage is directed towards conversion into glutamine via glutamine synthetase and later released (*21*, *22*, *294*). This would explain our observation that glutamate treatment resulted in increased mitochondrial oxidation (*256*, *295*), as our single-dose glutamate treatment would be directed towards the TCA cycle (*19*, *158*, *159*, *168*, *293*) as oxidation of highly available glutamate can occur in a quick and effective manner (*131*, *158*, *294*, *295*). If we would treat at higher doses and longer time, we would then expect that prolonged glutamate treatment would eventually increase the proportion of glutamine conversion and subsequent release (*294*).

Effect of glutamate on mitochondrial maintenance

Since glutamate-induced fatty acid import into mitochondria did not contribute to ATP production, it must play a different role. Analysis of mitochondrial morphology showed that glutamate increased mitochondrial quantity and mass. These changes in mitochondrial morphology were paired with an overall decrease in short chain acylcarnitines, decreased autophagy induction and decreased production of ROS.

There is sparse literature on the effects of glutamate on mitochondrial morphology in astrocytes. Some research shows that glutamate induces increased cell volume and increased mitochondrial volume without changing quantity due to swelling (*296*, *297*). These effects are temporary, and recovery is mostly achieved at 24 hours (*296*, *297*). The effects are dose dependent: higher glutamate doses induce higher swelling (*298*). Most of the studies that found glutamate-induced swelling, they were performed using cytotoxic concentrations of glutamate (≥5 mM), which would represent a state of pathophysiological activity levels. In contrast, the dose used in our research (100 μM) is well within the range of physiological glutamatergic neuronal activity (*299*, *300*), and we observed no change in cell volume (Figure 26B).

Increased mitochondrial mass could be a result of PGC1α activity, as it is a regulates signalling pathways that result in adaptation to high energy demands (*301*), including mitochondrial biogenesis (*302*). PGC1α is a tightly controlled gene that uses multiple promoters in addition to alternative splicing to generate multiple variants (>10), even brain-specific ones (*301*). Despite the importance of the role of PGC1α in multiple tissues, studies on role of PGC1α in the brain are sparse (*303*). Recently, expression of PGC1α-2 and PGC-1α-3 have been linked to the progression of reactive astrocytes (*304*). However, more research is needed to determine the activity and role of the multiple PGC1α variants in astrocytes responding to glutamate.

Our finding that glutamate reduces autophagy induction was unexpected, as glutamate induces autophagy in a dose and time dependent manner (*305*–*310*). Low glutamate doses (10 μM) transiently induce autophagy (*306*), however these studies were performed in immortalized astrocyte and neural cells. Therefore, its possible the

difference lies in the model system used. In that same study, glutamate also induced AMPK and ACC phosphorylation, replicating a similar result as our research (*306*).

We also confirmed that medium to long chain acylcarnitines are not accumulating in the mitochondria which can be toxic (*77*, *214*, *311*, *312*). Instead, we found decreased short-chain acylcarnitines. This is consistent with a recent report showing decreased acylcarnitine content reduced ROS without altering OXPHOS capacity (*313*). This paired with recent evidence that cardiolipin and other phospholipids modulate the stability of the ETC (*314*–*317*), further suggesting that acylcarnitines and phospholipids modulate ETC coupling. These findings coincide with our observations regarding decreased ROS (Figure 25A-B) and increased ATP-linked respiration (Figure 19A), suggesting increased ETC coupling in astrocytes in response to glutamate. More research is needed to test the role of acylcarnitine in ETC coupling, as the role of acylcarnitines in the brain is relatively unexplored.

The role of glutamate-induced lipid trafficking into the mitochondria remains to be elucidated. One possibility is that with decreased ROS and autophagy, there is less need to turnover whole mitochondria by autophagy, which coincides with our observations where glutamate did not alter mitochondrial turnover (Figure 27A-D). At the same time, expansion of mitochondrial mass requires the generation of more phospholipids and/or turnover of lipids on the mitochondrial membrane. For example, fatty acids imported into the mitochondria can be used for the turnover of mitochondrial phospholipids such as cardiolipin on the inner mitochondrial membrane (*318*, *319*). Since Red-C12 fluorescent tracer can be processed into phospholipids (*320*) its possible that this is what we are detecting.

There is also evidence that lipid composition regulates mitochondrial function (*250*). Phospholipids like cardiolipin, phosphatidylcholine and phosphatidylethanolamine bind to complex I to modulate the complex integrity and activity (*321*). Moreover, phosphatidylethanolamine can also bind to complex II (*322*), III (*323*) and IV (*324*); cardiolipin binds to complex III (*317*), IV (*317*, *324*) and V (*325*); while phosphatidylcholine binds to complex IV (*324*). Both phosphatidylethanolamine and cardiolipin are relevant for supercomplex formation (*314*, *316*, *317*) and the regulation of proton leak (*314*–*316*,

326). This also supports the idea that the fatty acid influx might be an adaptive response to sustain mitochondrial activity and health.

Finally, it is also important to mention that these explanations are not mutually exclusive. Fatty acid trafficking into the mitochondria could be used at a low level of fuel for oxidation while much of the lipid trafficking might be directed towards other processes like the turnover of mitochondrial membrane lipids or the regulation of the formation of supercomplexes, thus sustaining the increased mitochondrial oxidation by enhancing ETC complex activity/efficiency. More research is needed to determine the role of lipid trafficking into the mitochondria.

Chapter 5: Conclusion

Overall, our results show that exogenous application of glutamate regulates astrocyte lipid homeostasis. We demonstrated that glutamate activates AMPK and ACC through a yet unidentified receptor, facilitating the transport of fatty acids into the mitochondria. We have also confirmed that DDHD2 is the main triglyceride lipase in astrocytes. Glutamate-induced transport of fatty acids into the mitochondria is paired with increased ATP production rates. However, this increased ATP production rate is independent of fatty acid oxidation. This suggests that the influx of fatty acids into the mitochondria might have a different role than energy production. Analysis of mitochondrial morphology showed that glutamate increased mitochondrial quantity and mass. Consistently, glutamate decreased autophagy induction and decreased production of ROS. This suggests that lipid influx into the mitochondria likely contributes to mitochondrial function maintenance and overall mitochondrial health.

While our research raises many new questions about the role and regulation of fatty acids in the mitochondria of astrocytes, this work provides new and exciting insight into how astrocyte lipid metabolism is regulated by glutamate.

References

1. J. W. Mink, R. J. Blumenschine, D. B. Adams, Ratio of central nervous system to body metabolism in vertebrates: its constancy and functional basis. *American Journal of Physiology-Regulatory, Integrative and Comparative Physiology* **241**, 203–212 (1981).

2. J. L. Stobart, C. M. Anderson, Multifunctional role of astrocytes as gatekeepers of neuronal energy supply. *Front Cell Neurosci* **7** (2013).

3. J. V Andersen, K. H. Markussen, E. Jakobsen, A. Schousboe, H. S. Waagepetersen, P. A. Rosenberg, B. I. Aldana, Glutamate metabolism and recycling at the excitatory synapse in health and neurodegeneration. *Neuropharmacology* **196**, 108719 (2021).

4. G. Bonvento, J. P. Bolaños, Astrocyte-neuron metabolic cooperation shapes brain activity. *Cell Metab* **33**, 1546–1564 (2021).

5. J. P. Bolaños, Bioenergetics and redox adaptations of astrocytes to neuronal activity. *J Neurochem* **139**, 115–125 (2016).

6. M. R. van Horn, N. J. Benfey, C. Shikany, L. J. Severs, T. Deemyad, Neuron-astrocyte networking: Astrocytes orchestrate and respond to changes in neuronal network activity across brain states and behaviors. *J Neurophysiol* **126**, 627–636 (2021).

7. J. Lines, E. D. Martin, P. Kofuji, J. Aguilar, A. Araque, Astrocytes modulate sensory-evoked neuronal network activity. *Nature Communications 2020 11:1* **11**, 1–12 (2020).

8. A. Gasiorowska, M. Wydrych, P. Drapich, M. Zadrozny, M. Steczkowska, W. Niewiadomski, G. Niewiadomska, The Biology and Pathobiology of Glutamatergic, Cholinergic, and Dopaminergic Signaling in the Aging Brain. *Front Aging Neurosci* **13**, 654931 (2021).

9. C. R. Rose, L. Felix, A. Zeug, D. Dietrich, A. Reiner, C. Henneberger, Astroglial glutamate signaling and uptake in the hippocampus. *Front Mol Neurosci* **10**, 332221 (2018).

10. L. C. Jansson, K. E. Åkerman, The role of glutamate and its receptors in the proliferation, migration, differentiation and survival of neural progenitor cells. *J Neural Transm* **121**, 819–836 (2014).

11. A. Verkhratsky, A. Chvátal, NMDA Receptors in Astrocytes. *Neurochemical Research 2019 45:1* **45**, 122–133 (2019).

12. K. Skowrońska, M. Obara-Michlewska, M. Zielińska, J. Albrecht, NMDA receptors in astrocytes: In search for roles in neurotransmission and astrocytic homeostasis. *Int J Mol Sci* **20**, 309 (2019).

13. P. Montes de Oca Balderas, Flux-independent NMDAR signaling: Molecular mediators, cellular functions, and complexities. *Int J Mol Sci* **19** (2018).

14. J. W. McDonald, W. H. Trescher, M. V. Johnston, Susceptibility of brain to AMPA induced excitotoxicity transiently peaks during early postnatal development. *Brain Res* **583**, 54–70 (1992).

15. A. M. Palmer, D. W. Marion, M. L. Botscheller, P. E. Swedlow, S. D. Styren, S. T. DeKosky, Traumatic Brain Injury-Induced Excitotoxicity Assessed in a Controlled Cortical Impact Model. *J Neurochem* **61**, 2015–2024 (1993).

16. A. Granzotto, L. M. T. Canzoniero, S. L. Sensi, A Neurotoxic Ménage-à-trois: Glutamate, Calcium, and Zinc in the Excitotoxic Cascade. Frontiers Media S.A. [Preprint] (2020). https://doi.org/10.3389/fnmol.2020.600089.

17. D. Bano, M. Ankarcrona, Beyond the critical point: An overview of excitotoxicity, calcium overload and the downstream consequences. Elsevier Ireland Ltd [Preprint] (2018). https://doi.org/10.1016/j.neulet.2017.08.048.

18. M. Ankarcrona, J. M. Dypbukt, E. Bonfoco, B. Zhivotovsky, S. Orrenius, S. A. Lipton, P. Nicotera, Glutamate-induced neuronal death: A succession of necrosis or apoptosis depending on mitochondrial function. *Neuron* **15**, 961–973 (1995).

19. M. McKenna, J. T. Tildon, J. H. Stevenson, X. Huang, New Insights into the Compartmentation of Glutamate and Glutamine in Cultured Rat Brain Astrocytes. *Dev Neurosci* **18**, 380–390 (1996).

20. H. A. Krebs, The synthesis of glutamine from glutamic acid and ammonia, and the enzymic hydrolysis of glutamine in animal tissues. *Biochemical Journal* **29**, 1951–1969 (1935).

21. S. Bröer, N. Brookes, Transfer of glutamine between astrocytes and neurons. *J Neurochem* **77**, 705–719 (2001).

22. L. K. Bak, A. Schousboe, H. S. Waagepetersen, The glutamate/GABA-glutamine cycle: aspects of transport, neurotransmitter homeostasis and ammonia transfer. *J Neurochem* **98**, 641–653 (2006).

23. J. V. Andersen, A. Schousboe, A. Verkhratsky, Astrocyte energy and neurotransmitter metabolism in Alzheimer's disease: Integration of the glutamate/GABA-glutamine cycle. *Prog Neurobiol* **217**, 102331 (2022).

24. Y. Yu, P. Herman, D. L. Rothman, D. Agarwal, F. Hyder, Evaluating the gray and white matter energy budgets of human brain function. *Journal of Cerebral Blood Flow and Metabolism* **38**, 1339–1353 (2018).

25. J. J. Harris, R. Jolivet, D. Attwell, Synaptic Energy Use and Supply. *Neuron* **75**, 762–777 (2012).

26. J. J. Harris, R. Jolivet, D. Attwell, Synaptic Energy Use and Supply. *Neuron* **75**, 762–777 (2012).

27. V. Rangaraju, N. Calloway, T. A. Ryan, Activity-Driven Local ATP Synthesis Is Required for Synaptic Function. *Cell* **156**, 825–835 (2014).

28. C. N. Hall, M. C. Klein-Flügge, C. Howarth, D. Attwell, Oxidative Phosphorylation, Not Glycolysis, Powers Presynaptic and Postsynaptic Mechanisms Underlying Brain Information Processing. *Journal of Neuroscience* **32**, 8940–8951 (2012).

29. G. A. Dienel, Energy Metabolism in the Brain. *From Molecules to Networks: An Introduction to Cellular and Molecular Neuroscience: Third Edition*, 53–117 (2014).

30. G. A. Dienel, Brain glucose metabolism: Integration of energetics with function. *Physiol Rev* **99**, 949–1045 (2019).

31. R. Daneman, A. Prat, The blood–brain barrier. *Cold Spring Harb Perspect Biol* **7**, a020412 (2015).

32. R. Daneman, The blood–brain barrier in health and disease. *Ann Neurol* **72**, 648–672 (2012).

33. M. P. Bordone, M. M. Salman, H. E. Titus, E. Amini, J. V. Andersen, B. Chakraborti, A. V. Diuba, T. G. Dubouskaya, E. Ehrke, A. Espindola de Freitas, G. Braga de Freitas, R. A. Gonçalves, D. Gupta, R. Gupta, S. R. Ha, I. A. Hemming, M. Jaggar, E. Jakobsen, P. Kumari, N. Lakkappa, A. P. L. Marsh, J. Mitlöhner, Y. Ogawa, P. R. Kumar, F. C. Ribeiro, A. Salamian, S. Saleem, S. Sharma, J. M. Silva, S. Singh, K. Sulakhiya, T. W. Tefera, B. Vafadari, A. Yadav, R. Yamazaki, C. I. Seidenbecher, The energetic brain – A review from students to students. Blackwell Publishing Ltd [Preprint] (2019). https://doi.org/10.1111/jnc.14829.

34. H. Koepsell, H. De, Glucose transporters in brain in health and disease. *Pflügers Archiv - European Journal of Physiology 2020 472:9* **472**, 1299–1343 (2020).

35. H. Al Feteisi, Z. M. Al-Majdoub, B. Achour, N. Couto, A. Rostami-Hodjegan, J. Barber, Identification and quantification of blood-brain barrier transporters in isolated rat brain microvessels. *J Neurochem* **146**, 670–685 (2018).

36. K. A. Nałęcz, Solute Carriers in the Blood–Brain Barier: Safety in Abundance. *Neurochemical Research 2016 42:3* **42**, 795–809 (2016).

37. Y. T. K. Nguyen, H. T. T. Ha, T. H. Nguyen, L. N. Nguyen, The role of SLC transporters for brain health and disease. *Cellular and Molecular Life Sciences* **79**, 1–21 (2022).

38. O. H. Porras, I. Ruminot, A. Loaiza, L. F. Barros, Na+-Ca2+ cosignaling in the stimulation of the glucose transporter GLUT1 in cultured astrocytes. *Glia* **56**, 59–68 (2008).

39. A. Loaiza, O. H. Porras, L. F. Barros, Glutamate Triggers Rapid Glucose Transport Stimulation in Astrocytes as Evidenced by Real-Time Confocal Microscopy. *Journal of Neuroscience* **23**, 7337–7342 (2003).

40. A. Almeida, J. Almeida, J. P. Bolaños, S. Moncada, Different responses of astrocytes and neurons to nitric oxide: The role of glycolytically generated ATP in astrocyte protection. *Proc Natl Acad Sci U S A* **98**, 15294–15299 (2001).

41. A. Tabernero, C. Vicario, J. M. Medina, Lactate spares glucose as a metabolic fuel in neurons and astrocytes from primary culture. *Neurosci Res* **26**, 369–376 (1996).

42. L. Pellerin, G. Pellegri, P. G. Bittar, Y. Charnay, C. Bouras, J. L. Martin, N. Stella, P. J. Magistretti, Evidence Supporting the Existence of an Activity-Dependent Astrocyte-Neuron Lactate Shuttle. *Dev Neurosci* **20**, 291–299 (1998).

43. L. Pellerin, P. J. Magistretti, Glutamate Uptake Stimulates Na+,K+-ATPase Activity in Astrocytes via Activation of a Distinct Subunit Highly Sensitive to Ouabain. *J Neurochem* **69**, 2132–2137 (1997).

44. L. Pellerin, P. J. Magistretti, Excitatory Amino Acids Stimulate Aerobic Glycolysis in Astrocytes via an Activation of the Na+/K+ ATPase. *Dev Neurosci* **18**, 336–342 (1996).

45. L. Pellerin, P. J. Magistretti, Glutamate uptake into astrocytes stimulates aerobic glycolysis: a mechanism coupling neuronal activity to glucose utilization. *Proceedings of the National Academy of Sciences* **91**, 10625–10629 (1994).

46. M. Zonta, M. C. Angulo, S. Gobbo, B. Rosengarten, K. A. Hossmann, T. Pozzan, G. Carmignoto, Neuron-to-astrocyte signaling is central to the dynamic control of brain microcirculation. *Nat Neurosci* **6**, 43–50 (2002).

47. T. Takano, G. F. Tian, W. Peng, N. Lou, W. Libionka, X. Han, M. Nedergaard, Astrocyte-mediated control of cerebral blood flow. *Nat Neurosci* **9**, 260–267 (2005).

48. A. Devor, P. Tian, N. Nishimura, I. C. Teng, E. M. C. Hillman, S. N. Narayanan, I. Ulbert, D. A. Boas, D. Kleinfeld, A. M. Dale, Suppressed Neuronal Activity and Concurrent Arteriolar Vasoconstriction May Explain Negative Blood Oxygenation Level-Dependent Signal. *Journal of Neuroscience* **27**, 4452–4459 (2007).

49. S. J. Mulligan, B. A. MacVicar, Calcium transients in astrocyte endfeet cause cerebrovascular constrictions. *Nature* **431**, 195–199 (2004).

50. M. S. Ioannou, J. Jackson, S. H. Sheu, C. L. Chang, A. V. Weigel, H. Liu, H. A. Pasolli, C. S. Xu, S. Pang, D. Matthies, H. F. Hess, J. Lippincott-Schwartz, Z. Liu, Neuron-Astrocyte Metabolic Coupling Protects against Activity-Induced Fatty Acid Toxicity. *Cell* **177**, 1522-1535.e14 (2019).

51. C. C. C. R. De Carvalho, M. J. Caramujo, The Various Roles of Fatty Acids. *Molecules* **23**, 2583 (2018).

52. F. Kamp, H. V. Westerhoff, J. A. Hamilton, Movement of Fatty Acids, Fatty Acid Analogues, and Bile Acids across Phospholipid Bilayers. *Biochemistry* **32**, 11074–11085 (1993).

53. F. Kamp, D. Zakim, F. Zhang, N. Noy, J. A. Hamilton, Fatty Acid Flip-Flop in Phospholipid Bilayers Is Extremely Fast. *Biochemistry* **34**, 11928–11937 (1995).

54. R. W. Mitchell, G. M. Hatch, Fatty acid transport into the brain: Of fatty acid fables and lipid tails. *Prostaglandins, Leukotrienes and Essential Fatty Acids (PLEFA)* **85**, 293–302 (2011).

55. D. Samovski, M. Jacome-Sosa, N. A. Abumrad, Fatty Acid Transport and Signaling: Mechanisms and Physiological Implications. *Annu Rev Physiol* **85**, 317–337 (2023).

56. B. A. Fitscher, H. D. Riedel, K. C. Young, W. Stremmel, Tissue distribution and cDNA cloning of a human fatty acid transport protein (hsFATP4). *Biochimica et Biophysica Acta (BBA) - Gene Structure and Expression* **1443**, 381–385 (1998).

57. N. A. Abumrad, M. R. El-Maghrabi, E. Z. Amri, E. Lopez, P. A. Grimaldi, Cloning of a rat adipocyte membrane protein implicated in binding or transport of long-chain fatty acids that is induced during preadipocyte differentiation. Homology with human CD36. *Journal of Biological Chemistry* **268**, 17665–17668 (1993).

58. A. W. Zimmerman, H. T. B. Van Moerkerk, J. H. Veerkamp, Ligand specificity and conformational stability of human fatty acid-binding proteins. *Int J Biochem Cell Biol* **33**, 865–876 (2001).

59. Y. Owada, T. Yoshimoto, H. Kondo, Increased expression of the mRNA for brain- and skin-type but not heart-type fatty acid binding proteins following kainic acid systemic administration in the hippocampal glia of adult rats. *Molecular Brain Research* **42**, 156–160 (1996).

60. J. H. Veerkamp, A. W. Zimmerman, Fatty acid-binding proteins of nervous tissue. *Journal of Molecular Neuroscience* **16**, 133–142 (2001).

61. Y. Owada, T. Yoshimoto, H. Kondo, Spatio-temporally differential expression of genes for three members of fatty acid binding proteins in developing and mature rat brains. *J Chem Neuroanat* **12**, 113–122 (1996).

62. C. A. F. Kuate, O. Ebenhöh, B. M. Bakker, A. Raguin, Kinetic data for modeling the dynamics of the enzymes involved in animal fatty acid synthesis. *Biosci Rep* **43** (2023).

63. I. M. López-Lara, O. Geiger, “Formation of Fatty Acids” in *Biogenesis OfFatty Acids, Lipids and Membranes* (ed. 1, 2019; https://doi.org/10.1007/978-3-319-50430-8_5)vol. 1, pp. 43–55.

64. P. Paiva, F. E. Medina, M. Viegas, P. Ferreira, R. P. P. Neves, J. P. M. Sousa, M. J. Ramos, P. A. Fernandes, Animal Fatty Acid Synthase: A Chemical Nanofactory. *Chem Rev* **121**, 9502–9553 (2021).

65. E. D. Lewandowski, R. K. Kudej, L. T. White, J. M. O’Donnell, S. F. Vatner, Mitochondrial Preference for Short Chain Fatty Acid Oxidation During Coronary Artery Constriction. *Circulation* **105**, 367–372 (2002).

66. A. P. Halestrap, Pyruvate and ketone-body transport across the mitochondrial membrane. Exchange properties, pH-dependence and mechanism of the carrier. *Biochemical Journal* **172**, 377–387 (1978).

67. P. Rinaldo, D. Matern, M. J. Bennett, Fatty acid oxidation disorders. *Annu Rev Physiol* **64**, 477–502 (2002).

68. P. Schönfeld, L. Wojtczak, Short- and medium-chain fatty acids in energy metabolism: the cellular perspective. *J Lipid Res* **57**, 943 (2016).

69. J. M. O’Donnell, N. M. Alpert, L. T. White, E. Douglas Lewandowski, Coupling of mitochondrial fatty acid uptake to oxidative flux in the intact heart. *Biophys J* **82**, 11–18 (2002).

70. A. N. Carley, S. K. Maurya, M. Fasano, Y. Wang, C. H. Selzman, S. G. Drakos, E. D. Lewandowski, Short-Chain Fatty Acids Outpace Ketone Oxidation in the Failing Heart. *Circulation* **143**, 1797–1808 (2021).

71. B. Mesmin, D. Kovacs, G. D’Angelo, Lipid exchange and signaling at ER–Golgi contact sites. Elsevier Ltd [Preprint] (2019). https://doi.org/10.1016/j.ceb.2018.10.002.

72. Y. C. Wong, S. Kim, W. Peng, D. Krainc, Regulation and Function of Mitochondria–Lysosome Membrane Contact Sites in Cellular Homeostasis. *Trends Cell Biol* **29**, 500–513 (2019).

73. M. Hugenroth, M. Bohnert, Come a little bit closer! Lipid droplet-ER contact sites are getting crowded. *Biochim Biophys Acta Mol Cell Res* **1867** (2020).

74. J. A. Olzmann, P. Carvalho, Dynamics and functions of lipid droplets. *Nat Rev Mol Cell Biol* **20**, 137–155 (2019).

75. A. J. Mathiowetz, J. A. Olzmann, Lipid droplets and cellular lipid flux. *Nature Cell Biology 2024 26:3* **26**, 331–345 (2024).

76. J. Füllekrug, R. Ehehalt, M. Poppelreuther, Outlook: Membrane junctions enable the metabolic trapping of fatty acids by intracellular acyl-CoA synthetases. *Front Physiol* **3 OCT**, 32140 (2012).

77. M. Dambrova, M. Makrecka-Kuka, J. Kuka, R. Vilskersts, D. Nordberg, M. M. Attwood, S. Smesny, Z. Duygu Sen, A. Chi Guo, E. Oler, S. Tian, J. Zheng, D. S. Wishart, E. Liepinsh, H. B. Schi, C. Acg, Acylcarnitines: Nomenclature, Biomarkers, Therapeutic Potential, Drug Targets, and Clinical Trials. doi: 10.1124/pharmrev.121.000408 (2022).

78. T. J. Grevengoed, E. L. Klett, R. A. Coleman, Acyl-CoA metabolism and partitioning. *Annu Rev Nutr* **34**, 1–30 (2014).

79. Y. Guo, K. R. Cordes, R. V. Farese, T. C. Walther, Lipid droplets at a glance. *J Cell Sci* **122**, 749–752 (2009).

80. D. A. Gross, D. L. Silver, Cytosolic lipid droplets: From mechanisms of fat storage to disease. Informa Healthcare [Preprint] (2014). https://doi.org/10.3109/10409238.2014.931337.

81. A. Pol, S. P. Gross, R. G. Parton, Biogenesis of the multifunctional lipid droplet: Lipids, proteins, and sites. Rockefeller University Press [Preprint] (2014). https://doi.org/10.1083/jcb.201311051.

82. M. A. Roberts, J. A. Olzmann, Protein Quality Control and Lipid Droplet Metabolism. *Annu Rev Cell Dev Biol* **36**, 115–139 (2020).

83. Y. Ogasawara, T. Tsuji, T. Fujimoto, Multifarious roles of lipid droplets in autophagy – Target, product, and what else? *Semin Cell Dev Biol*, doi: 10.1016/j.semcdb.2020.02.013 (2020).

84. T. B. Nguyen, S. M. Louie, J. R. Daniele, Q. Tran, A. Dillin, R. Zoncu, D. K. Nomura, J. A. Olzmann, DGAT1-Dependent Lipid Droplet Biogenesis Protects Mitochondrial Function during Starvation-Induced Autophagy. *Dev Cell* **42**, 9-21.e5 (2017).

85. G. L. McLelland, M. Lopez-Osias, C. R. C. Verzijl, B. D. Ellenbroek, R. A. Oliveira, N. J. Boon, M. Dekker, L. G. van den Hengel, R. Ali, H. Janssen, J. Y. Song, P. Krimpenfort, T. van Zutphen, J. W. Jonker, T. R. Brummelkamp, Identification of an alternative triglyceride biosynthesis pathway. *Nature* **621**, 171–178 (2023).

86. M. Korber, I. Klein, G. Daum, Steryl ester synthesis, storage and hydrolysis: A contribution to sterol homeostasis. *Biochimica et Biophysica Acta (BBA) - Molecular and Cell Biology of Lipids* **1862**, 1534–1545 (2017).

87. J. A. Hamilton, D. M. Small, Solubilization and localization of triolein in phosphatidylcholine bilayers: a 13C NMR study. *Proceedings of the National Academy of Sciences* **78**, 6878–6882 (1981).

88. N. T. Nettebrock, M. Bohnert, Born this way – Biogenesis of lipid droplets from specialized ER subdomains. *Biochim Biophys Acta Mol Cell Biol Lipids* **1865** (2020).

89. A. Grippa, L. Buxó, G. Mora, C. Funaya, F. Z. Idrissi, F. Mancuso, R. Gomez, J. Muntanyà, E. Sabidó, P. Carvalho, The seipin complex Fld1/Ldb16 stabilizes ER-lipid droplet contact sites. *Journal of Cell Biology* **211**, 829–844 (2015).

90. H. Wang, M. Becuwe, B. E. Housden, C. Chitraju, A. J. Porras, M. M. Graham, X. N. Liu, A. R. Thiam, D. B. Savage, A. K. Agarwal, A. Garg, M. J. Olarte, Q. Lin, F. Frohlich, H. K. Hannibal-Bach, S. Upadhyayula, N. Perrimon, T. Kirchhausen, C. S.

Ejsing, T. C. Walther, R. V. Farese, Seipin is required for converting nascent to mature lipid droplets. *Elife* **5** (2016).

91. M. Henne, J. M. Goodman, H. Hariri, Spatial compartmentalization of lipid droplet biogenesis. *Biochim Biophys Acta Mol Cell Biol Lipids* **1865** (2020).

92. R. Zechner, F. Madeo, D. Kratky, Cytosolic lipolysis and lipophagy: Two sides of the same coin. *Nat Rev Mol Cell Biol* **18**, 671–684 (2017).

93. J. M. Inloes, K. L. Hsu, M. M. Dix, A. Viader, K. Masuda, T. Takei, M. R. Wood, B. F. Cravatt, The hereditary spastic paraplegia-related enzyme DDHD2 is a principal brain triglyceride lipase. *Proc Natl Acad Sci U S A* **111**, 14924–14929 (2014).

94. J. M. Inloes, W. B. Kiosses, H. Wang, T. C. Walther, R. V. Farese, B. F. Cravatt, Functional Contribution of the Spastic Paraplegia-Related Triglyceride Hydrolase DDHD2 to the Formation and Content of Lipid Droplets. *Biochemistry* **57**, 827–838 (2018).

95. A. R. Kimmel, C. Sztalryd, The Perilipins: Major Cytosolic Lipid Droplet–Associated Proteins and Their Roles in Cellular Lipid Storage, Mobilization, and Systemic Homeostasis*. *Annu Rev Nutr* **36**, 471–509 (2016).

96. H. Itabe, T. Yamaguchi, S. Nimura, N. Sasabe, Perilipins: a diversity of intracellular lipid droplet proteins. *Lipids Health Dis* **16**, 1–11 (2017).

97. C. Sztalryd, D. L. Brasaemle, The perilipin family of lipid droplet proteins: Gatekeepers of intracellular lipolysis. *Biochimica et Biophysica Acta (BBA) - Molecular and Cell Biology of Lipids* **1862**, 1221–1232 (2017).

98. B. C. Farmer, A. E. Walsh, J. C. Kluemper, L. A. Johnson, Lipid Droplets in Neurodegenerative Disorders. *Front Neurosci* **14** (2020).

99. X. Zhang, W. Xu, R. Xu, Z. Wang, X. Zhang, P. Wang, K. Peng, M. Li, J. Li, Y. Tan, X. Wang, H. Pei, Plin5 Bidirectionally Regulates Lipid Metabolism in Oxidative Tissues. *Oxid Med Cell Longev* **2022** (2022).

100. S. Kaushik, A. M. Cuervo, AMPK-dependent phosphorylation of lipid droplet protein PLIN2 triggers its degradation by CMA. *Autophagy* **12**, 432–438 (2016).

101. F. Cingolani, M. J. Czaja, Regulation and Functions of Autophagic Lipolysis. *Trends in Endocrinology and Metabolism* **27** (2016).

102. W. Cui, A. Sathyanarayan, M. Lopresti, M. Aghajan, C. Chen, D. G. Mashek, Lipophagy-derived fatty acids undergo extracellular efflux via lysosomal exocytosis. *Autophagy*, doi: 10.1080/15548627.2020.1728097 (2020).

103. G. F. Grabner, H. Xie, M. Schweiger, R. Zechner, Lipolysis: cellular mechanisms for lipid mobilization from fat stores. *Nature Metabolism 2021 3:11* **3**, 1445–1465 (2021).

104. R. P. Chakrabarty, N. S. Chandel, Mitochondria as Signaling Organelles Control Mammalian Stem Cell Fate. *Cell Stem Cell* **28**, 394–408 (2021).

105. R. P. Chakrabarty, N. S. Chandel, Beyond ATP, new roles of mitochondria. *Biochem (Lond)* **44**, 2–8 (2022).

106. T. TeSlaa, M. A. Teitell, “Techniques to Monitor Glycolysis” in *Methods in Enzymology* (Academic Press, 2014)vol. 542, pp. 91–114.

107. J. G. Salway, *Metabolism at a Glance* (Wiley-Blackwell, ed. 4, 2017; https://www-wiley-com.login.ezproxy.library.ualberta.ca/en-us/Metabolism+at+a+Glance%2C+4th+Edition-p-9780470674710).

108. I. Mesquita, F. Rodrigues, “Cellular Metabolism at a Glance” in *Metabolic Interaction in Infection*, R. Silvestre, E. Torrado, Eds. (Springer, Cham, ed. 1, 2018; https://link-springer-com.login.ezproxy.library.ualberta.ca/chapter/10.1007/978-3-319-74932-7_1)vol. 109, pp. 3–27.

109. D. Voet, J. G. Voet, C. W. Pratt, *Fundamentals of Biochemistry: Life at the Molecular Level* (Wiley, ed. 5, 2016; https://www.wiley.com/en-us/Fundamentals+of+Biochemistry%3A+Life+at+the+Molecular+Level%2C+5th+Edition-p-9781118918401).

110. W. Walz, S. Mukerji, Lactate production and release in cultured astrocytes. *Neurosci Lett* **86**, 296–300 (1988).

111. K. Pierre, L. Pellerin, Monocarboxylate transporters in the central nervous system: Distribution, regulation and function. *J Neurochem* **94**, 1–14 (2005).

112. H. Roumes, L. Pellerin, A. K. Bouzier-Sore, Astrocytes as metabolic suppliers to support neuronal activity and brain functions. *Essays Biochem* **67**, 27–37 (2023).

113. G. Descalzi, V. Gao, M. Q. Steinman, A. Suzuki, C. M. Alberini, Lactate from astrocytes fuels learning-induced mRNA translation in excitatory and inhibitory neurons. *Commun Biol* **2**, 1–11 (2019).

114. G. A. Dienel, M. C. McKenna, A dogma-breaking concept: glutamate oxidation in astrocytes is the source of lactate during aerobic glycolysis in resting subjects. *J Neurochem* **131**, 395–398 (2014).

115. H. S. Waagepetersen, I. J. Bakken, O. M. Larsson, U. Sonnewald, A. Schousboe, Comparison of Lactate and Glucose Metabolism in Cultured Neocortical Neurons and Astrocytes Using 13C-NMR Spectroscopy. *Dev Neurosci* **20**, 310–320 (1998).

116. M. C. McKenna, Substrate Competition Studies Demonstrate Oxidative Metabolism of Glucose, Glutamate, Glutamine, Lactate and 3-Hydroxybutyrate in Cortical Astrocytes from Rat Brain. *Neurochem Res* **37**, 2613–2626 (2012).

117. H. Li, C. Guglielmetti, Y. J. Sei, M. Zilberter, L. M. Le Page, L. Shields, J. Yang, K. Nguyen, B. Tiret, X. Gao, N. Bennett, I. Lo, T. L. Dayton, M. Kampmann, Y. Huang, J. C. Rathmell, M. Vander Heiden, M. M. Chaumeil, K. Nakamura, Neurons require glucose uptake and glycolysis in vivo. *Cell Rep* **42**, 112335 (2023).

118. O. H. Porras, A. Loaiza, L. Felipe Barros, Glutamate Mediates Acute Glucose Transport Inhibition in Hippocampal Neurons. *Journal of Neuroscience* **24**, 9669–9673 (2004).

119. I. Lundgaard, B. Li, L. Xie, H. Kang, S. Sanggaard, J. D. R. Haswell, W. Sun, S. Goldman, S. Blekot, M. Nielsen, T. Takano, R. Deane, M. Nedergaard, Direct

neuronal glucose uptake heralds activity-dependent increases in cerebral metabolism. *Nat Commun* **6**, 1–12 (2015).

120. L. B. Achanta, B. D. Rowlands, D. S. Thomas, G. D. Housley, C. D. Rae, β-Hydroxybutyrate Boosts Mitochondrial and Neuronal Metabolism but is not Preferred Over Glucose Under Activated Conditions. *Neurochem Res* **42**, 1710–1723 (2017).

121. C. Vicente-Gutierrez, N. Bonora, V. Bobo-Jimenez, D. Jimenez-Blasco, I. Lopez-Fabuel, E. Fernandez, C. Josephine, G. Bonvento, J. A. Enriquez, A. Almeida, J. P. Bolaños, Astrocytic mitochondrial ROS modulate brain metabolism and mouse behaviour. *Nat Metab* **1**, 201–211 (2019).

122. J. -i Sagara, K. Miura, S. Bannai, Maintenance of Neuronal Glutathione by Glial Cells. *J Neurochem* **61**, 1672–1676 (1993).

123. R. Dringen, B. Pfeiffer, B. Hamprecht, Synthesis of the Antioxidant Glutathione in Neurons: Supply by Astrocytes of CysGly as Precursor for Neuronal Glutathione. *Journal of Neuroscience* **19**, 562–569 (1999).

124. J. Hirrlinger, J. B. Schulz, R. Dringen, Glutathione release from cultured brain cells: Multidrug resistance protein 1 mediates the release of GSH from rat astroglial cells. *J Neurosci Res* **69**, 318–326 (2002).

125. J. R. Liddell, S. R. Robinson, R. Dringen, G. M. Bishop, Astrocytes retain their antioxidant capacity into advanced old age. *Glia* **58**, 1500–1509 (2010).

126. Y. Oe, O. Baba, H. Ashida, K. C. Nakamura, H. Hirase, Glycogen distribution in the microwave-fixed mouse brain reveals heterogeneous astrocytic patterns. *Glia* **64**, 1532–1545 (2016).

127. A. M. Brown, B. R. Ransom, Astrocyte glycogen as an emergency fuel under conditions of glucose deprivation or intense neural activity. *Metab Brain Dis* **30**, 233–239 (2015).

128. A. M. Cataldo, R. D. Broadwell, A. M. Cataldo, R. D. Broadwell, Cytochemical identification of cerebral glycogen and glucose-6-phosphatase activity under normal and experimental conditions: I. Neurons and glia. *J Electron Microsc Tech* **3**, 413–437 (1986).

129. L. K. Bak, A. B. Walls, Astrocytic glycogen metabolism in the healthy and diseased brain. *Journal of Biological Chemistry* **293**, 7108–7116 (2018).

130. Y. Shen, Y. Tian, X. Shi, J. Yang, L. Ouyang, J. Gao, J. Lu, Exposure to high glutamate concentration activates aerobic glycolysis but inhibits ATP-linked respiration in cultured cortical astrocytes. *Cell Biochem Funct* **32**, 530–537 (2014).

131. L. Peng, R. A. Swanson, L. Hertz, Effects of l-glutamate, d-aspartate, and monensin on glycolytic and oxidative glucose metabolism in mouse astrocyte cultures: further evidence that glutamate uptake is metabolically driven by oxidative metabolism. *Neurochem Int* **38**, 437–443 (2001).

132. L. Hertz, L. Peng, G. A. Dienel, Energy metabolism in astrocytes: High rate of oxidative metabolism and spatiotemporal dependence on glycolysis/glycogenolysis. *Journal of Cerebral Blood Flow and Metabolism* **27**, 219–249 (2007).

133. Y. Mi, G. Qi, F. Vitali, Y. Shang, A. C. Raikes, T. Wang, Y. Jin, R. D. Brinton, H. Gu, F. Yin, Loss of fatty acid degradation by astrocytic mitochondria triggers neuroinflammation and neurodegeneration. *Nature Metabolism 2023 5:3* **5**, 445–465 (2023).

134. P. K. Arnold, L. W. S. Finley, Regulation and function of the mammalian tricarboxylic acid cycle. *Journal of Biological Chemistry* **299** (2023).

135. A. R. Harders, P. Spellerberg, R. Dringen, Exogenous Substrates Prevent the Decline in the Cellular ATP Content of Primary Rat Astrocytes During Glucose Deprivation. *Neurochem Res* **49**, 1188–1199 (2024).

136. I. Fernández-González, E. Galea, Astrocyte strategies in the energy-efficient brain. *Essays Biochem* **67**, 3–16 (2022).

137. A. R. Harders, C. Arend, S. C. Denieffe, J. Berger, R. Dringen, Endogenous Energy Stores Maintain a High ATP Concentration for Hours in Glucose-Depleted Cultured Primary Rat Astrocytes. *Neurochem Res* **48**, 2241–2252 (2023).

138. J. Edmond, R. A. Robbins, J. D. Bergstrom, R. A. Cole, J. de Vellis, Capacity for substrate utilization in oxidative metabolism by neurons, astrocytes, and oligodendrocytes from developing brain in primary culture. *J Neurosci Res* **18**, 551–561 (1987).

139. S. Herzig, E. Raemy, S. Montessuit, J. L. Veuthey, N. Zamboni, B. Westermann, E. R. S. Kunji, J. C. Martinou, Identification and functional expression of the mitochondrial pyruvate carrier. *Science (1979)* **336**, 93–96 (2012).

140. I. Martínez-Reyes, N. S. Chandel, Mitochondrial TCA cycle metabolites control physiology and disease. *Nat Commun* **11**, 1–11 (2020).

141. R. Guo, S. Zong, M. Wu, J. Gu, M. Yang, Architecture of Human Mitochondrial Respiratory Megacomplex I2III2IV2. *Cell* **170**, 1247-1257.e12 (2017).

142. R.-Z. Zhao, S. Jiang, L. Zhang, Z.-B. Yu, Mitochondrial electron transport chain, ROS generation and uncoupling. *International Journal of Molecular Science* **44**, 315 (2019).

143. Y. Wang, J. Palmfeldt, N. Gregersen, A. M. Makhov, J. F. Conway, M. Wang, S. P. McCalley, S. Basu, H. Alharbi, C. St. Croix, M. J. Calderon, S. Watkins, J. Vockley, Mitochondrial fatty acid oxidation and the electron transport chain comprise a multifunctional mitochondrial protein complex. *Journal of Biological Chemistry* **294**, 12380–12391 (2019).

144. A. Mühleip, R. K. Flygaard, R. Baradaran, O. Haapanen, T. Gruhl, V. Tobiasson, A. Maréchal, V. Sharma, A. Amunts, Structural basis of mitochondrial membrane bending by the I–II–III2–IV2 supercomplex. *Nature* **615**, 934–938 (2023).

145. D. Nolfi-Donegan, A. Braganza, S. Shiva, Mitochondrial electron transport chain: Oxidative phosphorylation, oxidant production, and methods of measurement. *Redox Biol* **37**, 101674 (2020).

146. J. A. Letts, L. A. Sazanov, Clarifying the supercomplex: the higher-order organization of the mitochondrial electron transport chain. *Nat Struct Mol Biol* **24**, 800–808 (2017).

147. S. H. Lee, H. E. Duron, D. Chaudhuri, Beyond the TCA cycle: new insights into mitochondrial calcium regulation of oxidative phosphorylation. *Biochem Soc Trans* **51**, 1661–1673 (2023).

148. R. Guo, J. Gu, S. Zong, M. Wu, M. Yang, Structure and mechanism of mitochondrial electron transport chain. *Biomed J* **41**, 9–20 (2018).

149. S. Cogliati, J. L. Cabrera-Alarcón, J. A. Enriquez, Regulation and functional role of the electron transport chain supercomplexes. *Biochem Soc Trans* **49**, 2655–2668 (2021).

150. I. Lopez-Fabuel, J. Le Douce, A. Logan, A. M. James, G. Bonvento, M. P. Murphy, A. Almeida, J. P. Bolaños, Complex I assembly into supercomplexes determines differential mitochondrial ROS production in neurons and astrocytes. *Proc Natl Acad Sci U S A* **113**, 13063–13068 (2016).

151. B. Millare, B. O'Rourke, N. Trayanova, Hydrogen peroxide diffusion and scavenging shapes mitochondrial network instability and failure by sensitizing ROS-induced ROS release. *Scientific Reports 2020 10:1* **10**, 1–15 (2020).

152. S. García-Santamarina, S. Boronat, E. Hidalgo, Reversible cysteine oxidation in hydrogen peroxide sensing and signal transduction. *Biochemistry* **53**, 2560–2580 (2014).

153. S. Stöcker, K. Van Laer, A. Mijuskovic, T. P. Dick, The Conundrum of Hydrogen Peroxide Signaling and the Emerging Role of Peroxiredoxins as Redox Relay Hubs. *Antioxid Redox Signal* **28**, 558–573 (2018).

154. H. Sies, V. V. Belousov, N. S. Chandel, M. J. Davies, D. P. Jones, G. E. Mann, M. P. Murphy, M. Yamamoto, C. Winterbourn, Defining roles of specific reactive oxygen species (ROS) in cell biology and physiology. *Nature Reviews Molecular Cell Biology 2022 23:7* **23**, 499–515 (2022).

155. A. Elsayed Azab, Almokhtar A Adwas, A. S. Ibrahim Elsayed, A. A Adwas, Ata Sedik Ibrahim Elsayed, F. A. Quwaydir, Oxidative stress and antioxidant mechanisms in human body. *Journal of Applied Biotechnology & Bioengineering* **Volume 6**, 43–47 (2019).

156. Y. Chen, C. Qin, J. Huang, X. Tang, C. Liu, K. Huang, J. Xu, G. Guo, A. Tong, L. Zhou, The role of astrocytes in oxidative stress of central nervous system: A mixed blessing. *Cell Prolif* **53**, e12781 (2020).

157. P. R. Angelova, A. Y. Abramov, Role of mitochondrial ROS in the brain: from physiology to neurodegeneration. *FEBS Lett* **592**, 692–702 (2018).

158. M. C. McKenna, Glutamate pays its own way in astrocytes. *Front Endocrinol (Lausanne)* **4**, 191 (2013).

159. M. C. McKenna, M. H. Stridh, L. F. McNair, U. Sonnewald, H. S. Waagepetersen, A. Schousboe, Glutamate oxidation in astrocytes: Roles of glutamate dehydrogenase and aminotransferases. *J Neurosci Res* **94**, 1561–1571 (2016).

160. C. F. Rose, A. Verkhratsky, V. Parpura, Astrocyte glutamine synthetase: pivotal in health and disease. *Biochem Soc Trans* **41**, 1518–1524 (2013).

161. S. Sreedharan, J. H. Shaik, P. K. Olszewski, A. S. Levine, H. B. Schiöth, R. Fredriksson, Glutamate, aspartate and nucleotide transporters in the SLC17 family form four main phylogenetic clusters: Evolution and tissue expression. *BMC Genomics* **11** (2010).

162. Y. Shigeri, R. P. Seal, K. Shimamoto, Molecular pharmacology of glutamate transporters, EAATs and VGLUTs. *Brain Res Rev* **45**, 250–265 (2004).

163. M. B. Robinson, M. L. Lee, S. DaSilva, Glutamate Transporters and Mitochondria: Signaling, Co-compartmentalization, Functional Coupling, and Future Directions. *Neurochem Res* **45**, 526–540 (2020).

164. J. D. Nissen, K. Lykke, J. Bryk, M. H. Stridh, I. Zaganas, D. M. Skytt, A. Schousboe, L. K. Bak, W. Enard, S. Pääbo, H. S. Waagepetersen, Expression of the human isoform of glutamate dehydrogenase, hGDH2, augments TCA cycle capacity and oxidative metabolism of glutamate during glucose deprivation in astrocytes. *Glia* **65**, 474–488 (2017).

165. G. A. Dienel, Astrocytic energetics during excitatory neurotransmission: What are contributions of glutamate oxidation and glycolysis? *Neurochem Int* **63**, 244–258 (2013).

166. A. Schousboe, G. Svenneby, L. Hertz, Uptake and metabolism of glutamate in astrocytes cultured from dissociated mouse brain hemispheres. *J Neurochem* **29**, 999–1005 (1977).

167. N. Westergaard, J. Drejer, A. Schousboe, U. Sonnewald, Evaluation of the Importance of Transamination Versus Deamination in Astrocytic Metabolism of [U-13C]Glutamate. *Glia* **17**, 160–168 (1996).

168. M. C. McKenna, U. Sonnewald, X. Huang, J. Stevenson, H. R. Zielke, Exogenous Glutamate Concentration Regulates the Metabolic Fate of Glutamate in Astrocytes. *J Neurochem* **66**, 386–393 (1996).

169. U. Sonnewald, N. Westergaard, P. Jones, A. Taylor, H. S. Bachelard, A. Schousboe, Metabolism of [U-13C5]Glutamine in Cultured Astrocytes Studied by NMR Spectroscopy: First Evidence of Astrocytic Pyruvate Recycling. *J Neurochem* **67**, 2566–2572 (1996).

170. H. S. Waagepetersen, H. Qu, L. Hertz, U. Sonnewald, A. Schousboe, Demonstration of pyruvate recycling in primary cultures of neocortical astrocytes but not in neurons. *Neurochem Res* **27**, 1431–1437 (2002).

171. L. L. Jones, D. A. McDonald, P. R. Borum, Acylcarnitines: Role in brain. *Prog Lipid Res* **49**, 61–75 (2010).

172. S. E. Reuter, A. M. Evans, Carnitine and Acylcarnitines. *Clin Pharmacokinet* **51**, 553–572 (2012).

173. M. R. McCann, M. V. G. De la Rosa, G. R. Rosania, K. A. Stringer, L-Carnitine and Acylcarnitines: Mitochondrial Biomarkers for Precision Medicine. *Metabolites 2021, Vol. 11, Page 51* **11**, 51 (2021).

174. S. Violante, L. Ijlst, H. Te Brinke, J. Koster, I. T. De Almeida, R. J. A. Wanders, F. V. Ventura, S. M. Houten, Peroxisomes contribute to the acylcarnitine production when the carnitine shuttle is deficient. *Biochimica et Biophysica Acta (BBA) - Molecular and Cell Biology of Lipids* **1831**, 1467–1474 (2013).

175. S. M. Houten, S. Violante, F. V Ventura, R. J. A. Wanders, The Biochemistry and Physiology of Mitochondrial Fatty Acid β-Oxidation and Its Genetic Disorders. *The Annual Review of Physiology is online at* **78**, 23–44 (2016).

176. J. Kerner, C. Hoppel, Fatty acid import into mitochondria. *Biochimica et Biophysica Acta (BBA) - Molecular and Cell Biology of Lipids* **1486**, 1–17 (2000).

177. S. Eaton, Control of mitochondrial β-oxidation flux. *Prog Lipid Res* **41**, 197–239 (2002).

178. M. J. Bennett, Assays of Fatty Acid β-Oxidation Activity. *Methods Cell Biol* **80**, 179–197 (2007).

179. M. J. Bennett, F. Sheng, A. Saada, Biochemical assays of TCA cycle and β-oxidation metabolites. *Methods Cell Biol* **155**, 83–120 (2020).

180. M. M. Adeva-Andany, N. Carneiro-Freire, M. Seco-Filgueira, C. Fernández-Fernández, D. Mouriño-Bayolo, Mitochondrial β-oxidation of saturated fatty acids in humans. *Mitochondrion* **46**, 73–90 (2019).

181. I. J. Lodhi, C. F. Semenkovich, Peroxisomes: A Nexus for Lipid Metabolism and Cellular Signaling. *Cell Metab* **19**, 380–392 (2014).

182. S. M. Houten, R. J. A. Wanders, P. Ranea-Robles, Metabolic interactions between peroxisomes and mitochondria with a special focus on acylcarnitine metabolism. *Biochimica et Biophysica Acta (BBA) - Molecular Basis of Disease* **1866**, 165720 (2020).

183. M. Fransen, C. Lismont, P. Walton, The Peroxisome-Mitochondria Connection: How and Why? *International Journal of Molecular Sciences 2017, Vol. 18, Page 1126* **18**, 1126 (2017).

184. R. J. A. Wanders, H. R. Waterham, S. Ferdinandusse, Metabolic interplay between peroxisomes and other subcellular organelles including mitochondria and the endoplasmic reticulum. *Front Cell Dev Biol* **3**, 83 (2016).

185. R. J. A. Wanders, Metabolic functions of peroxisomes in health and disease. *Biochimie* **98**, 36–44 (2014).

186. A. Esfandiari, D. Soifiyoudine, M. Paturneau-Jouas, Inhibition of Fatty Acid ß-Oxidation in Rat Brain Cultured Astrocytes Exposed to the Neurotoxin 3-Nitropropionic Acid. *Dev Neurosci* **19**, 312–320 (1997).

187. S. A. Liddelow, K. A. Guttenplan, L. E. Clarke, F. C. Bennett, C. J. Bohlen, L. Schirmer, M. L. Bennett, alexandra E. Münch, W. S. Chung, T. C. Peterson, D. K. Wilton, A. Frouin, B. A. Napier, N. Panicker, M. Kumar, M. S. Buckwalter, D. H. Rowitch, V. L. Dawson, T. M. Dawson, B. Stevens, B. A. Barres, Neurotoxic reactive astrocytes are induced by activated microglia. *Nature* **541**, 481–487 (2017).

188. K. A. Guttenplan, B. K. Stafford, R. N. El-Danaf, D. I. Adler, A. E. Münch, M. K. Weigel, A. D. Huberman, S. A. Liddelow, Neurotoxic reactive astrocytes drive neuronal death after retinal injury. *Cell Rep.* **31**, 107776 (2020).

189. K. A. Guttenplan, M. K. Weigel, P. Prakash, P. R. Wijewardhane, P. Hasel, U. Rufen-Blanchette, A. E. Münch, J. A. Blum, J. Fine, M. C. Neal, K. D. Bruce, A. D.

Gitler, G. Chopra, S. A. Liddelow, B. A. Barres, Neurotoxic reactive astrocytes induce cell death via saturated lipids. *Nature 2021 599:7883* **599**, 102–107 (2021).

190. N. Auestad, R. A. Korsak, J. W. Morrow, J. Edmond, Fatty Acid Oxidation and Ketogenesis by Astrocytes in Primary Culture. *J Neurochem* **56**, 1376–1386 (1991).

191. Q. Wang, S. Liu, A. Zhai, B. Zhang, G. Tian, AMPK-mediated regulation of lipid metabolism by phosphorylation. *Biol Pharm Bull* **41**, 985–993 (2018).

192. S. Herzig, R. J. Shaw, AMPK: guardian of metabolism and mitochondrial homeostasis. *Nat Rev Mol Cell Biol* **19**, 121–135 (2017).

193. S. C. Lin, D. G. Hardie, AMPK: Sensing Glucose as well as Cellular Energy Status. *Cell Metab* **27**, 299–313 (2018).

194. G. R. Steinberg, D. G. Hardie, New insights into activation and function of the AMPK. *Nat Rev Mol Cell Biol* **24**, 255–272 (2022).

195. S. M. Jeon, Regulation and function of AMPK in physiology and diseases. *Experimental & Molecular Medicine 2016 48:7* **48**, e245–e245 (2016).

196. N. Dzamko, J. D. Schertzer, J. G. Ryall, R. Steel, S. L. Macaulay, S. Wee, Z. P. Chen, B. J. Michell, J. S. Oakhill, M. J. Watt, S. B. Jørgensen, G. S. Lynch, B. E. Kemp, G. R. Steinberg, AMPK-independent pathways regulate skeletal muscle fatty acid oxidation. *Journal of Physiology* **586**, 5819–5831 (2008).

197. C. M. Voss, K. Pajęcka, M. H. Stridh, J. D. Nissen, A. Schousboe, H. S. Waagepetersen, AMPK Activation Affects Glutamate Metabolism in Astrocytes. *Neurochem Res* **40**, 2431–2442 (2015).

198. R. W. Brownsey, A. N. Boone, J. E. Elliott, J. E. Kulpa, W. M. Lee, Regulation of acetyl-CoA carboxylase. *Biochem Soc Trans* **34**, 223–227 (2006).

199. J. Ha, S. Daniel, S. S. Broyles, K. H. Kim, Critical phosphorylation sites for acetyl-CoA carboxylase activity. *Journal of Biological Chemistry* **269**, 22162–22168 (1994).

200. P. Hasel, O. Dando, Z. Jiwaji, P. Baxter, A. C. Todd, S. Heron, N. M. Márkus, J. McQueen, D. W. Hampton, M. Torvell, S. S. Tiwari, S. McKay, A. Eraso-Pichot, A. Zorzano, R. Masgrau, E. Galea, S. Chandran, D. J. A. Wyllie, T. I. Simpson, G. E. Hardingham, Neurons and neuronal activity control gene expression in astrocytes to regulate their development and metabolism. *Nat Commun* **8**, 1–18 (2017).

201. I. Farhy-Tselnicker, M. M. Boisvert, H. Liu, C. Dowling, G. A. Erikson, E. Blanco-Suarez, C. Farhy, M. N. Shokhirev, J. R. Ecker, N. J. Allen, Activity-dependent modulation of synapse-regulating genes in astrocytes. *Elife* **10** (2021).

202. T. Smolič, R. Zorec, N. Vardjan, Pathophysiology of Lipid Droplets in Neuroglia. *Antioxidants 2022, Vol. 11, Page 22* **11**, 22 (2021).

203. F. Petrelli, M. Knobloch, F. Amati, Brain lipid metabolism: The emerging role of lipid droplets in glial cells. *Curr Opin Lipidol* **33**, 86–87 (2022).

204. T. Smolič, P. Tavčar, A. Horvat, U. Černe, A. Halužan Vasle, L. Tratnjek, M. E. Kreft, N. Scholz, M. Matis, T. Petan, R. Zorec, N. Vardjan, Astrocytes in stress accumulate lipid droplets. *Glia* **69**, 1540–1562 (2021).

205. L. C. Foo, N. J. Allen, E. A. Bushong, P. B. Ventura, W. S. Chung, L. Zhou, J. D. Cahoy, R. Daneman, H. Zong, M. H. Ellisman, B. A. Barres, Development of a method for the purification and culture of rodent astrocytes. *Neuron* **71**, 799–811 (2011).

206. J. Prah, A. Winters, K. Chaudhari, J. Hersh, R. Liu, S. H. Yang, A novel serum free primary astrocyte culture method that mimic quiescent astrocyte phenotype. *J Neurosci Methods* **320**, 50–63 (2019).

207. M. Dahlmanns, J. K. Dahlmanns, N. Savaskan, H. H. Steiner, E. Yakubov, Glial Glutamate Transporter-Mediated Plasticity: System xc -/xCT/SLC7A11 and EAAT1/2 in Brain Diseases. *Frontiers in Bioscience* **28**, 57 (2023).

208. J. Han, K. Lin, C. Sequeira, C. H. Borchers, An isotope-labeled chemical derivatization method for the quantitation of short-chain fatty acids in human feces

by liquid chromatography–tandem mass spectrometry. *Anal Chim Acta* **854**, 86–94 (2015).

209. J. Han, R. Higgins, M. D. Lim, K. Atkinson, J. Yang, K. Lin, C. H. Borchers, Isotope-labeling derivatization with 3-nitrophenylhydrazine for LC/multiple-reaction monitoring-mass-spectrometry-based quantitation of carnitines in dried blood spots. *Anal Chim Acta* **1037**, 177–187 (2018).

210. R. A. Gottlieb, A. Stotland, MitoTimer: a novel protein for monitoring mitochondrial turnover in the heart. *J Mol Med* **93**, 271–278 (2015).

211. G. Hernandez, C. Thornton, A. Stotland, D. Lui, J. Sin, J. Ramil, N. Magee, A. Andres, G. Quarato, R. S. Carreira, M. R. Sayen, R. Wolkowicz, R. A. Gottlieb, MitoTimer: A novel tool for monitoring mitochondrial turnover. *Autophagy* **9**, 1852–1861 (2013).

212. L. Pellerin, A. K. Bouzier-Sore, A. Aubert, S. Serres, M. Merle, R. Costalat, P. J. Magistretti, Activity-dependent regulation of energy metabolism by astrocytes: An update. *Glia* **55**, 1251–1262 (2007).

213. H. Tominaga, H. Katoh, K. Odagiri, Y. Takeuchi, H. Kawashima, M. Saotome, T. Urushida, H. Satoh, H. Hayashi, Different effects of palmitoyl-L-carnitine and palmitoyl-CoA on mitochondrial function in rat ventricular myocytes. *Am J Physiol Heart Circ Physiol* **295**, 105–112 (2008).

214. E. Liepinsh, M. Makrecka-Kuka, K. Volska, J. Kuka, E. Makarova, U. Antone, E. Sevostjanovs, R. Vilskersts, A. Strods, K. Tars, M. Dambrova, Long-chain acylcarnitines determine ischaemia/reperfusion-induced damage in heart mitochondria. *Biochemical Journal* **473**, 1191–1202 (2016).

215. T. Maruyama, T. Baba, Y. Maemoto, C. Hara-Miyauchi, M. Hasegawa-Ogawa, H. J. Okano, Y. Enda, K. Matsumoto, N. Arimitsu, K. Nakao, H. Hamamoto, K. Sekimizu, T. Ohto-Nakanishi, H. Nakanishi, T. Tokuyama, S. Yanagi, M. Tagaya, K. Tani, Loss of DDHD2, whose mutation causes spastic paraplegia, promotes

reactive oxygen species generation and apoptosis. *Cell Death & Disease 2018 9:8* **9**, 1–15 (2018).

216. R. J. Schulze, A. Sathyanarayan, D. G. Mashek, Breaking fat: The regulation and mechanisms of lipophagy. *Biochim Biophys Acta Mol Cell Biol Lipids* **1862**, 1178–1187 (2017).

217. H. Choi, Z. Yang, J. C. Weisshaar, Single-cell, real-time detection of oxidative stress induced in escherichia coli by the antimicrobial peptide CM15. *Proc Natl Acad Sci U S A* **112**, E303–E310 (2015).

218. L. C. Foo, Purification of rat and mouse astrocytes by immunopanning. *Cold Spring Harb Protoc* **8**, 421–432 (2013).

219. J. L. Zamanian, L. Xu, L. C. Foo, N. Nouri, L. Zhou, R. G. Giffard, B. A. Barres, Genomic Analysis of Reactive Astrogliosis. *Journal of Neuroscience* **32**, 6391–6410 (2012).

220. K. Freitag, P. Eede, A. Ivanov, N. Sterczyk, S. Schneeberger, T. Borodina, S. Sauer, D. Beule, F. L. Heppner, Diverse but unique astrocytic phenotypes during embryonic stem cell differentiation, culturing and development. *Communications Biology 2023 6:1* **6**, 1–12 (2023).

221. M. Magistri, N. Khoury, E. M. C. Mazza, D. Velmeshev, J. K. Lee, S. Bicciato, P. Tsoulfas, M. A. Faghihi, A comparative transcriptomic analysis of astrocytes differentiation from human neural progenitor cells. *European Journal of Neuroscience* **44**, 2858–2870 (2016).

222. J. D. Cahoy, B. Emery, A. Kaushal, L. C. Foo, J. L. Zamanian, K. S. Christopherson, Y. Xing, J. L. Lubischer, P. A. Krieg, S. A. Krupenko, W. J. Thompson, B. A. Barres, A transcriptome database for astrocytes, neurons, and oligodendrocytes: A new resource for understanding brain development and function. *Journal of Neuroscience* **28**, 264–278 (2008).

223. X. Y. Xiong, Y. Tang, Q. W. Yang, Metabolic changes favor the activity and heterogeneity of reactive astrocytes. *Trends in Endocrinology & Metabolism* **33**, 390–400 (2022).

224. C. Salcedo, V. Pozo Garcia, B. García-Adán, A. O. Ameen, G. Gegelashvili, H. S. Waagepetersen, K. K. Freude, B. I. Aldana, Increased glucose metabolism and impaired glutamate transport in human astrocytes are potential early triggers of abnormal extracellular glutamate accumulation in hiPSC-derived models of Alzheimer's disease. *J Neurochem* **00**, 1–19 (2023).

225. N. Itoh, Y. Itoh, A. Tassoni, E. Ren, M. Kaito, A. Ohno, Y. Ao, V. Farkhondeh, H. Johnsonbaugh, J. Burda, M. V. Sofroniew, R. R. Voskuhl, Cell-specific and region-specific transcriptomics in the multiple sclerosis model: Focus on astrocytes. *Proc Natl Acad Sci U S A* **115**, E302–E309 (2017).

226. Y. Zhang, B. A. Barres, Astrocyte heterogeneity: An underappreciated topic in neurobiology. *Curr Opin Neurobiol* **20**, 588–594 (2010).

227. S. A. Liddelow, B. A. Barres, Reactive Astrocytes: Production, Function, and Therapeutic Potential. *Immunity* **46**, 957–967 (2017).

228. C. Escartin, E. Galea, J. P. Oamp, G. C. Petzold, A. Serrano-Pozo, C. Steinhamp, A. Volterra, G. Carmignoto, A. Agarwal, N. J. Allen, A. Araque, L. Barbeito, A. Barzilai, D. E. Bergles, G. Bonvento, A. M. Butt, W.-T. Chen, M. Cohen-Salmon, C. Cunningham, B. Deneen, B. Strooper, B. Damp, C. Farina, M. Freeman, V. Gallo, J. E. Goldman, S. A. Goldman, M. Gamp, A. Gutiamp, P. G. Haydon, D. H. Heiland, E. M. Hol, M. G. Holt, M. Iino, K. V Kastanenka, H. Kettenmann, B. S. Khakh, S. Koizumi, C. Justin Lee, S. A. Liddelow, B. A. MacVicar, P. Magistretti, A. Messing, A. Mishra, A. V Molofsky, K. K. Murai, C. M. Norris, S. Okada, phane H. R Oliet, F. Oliveira, A. Panatier, V. Parpura, M. Pekna, M. Pekny, L. Pellerin, G. Perea, B. G. Pamp, F. W. Pfrieger, K. E. Poskanzer, F. J. Quintana, R. M. Ransohoff, M. Riquelme-Perez, S. Robel, C. R. Rose, J. D. Rothstein, N. Rouach, D. H. Rowitch, A. Semyanov, S. Sirko, H. Sontheimer, R. A. Swanson, J. Vitorica, I.-B. Wanner, L. B. Wood, J. Wu, B. Zheng, E. R. Zimmer, R. Zorec, M. V Sofroniew, A. Verkhratsky,

Reactive astrocyte nomenclature, definitions, and future directions. *Nat Neurosci*, 1–14 (2021).

229. J. L. Ridet, S. K. Malhotra, A. Privat, F. H. Gage, Reactive astrocytes: Cellular and molecular cues to biological function. *Trends Neurosci* **20**, 570–577 (1997).

230. K. Skowrońska, M. Obara-Michlewska, M. Zielińska, J. Albrecht, NMDA Receptors in Astrocytes: In Search for Roles in Neurotransmission and Astrocytic Homeostasis. *International Journal of Molecular Sciences 2019, Vol. 20, Page 309* **20**, 309 (2019).

231. V. Rusnakova, P. Honsa, D. Dzamba, A. Ståhlberg, M. Kubista, M. Anderova, Heterogeneity of Astrocytes: From Development to Injury – Single Cell Gene Expression. *PLoS One* **8**, e69734 (2013).

232. M. C. Lee, K. K. Ting, S. Adams, B. J. Brew, R. Chung, G. J. Guillemin, Characterisation of the Expression of NMDA Receptors in Human Astrocytes. *PLoS One* **5**, e14123 (2010).

233. P. H. Chipman, C. Chung Alan Fung, A. Pazo Fernandez, A. Sawant, A. Tedoldi, A. Kawai, S. Ghimire Gautam, M. Kurosawa, M. Abe, K. Sakimura, T. Fukai, Y. Goda, Astrocyte GluN2C NMDA receptors control basal synaptic strengths of hippocampal CA1 pyramidal neurons in the stratum radiatum. *Elife* **10:e70818**, 1–32 (2021).

234. M. Daniels, D. R. Brown, Astrocytes Regulate N-Methyl-d-aspartate Receptor Subunit Composition Increasing Neuronal Sensitivity to Excitotoxicity. *Journal of Biological Chemistry* **276**, 22446–22452 (2001).

235. M. K. Shelton, K. D. Mccarthy, Mature Hippocampal Astrocytes Exhibit Functional Metabotropic and Ionotropic Glutamate Receptors In Situ. *Glia* **26**, 1–11 (1999).

236. Z. Cai, H. K. Kimelberg, Glutamate Receptor-Mediated Calcium Responses in Acutely Isolated Hippocampal Astrocytes. *Glia* **21**, 380–389 (1997).

237. G. Seifert, C. Steinhäuser, Glial Cells in the Mouse Hippocampus Express AMPA Receptors with an Intermediate Ca2+ Permeability. *European Journal of Neuroscience* **7**, 1872–1881 (1995).

238. U. Lalo, Y. Pankratov, F. Kirchhoff, R. A. North, A. Verkhratsky, NMDA Receptors Mediate Neuron-to-Glia Signaling in Mouse Cortical Astrocytes. *Journal of Neuroscience* **26**, 2673–2683 (2006).

239. I. S. Stein, J. A. Gray, K. Zito, Non-Ionotropic NMDA Receptor Signaling Drives Activity-Induced Dendritic Spine Shrinkage. *Journal of Neuroscience* **35**, 12303–12308 (2015).

240. J. L. Parker, J. C. Deme, D. Kolokouris, G. Kuteyi, P. C. Biggin, S. M. Lea, S. Newstead, Molecular basis for redox control by the human cystine/glutamate antiporter system xc−. *Nature Communications 2021 12:1* **12**, 1–11 (2021).

241. D. A. Baker, Z. X. Xi, H. Shen, C. J. Swanson, P. W. Kalivas, The Origin and Neuronal Function of In Vivo Nonsynaptic Glutamate. *Journal of Neuroscience* **22**, 9134–9141 (2002).

242. S. Bannai, E. Kitamura, Transport Interaction of t-Cystine and L-Glutamate in Human Diploid Fibroblasts in Culture. *Journal of Biological Chemistry* **255**, 2372–2376 (1980).

243. T. H. Murphy, M. Miyamoto, A. Sastre, R. L. Schnaar, J. T. Coyle, Glutamate toxicity in a neuronal cell line involves inhibition of cystine transport leading to oxidative stress. *Neuron* **2**, 1547–1558 (1989).

244. S. J. Dixon, K. M. Lemberg, M. R. Lamprecht, R. Skouta, E. M. Zaitsev, C. E. Gleason, D. N. Patel, A. J. Bauer, A. M. Cantley, W. S. Yang, B. Morrison, B. R. Stockwell, Ferroptosis: An iron-dependent form of nonapoptotic cell death. *Cell* **149**, 1060–1072 (2012).

245. S. J. Dixon, D. A. Pratt, Ferroptosis: A flexible constellation of related biochemical mechanisms. *Mol Cell* **83**, 1030–1042 (2023).

246. A. N. Boone, A. Chan, J. E. Kulpa, R. W. Brownsey, Bimodal Activation of Acetyl-CoA Carboxylase by Glutamate. *Journal of Biological Chemistry* **275**, 10819–10825 (2000).

247. A. Bianchi, J. L. Evans, A. J. Iverson, A. C. Nordlund, T. D. Watts, L. A. Witters, Identification of an isozymic form of acetyl-CoA carboxylase. *Journal of Biological Chemistry* **265**, 1502–1509 (1990).

248. M. Hunkeler, A. Hagmann, E. Stuttfeld, M. Chami, Y. Guri, H. Stahlberg, T. Maier, Structural basis for regulation of human acetyl-CoA carboxylase. *Nature* **558**, 470–474 (2018).

249. B. N. M. Zordoky, J. Nagendran, T. Pulinilkunnil, P. C. Kienesberger, G. Masson, T. J. Waller, B. E. Kemp, G. R. Steinberg, J. R. B. Dyck, AMPK-dependent inhibitory phosphorylation of ACC is not essential for maintaining myocardial fatty acid oxidation. *Circ Res* **115**, 518–524 (2014).

250. K. Funai, S. A. Summers, J. Rutter, Reign in the membrane: How common lipids govern mitochondrial function. *Curr Opin Cell Biol* **63**, 162–173 (2020).

251. S. E. Horvath, G. Daum, Lipids of mitochondria. *Prog Lipid Res* **52**, 590–614 (2013).

252. M. B. Schott, S. G. Weller, R. J. Schulze, E. W. Krueger, K. Drizyte-Miller, C. A. Casey, M. A. McNiven, Lipid droplet size directs lipolysis and lipophagy catabolism in hepatocytes. *Journal of Cell Biology* **218**, 3320–3335 (2019).

253. J. Yu, P. Li, The size matters: regulation of lipid storage by lipid droplet dynamics. *Sci China Life Sci* **60**, 46–56 (2017).

254. X. Lu, X. Yang, J. Liu, Cell Cycle Differential control of ATGL-mediated lipid droplet degradation by CGI-58 and G0S2. *Cell Cycle* **9**, 2791–2797 (2010).

255. P. Hofer, G. F. Grabner, M. König, H. Xie, D. Bulfon, A. E. Ludwig, H. Wolinski, R. Zimmermann, R. Zechner, C. Heier, Cooperative lipolytic control of neuronal triacylglycerol by spastic paraplegia-associated enzyme DDHD2 and ATGL. *J Lipid Res* **64**, 100457 (2023).

256. I. Juaristi, I. Llorente-Folch, J. Satrústegui, A. del Arco, Extracellular ATP and glutamate drive pyruvate production and energy demand to regulate mitochondrial respiration in astrocytes. *Glia* **67**, 759–774 (2019).

257. C. X. Bittner, R. Valdebenito, I. Ruminot, A. Loaiza, V. Larenas, T. Sotelo-Hitschfeld, H. Moldenhauer, A. San Martín, R. Gutiérrez, M. Zambrano, L. F. Barros, Fast and Reversible Stimulation of Astrocytic Glycolysis by K+ and a Delayed and Persistent Effect of Glutamate. *Journal of Neuroscience* **31**, 4709–4713 (2011).

258. C. L. Bowman, H. K. Kimelberg, Excitatory amino acids directly depolarize rat brain astrocytes in primary culture. *Nature 1984 311:5987* **311**, 656–659 (1984).

259. T. Masuda, Y. Ozono, S. Mikuriya, Y. Kohro, H. Tozaki-Saitoh, K. Iwatsuki, H. Uneyama, R. Ichikawa, M. W. Salter, M. Tsuda, K. Inoue, Dorsal horn neurons release extracellular ATP in a VNUT-dependent manner that underlies neuropathic pain. *Nat Commun* **7** (2016).

260. T. Pangršič, M. Potokar, M. Stenovec, M. Kreft, E. Fabbretti, A. Nistri, E. Pryazhnikov, L. Khiroug, R. Giniatullin, R. Zorec, Exocytotic release of ATP from cultured astrocytes. *Journal of Biological Chemistry* **282**, 28749–28758 (2007).

261. P. B. Guthrie, J. Knappenberger, M. Segal, M. V. L. Bennett, A. C. Charles, S. B. Kater, ATP released from astrocytes mediates glial calcium waves. *Journal of Neuroscience* **19**, 520–528 (1999).

262. Z. Zhang, G. Chen, W. Zhou, A. Song, T. Xu, Q. Luo, W. Wang, X. S. Gu, S. Duan, Regulated ATP release from astrocytes through lysosome exocytosis. *Nat Cell Biol* **9**, 945–953 (2007).

263. J.-M. Zhang, H.-K. Wang, C.-Q. Ye, W. Ge, Y. Chen, Z.-L. Jiang, C.-P. Wu, M.-M. Poo, S. Duan, ATP Released by Astrocytes Mediates Glutamatergic Activity-Dependent Heterosynaptic Suppression. *Neuron* **40**, 971–982 (2003).

264. A. V Singh, M. Raymond, F. Pace, A. Certo, J. M. Zuidema, C. A. McKay, R. J. Gilbert, X. L. Lu, L. Q. Wan, Astrocytes increase ATP exocytosis mediated calcium signaling in response to microgroove structures. *Sci Rep* **5** (2015).

265. Q. Cao, K. Zhao, X. Z. Zhong, Y. Zou, H. Yu, P. Huang, T. Le Xu, X. P. Dong, SLC17A9 protein functions as a lysosomal ATP transporter and regulates cell viability. *Journal of Biological Chemistry* **289**, 23189–23199 (2014).

266. X. Z. Zhong, Q. Cao, X. Sun, X. P. Dong, Activation of lysosomal P2X4 by ATP transported into lysosomes via VNUT/SLC17A9 using V-ATPase generated voltage gradient as the driving force. *Journal of Physiology* **594**, 4253–4266 (2016).

267. A. M. Falchi, V. Sogos, F. Saba, M. Piras, T. Congiu, M. Piludu, Astrocytes shed large membrane vesicles that contain mitochondria, lipid droplets and ATP. *Histochem Cell Biol* **139**, 221–231 (2013).

268. U. Lalo, O. Palygin, S. Rasooli-Nejad, J. Andrew, P. G. Haydon, Y. Pankratov, Exocytosis of ATP From Astrocytes Modulates Phasic and Tonic Inhibition in the Neocortex. *PLoS Biol* **12** (2014).

269. M. Oya, T. Kitaguchi, Y. Yanagihara, R. Numano, M. Kakeyama, K. Ikematsu, T. Tsuboi, Vesicular nucleotide transporter is involved in ATP storage of secretory lysosomes in astrocytes. *Biochem Biophys Res Commun* **438**, 145–151 (2013).

270. C. Verderio, C. Cagnoli, M. Bergami, M. Francolini, U. Schenk, A. Colombo, L. Riganti, C. Frassoni, E. Zuccaro, L. Danglot, C. Wilhelm, T. Galli, M. Canossa, M. Matteoli, TI-VAMP/VAMP7 is the SNARE of secretory lysosomes contributing to ATP secretion from astrocytes. *Biol Cell* **104**, 213–228 (2012).

271. C. A. Schmidt, K. H. Fisher-Wellman, P. Darrell Neufer, From OCR and ECAR to energy: Perspectives on the design and interpretation of bioenergetics studies. American Society for Biochemistry and Molecular Biology Inc. [Preprint] (2021). https://doi.org/10.1016/j.jbc.2021.101140.

272. S. A. Mookerjee, R. L. S. Goncalves, A. A. Gerencser, D. G. Nicholls, M. D. Brand, The contributions of respiration and glycolysis to extracellular acid production. *Biochimica et Biophysica Acta (BBA) - Bioenergetics* **1847**, 171–181 (2015).

273. N. Romero, G. Rogers, A. Neilson, B. P. Dranka, “White Paper: Quantifying Cellular ATP Production Rate Using Agilent Seahorse XF Technology” (Lexington, MA, USA, 2018).

274. M. A. Lobas, R. Tao, J. Nagai, M. T. Kronschläger, P. M. Borden, J. S. Marvin, L. L. Looger, B. S. Khakh, A genetically encoded single-wavelength sensor for imaging cytosolic and cell surface ATP. *Nat Commun* **10** (2019).

275. A. Almeida, S. Moncada, J. P. Bolaños, Nitric oxide switches on glycolysis through the AMP protein kinase and 6-phosphofructo-2-kinase pathway. *Nature Cell Biology 2003 6:1* **6**, 45–51 (2003).

276. S. Duan, C. M. Anderson, B. A. Stein, R. A. Swanson, Glutamate Induces Rapid Upregulation of Astrocyte Glutamate Transport and Cell-Surface Expression of GLAST. *Journal of Neuroscience* **19**, 10193–10200 (1999).

277. S. L. Liao, C. J. Chen, l-Glutamate decreases glucose utilization by rat cortical astrocytes. *Neurosci Lett* **348**, 81–84 (2003).

278. H. Qu, H. Eloqayli, G. Unsgård, U. Sonnewald, Glutamate decreases pyruvate carboxylase activity and spares glucose as energy substrate in cultured cerebellar astrocytes. *J Neurosci Res* **66**, 1127–1132 (2001).

279. J. Edmond, R. A. Robbins, J. D. Bergstrom, R. A. Cole, J. de Vellis, Capacity for substrate utilization in oxidative metabolism by neurons, astrocytes, and oligodendrocytes from developing brain in primary culture. *J Neurosci Res* **18**, 551–561 (1987).

280. A. Eraso-Pichot, M. Brasó-Vives, A. Golbano, C. Menacho, E. Claro, E. Galea, R. Masgrau, GSEA of mouse and human mitochondriomes reveals fatty acid oxidation in astrocytes. *Glia* **66**, 1724–1735 (2018).

281. K. Hofmann, R. Rodriguez-Rodriguez, A. Gaebler, N. Casals, A. Scheller, L. Kuerschner, Astrocytes and oligodendrocytes in grey and white matter regions of the brain metabolize fatty acids. *Sci Rep* **7** (2017).

282. D. Fitzner, J. M. Bader, H. Penkert, C. G. Bergner, M. Su, M. T. Weil, M. A. Surma, M. Mann, C. Klose, M. Simons, Cell-Type- and Brain-Region-Resolved Mouse Brain Lipidome. *Cell Rep* **32** (2020).

283. P. G. Weightman Potter, J. M. Vlachaki Walker, J. L. Robb, J. K. Chilton, R. Williamson, A. D. Randall, K. L. J. Ellacott, C. Beall, Basal fatty acid oxidation increases after recurrent low glucose in human primary astrocytes. *Diabetologia* **62**, 187–198 (2019).

284. J. Thevenet, U. De Marchi, J. S. Domingo, N. Christinat, L. Bultot, G. Lefebvre, K. Sakamoto, P. Descombes, M. Masoodi, A. Wiederkehr, Medium-chain fatty acids inhibit mitochondrial metabolism in astrocytes promoting astrocyte-neuron lactate and ketone body shuttle systems. *FASEB Journal* **30**, 1913–1926 (2016).

285. S. Sonnay, A. Chakrabarti, J. Thevenet, A. Wiederkehr, N. Christinat, M. Masoodi, Differential Metabolism of Medium-Chain Fatty Acids in Differentiated Human-Induced Pluripotent Stem Cell-Derived Astrocytes. *Front Physiol* **10** (2019).

286. A. O. Wagner, R. Markt, T. Puempel, P. Illmer, H. Insam, C. Ebner, Sample preparation, preservation, and storage for volatile fatty acid quantification in biogas plants. *Eng Life Sci* **17**, 132–139 (2017).

287. J. F. Hütter, C. Schweickhardt, H. M. Piper, P. G. Spieckermann, Inhibition of fatty acid oxidation and decrease of oxygen consumption of working rat heart by 4-bromocrotonic acid. *J Mol Cell Cardiol* **16**, 105–108 (1984).

288. Y. Olowe, H. Schulz, 4-Bromocrotonic acid, an effective inhibitor of fatty acid oxidation and ketone body degradation in rat heart mitochondria. On the rate-determining step of beta-oxidation and ketone body degradation in heart. *Journal of Biological Chemistry* **257**, 5408–5413 (1982).

289. H. Rupp, A. Zarain-Herzberg, B. Maisch, The use of partial fatty acid oxidation inhibitors for metabolic therapy of angina pectoris and heart failure. *Herz* **27**, 621–636 (2002).

290. D. Grünig, U. Duthaler, S. Krähenbühl, Effect of toxicants on fatty acid metabolism in HepG2 cells. *Front Pharmacol* **9**, 322850 (2018).

291. A. MacInnes, D. A. Fairman, P. Binding, J. ann Rhodes, M. J. Wyatt, A. Phelan, P. S. Haddock, E. H. Karran, The antianginal agent trimetazidine does not exert its functional benefit via inhibition of mitochondrial long-chain 3-ketoacyl coenzyme A thiolase. *Circ Res* **93** (2003).

292. B. Morant-Ferrando, D. Jimenez-Blasco, P. Alonso-Batan, J. Agulla, R. Lapresa, D. Garcia-Rodriguez, S. Yunta-Sanchez, I. Lopez-Fabuel, E. Fernandez, P. Carmeliet, A. Almeida, M. Garcia-Macia, J. P. Bolaños, Fatty acid oxidation organizes mitochondrial supercomplexes to sustain astrocytic ROS and cognition. *Nat Metab* **5**, 1290–1302 (2023).

293. M. C. Mckenna, J. T. Tildon, J. H. Stevenson, X. Huang, K. G. Kingwelp, “Regulation of Mitochondrial and Cytosolic Malic Enzymes from Cultured Rat Brain Astrocytes*” (1995).

294. L. L. Fonseca, M. A. R. Monteiro, P. M. Alves, M. J. T. Carrondo, H. Santos, Cultures of rat astrocytes challenged with a steady supply of glutamate: New model to study flux distribution in the glutamate-glutamine cycle. *Glia* **51**, 286–296 (2005).

295. L. Hertz, E. Hertz, Cataplerotic TCA cycle flux determined as glutamate-sustained oxygen consumption in primary cultures of astrocytes. *Neurochem Int* **43**, 355–361 (2003).

296. P. H. Chan, L. Chu, Mechanisms underlying glutamate-induced swelling of astrocytes in primary culture. *Acta Neurochir Suppl (Wien)* **51**, 7–10 (1990).

297. L. J. Noble, J. J. Hall, S. Chen, P. H. Chan, Morphologic Changes in Cultured Astrocytes After Exposure to Glutamate. *J Neurotrauma* **9**, 255–267 (2009).

298. P. H. Chan, L. Chu, S. Chen, Effects of MK-801 on glutamate-induced swelling of astrocytes in primary cell culture. *J Neurosci Res* **25**, 87–93 (1990).

299. J. A. Dzubay, C. E. Jahr, The Concentration of Synaptically Released Glutamate Outside of the Climbing Fiber–Purkinje Cell Synaptic Cleft. *Journal of Neuroscience* **19**, 5265–5274 (1999).

300. K. Moussawi, A. Riegel, S. Nair, P. W. Kalivas, Extracellular glutamate: Functional compartments operate in different concentration ranges. *Front Syst Neurosci* **5**, 11030 (2011).

301. V. Martínez-Redondo, A. T. Pettersson, J. L. Ruas, The hitchhiker's guide to PGC-1α isoform structure and biological functions. *Diabetologia* **58**, 1969–1977 (2015).

302. S. Tan, B. Kennedy, E. Wong, Mitochondrial biogenesis and mitophagy. *Mitochondrial Physiology and Vegetal Molecules: Therapeutic Potential of Natural Compounds on Mitochondrial Health*, 35–90 (2021).

303. Z. Kuczynska, E. Metin, M. Liput, L. Buzanska, Covering the Role of PGC-1α in the Nervous System. *Cells* **11**, 1–16 (2021).

304. M. J. Nunes, A. N. Carvalho, C. Sá-Lemos, M. Colaço, I. Cervenka, V. Ciraci, S. G. Santos, M. M. Ribeiro, M. Castanheira, P. R. Jannig, M. J. Gama, M. Castro-Caldas, C. M. P. Rodrigues, E. Rodrigues, J. L. Ruas, Sustained PGC-1α2 or PGC-1α3 expression induces astrocyte dysfunction and degeneration. *Eur J Cell Biol* **103**, 151377 (2024).

305. C. J. Lin, T. H. Chen, L. Y. Yang, C. M. Shih, Resveratrol protects astrocytes against traumatic brain injury through inhibiting apoptotic and autophagic cell death. *Cell Death & Disease 2014 5:3* **5**, e1147–e1147 (2014).

306. G. J. S. Pereira, M. Antonioli, H. Hirata, R. P. Ureshino, A. R. Nascimento, C. Bincoletto, T. Vescovo, M. Piacentini, G. M. Fimia, S. S. Smaili, Glutamate induces autophagy via the two-pore channels in neural cells. *Oncotarget* **8**, 12730–12740 (2017).

307. S. Kumari, S. L. Mehta, P. A. Li, Glutamate Induces Mitochondrial Dynamic Imbalance and Autophagy Activation: Preventive Effects of Selenium. *PLoS One* **7**, e39382 (2012).

308. B. Gabryel, A. Kost, D. Kasprowska, S. Liber, G. Machnik, R. Wiaderkiewicz, K. Łabuzek, AMP-activated protein kinase is involved in induction of protective autophagy in astrocytes exposed to oxygen-glucose deprivation. *Cell Biol Int* **41**, 928–931 (2017).

309. S. J. Lee, K. S. Cho, J. Y. Koh, Oxidative injury triggers autophagy in astrocytes: The role of endogenous zinc. *Glia* **57**, 1351–1361 (2009).

310. G. J. S. Pereira, H. Hirata, G. M. Fimia, L. G. Do Carmo, C. Bincoletto, S. W. Han, R. S. Stilhano, R. P. Ureshino, D. Bloor-Young, G. Churchill, M. Piacentini, S. Patel, S. S. Smaili, Nicotinic Acid Adenine Dinucleotide Phosphate (NAADP) regulates autophagy in cultured astrocytes. *Journal of Biological Chemistry* **286**, 27875–27881 (2011).

311. N. I. Fedotcheva, E. V. Grishina, V. V. Dynnik, Induction of Mitochondrial Cyclosporin-Dependent Permeability Transition Pore by Acylcarnitines. Effects of Concentrations and Carbon Chain Length. *Biochem (Mosc) Suppl Ser A Membr Cell Biol* **16**, 72–78 (2022).

312. H. X. Liu, Q. J. Liu, Logistic role of carnitine shuttle system on radiation-induced L-carnitine and acylcarnitines alteration. *https://doi-org.login.ezproxy.library.ualberta.ca/10.1080/09553002.2022.2063430* **98**, 1595–1608 (2022).

313. L. Zvejniece, B. Svalbe, E. Vavers, M. Ozola, S. Grinberga, B. Gukalova, E. Sevostjanovs, E. Liepinsh, M. Dambrova, Decreased long-chain acylcarnitine content increases mitochondrial coupling efficiency and prevents ischemia-induced brain damage in rats. *Biomedicine & Pharmacotherapy* **168**, 115803 (2023).

314. L. Böttinger, S. E. Horvath, T. Kleinschroth, C. Hunte, G. Daum, N. Pfanner, T. Becker, Phosphatidylethanolamine and Cardiolipin Differentially Affect the Stability

of Mitochondrial Respiratory Chain Supercomplexes. *J Mol Biol* **423**, 677–686 (2012).

315. Y. Lee, C. Willers, E. R. S. Kunji, P. G. Crichton, Uncoupling protein 1 binds one nucleotide per monomer and is stabilized by tightly bound cardiolipin. *Proc Natl Acad Sci U S A* **112**, 6973–6978 (2015).

316. M. Zhang, E. Mileykovskaya, W. Dowhan, Gluing the Respiratory Chain Together: Cardiolipin is required fro supercomplex formation in the inner mitochondrial membrane. *Journal of Biological Chemistry* **277**, 43553–43556 (2002).

317. M. Zhang, E. Mileykovskaya, W. Dowhan, Cardiolipin Is Essential for Organization of Complexes III and IV into a Supercomplex in Intact Yeast Mitochondria. *Journal of Biological Chemistry* **280**, 29403–29408 (2005).

318. M. Schlame, M. L. Greenberg, Biosynthesis, remodeling and turnover of mitochondrial cardiolipin. *Biochimica et Biophysica Acta (BBA) - Molecular and Cell Biology of Lipids* **1862**, 3–7 (2017).

319. G. Oemer, J. Koch, Y. Wohlfarter, M. T. Alam, K. Lackner, S. Sailer, L. Neumann, H. H. Lindner, K. Watschinger, M. Haltmeier, E. R. Werner, J. Zschocke, M. A. Keller, Phospholipid Acyl Chain Diversity Controls the Tissue-Specific Assembly of Mitochondrial Cardiolipins. *Cell Rep* **30**, 4281-4291.e4 (2020).

320. V. H. Quinlivan, M. H. Wilson, J. Ruzicka, S. A. Farber, An HPLC-CAD/fluorescence lipidomics platform using fluorescent fatty acids as metabolic tracers. *J Lipid Res* **58**, 1008–1020 (2017).

321. M. S. Sharpley, R. J. Shannon, F. Draghi, J. Hirst, Interactions between phospholipids and NADH:ubiquinone oxidoreductase (complex I) from bovine mitochondrial. *Biochemistry* **45**, 241–248 (2006).

322. F. Sun, X. Huo, Y. Zhai, A. Wang, J. Xu, D. Su, M. Bartlam, Z. Rao, Crystal Structure of Mitochondrial Respiratory Membrane Protein Complex II. *Cell* **121**, 1043–1057 (2005).

323. E. Calzada, E. Avery, P. N. Sam, A. Modak, C. Wang, J. M. McCaffery, X. Han, N. N. Alder, S. M. Claypool, Phosphatidylethanolamine made in the inner mitochondrial membrane is essential for yeast cytochrome bc1 complex function. *Nat Commun* **10**, 1–17 (2019).

324. K. Shinzawa-Itoh, H. Aoyama, K. Muramoto, H. Terada, T. Kurauchi, Y. Tadehara, A. Yamasaki, T. Sugimura, S. Kurono, K. Tsujimoto, T. Mizushima, E. Yamashita, T. Tsukihara, S. Yoshikawa, Structures and physiological roles of 13 integral lipids of bovine heart cytochrome c oxidase. *EMBO Journal* **26**, 1713–1725 (2007).

325. A. R. Mehdipour, G. Hummer, Cardiolipin puts the seal on ATP synthase. *Proc Natl Acad Sci U S A* **113**, 8568–8570 (2016).

326. A. M. Bertholet, E. T. Chouchani, L. Kazak, A. Angelin, A. Fedorenko, J. Z. Long, S. Vidoni, R. Garrity, J. Cho, N. Terada, D. C. Wallace, B. M. Spiegelman, Y. Kirichok, H+ transport is an integral function of the mitochondrial ADP/ATP carrier. *Nature* **571**, 515–520 (2019).